

NAVAL POSTGRADUATE SCHOOL  
Monterey, California

JN-05-CR

204247  
P. 129

(NASA-CR-195510) DESIGN PROJECT:  
LONGBOW SUPERSONIC INTERCEPTOR  
(Naval Postgraduate School) 129 p



DESIGN PROJECT

**LONGBOW Supersonic Interceptor**

**by**

**FASTGUYS CORPORATION**

**March, 1993**

**Project Advisor: Prof. C.F. Newberry**

N94-24581

Unclass

63/05 0204247




# Longbow Supersonic Interceptor


## AE4273 Aircraft Design

March, 1993

Bob Stoney

  
Project Engineer

Matt Baker

  
Performance/Weights

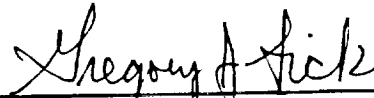
Joe Capstaff

  
Subsonic Aerodynamics

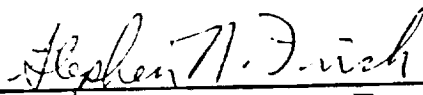
Bob Dishman

  
Structures/Materials

Greg Fick

  
Stability and Control

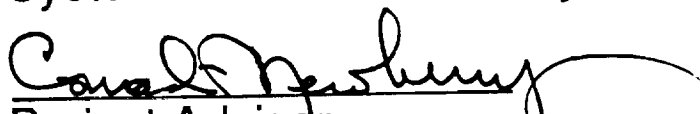
Steve Frick

  
Supersonic Aero/Propulsion

Mark Kelly

  
Systems/R&M/Survivability

Professor Newberry

  
Project Advisor



## TABLE OF CONTENTS

- I. INTRODUCTION
- II. BASIC CONFIGURATION
- III. WAVERIDER DESIGN
- IV. SUBSONIC CONFIGURATION
- V. AERODYNAMICS
- VI. PROPULSION
- VII. STABILITY AND CONTROL
- VIII. PERFORMANCE
- IX. STRUCTURES
- X. AIRCRAFT SYSTEMS
- XI. COST
- XII. MANAGEMENT
- XIII. PRODUCTION FACILITIES
- XIV. SUMMARY



## INTRODUCTION

### A. BACKGROUND/MISSION NEED

A recent white paper entitled "From the Sea" has spotlighted the need for Naval Aviation to provide overland support to joint operations. The base for this support, the Aircraft Carrier (CVN), will frequently be unable to operate within close range of the battleground because of littoral land-based air and subsurface threats. A high speed, long range, carrier capable aircraft would allow the CVN to provide timely support to distant battleground operations. Such an aircraft, operating as a Deck-Launched Interceptor (DLI), would also be an excellent counter to Next Generation Russian Naval Aviation (NGRNA) threats consisting of supersonic bombers, such as the Backfire, equipped with the next generation of high-speed, long-range missiles. Additionally, it would serve as an excellent high speed Reconnaissance airplane, capable of providing Battle Force commanders with timely, accurate pre-mission targeting information and post-mission Bomb Damage Assessment (BDA).

Recent advances in computational hypersonic airflow modeling has produced a method of defining aircraft shapes that fit a conical shock flow model to maximize the efficiency of the vehicle. This "Waverider" concept provides one means of achieving long ranges at high speeds. A Request for Proposal (RFP) was issued by Professor Conrad Newberry that contained design requirements for an aircraft to accomplish the above stated missions, utilizing Waverider technology. The FASTGUYS Corporation's response to this RFP is a design called the LONGBOW. Table I outlines the significant detailed requirements and compares LONGBOW's performance with them.

Table I.1  
WAVERIDER RFP DETAILED REQUIREMENTS

RFP REQUIREMENT	SPECIFICATION	Longbow
Minimum Mission Radius (DLI)	1500 nm	775
Cruise Mach Number	3 to 5	3
Carrier Suitable (FQ&P, S) (1)	All Applicable	Satisfies
Weapons Load (A/A missile)	2	2
External Weapons (400 nm mission)	2 X 1000 LGB	2
Maximum Weight	70,000	68,000
Sustained Turn Performance (2)	2.5 g	2.8 g
Crew	1	1

Notes: (1) Flying Qualities, Performance, Support

(2) 50,000 ft, Mach=2.0



## **B. MISSION PROFILE**

The mission profile, Figure I.1, consists of : CVN launch, climb/accelerate, cruise, A/A missile shot, high efficiency return cruise, loiter/descent, and CVN arrestment.

## **C. REGULATIONS/SPECIFICATIONS**

In addition to the RFP specifications, the LONGBOW was designed to meet the requirements of the following specifications and standards:

- MIL-F-8785C (Flying Qualities)
- MIL-STD-805A (Field of View)
- MIL-STD-2069 (Survivability)
- MIL-A-8860 (Strength and Rigidity)
- MIL-A-8861 (Flight Loads)
- MIL-A-8863 (Carrier Suitability)
- MIL-STD-8552 (Landing gear design)
- MIL-A-8870 (Vibration and Flutter)
- MIL-A-2066 (Carrier Launch and Arrestment)

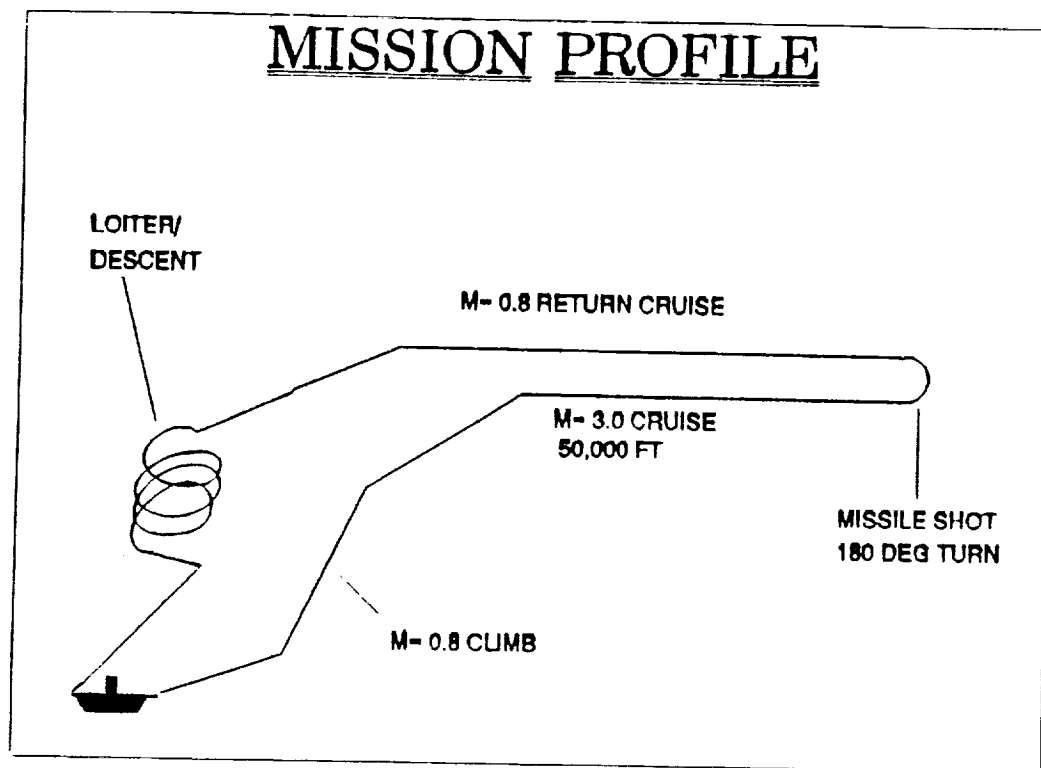


Figure I.1  
LONGBOW Mission Profile

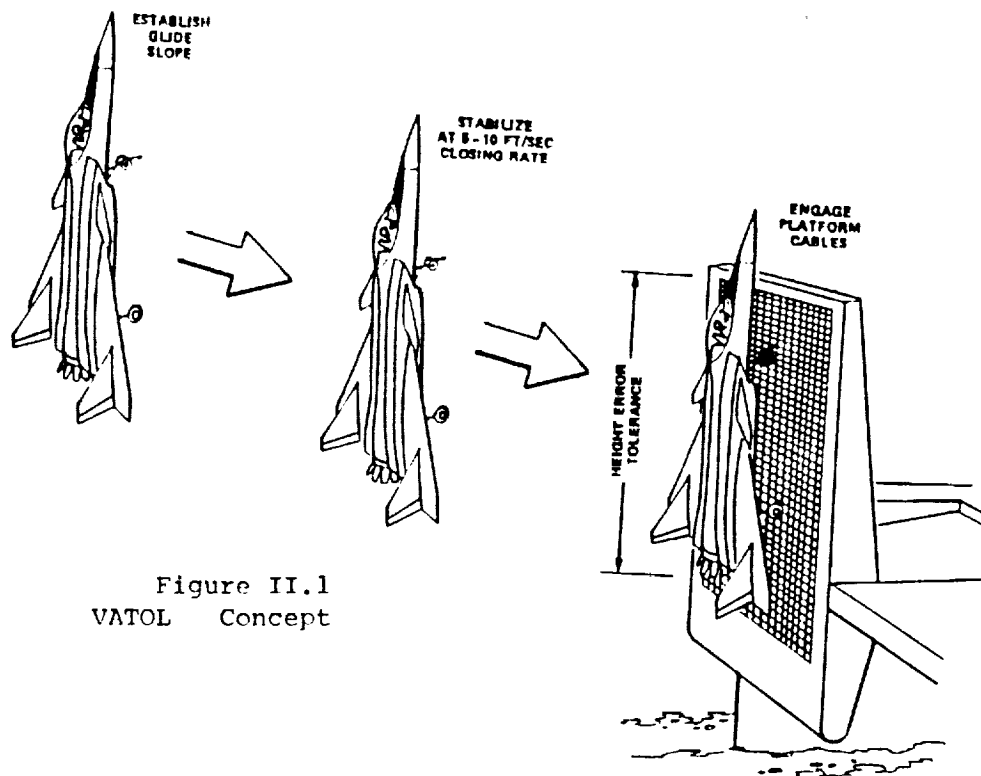


Figure II.1  
VATOL Concept

## II. BASIC CONFIGURATION

After studying several historical designs the team selected three basic design types:

- 1) A conventional aircraft; in other words one that performs horizontal takeoff and landing.

- 2) Lift/Cruise (L/C) VSTOL; similar in concept to the Harrier design: takeoff and landing augmented by thrust from swiveling exhaust nozzles.

- 3) Vertical Attitude Takeoff and Landing (VATOL); shown in figure II.1, also called a "tailsitter".

The design began with a basic constraint analysis of Sea Level Thrust to Takeoff Weight versus Wing Loading for the various phases of the mission. Figure II.2 shows the results of this analysis, with an initial design target of 0.55 Thrust to Weight and 120 lb/ft<sup>2</sup> Wing Loading. A trade-off study of the three basic design alternatives was then conducted, as described in Table II.1

# Contraint analysis.

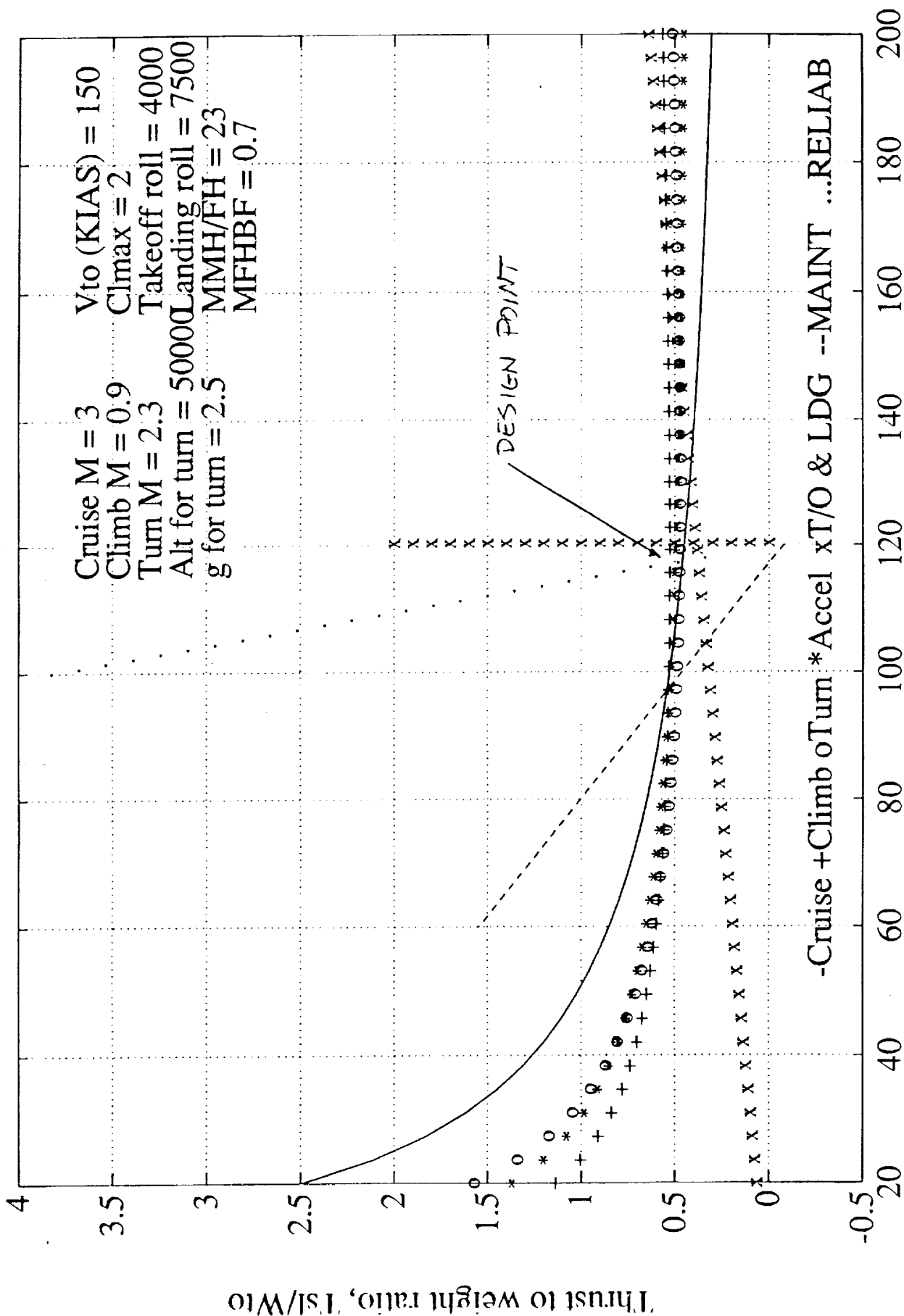


Figure II.2: LONGBCW Constraint Analysis

# BASIC DESIGN TYPES--TRADEOFF STUDY

	CONVENTIONAL	VSTOL	VATOL
ADVANTAGES	<ul style="list-style-type: none"> <li>-Proven Design</li> <li>-Easier S&amp;C</li> <li>-On Constraint (T/W vs. W/S)</li> <li>-CVN suitable</li> </ul>	<ul style="list-style-type: none"> <li>-Easier integration of Waverider shape</li> <li>-S&amp;C known (Harrier)</li> </ul>	<ul style="list-style-type: none"> <li>-Most efficient V/STOL design</li> <li>-Easy to match with Waverider shape</li> </ul>
DISADVANTAGES	<ul style="list-style-type: none"> <li>-Wt Penalty for swing wing, etc</li> <li>-Hypersonic losses caused by slow speed devices (swing wing, etc)</li> </ul>	<ul style="list-style-type: none"> <li>-Off Constraint (T/W too high)</li> <li>-Nozzle losses</li> <li>-Wt penalty for nozzles</li> </ul>	<ul style="list-style-type: none"> <li>-Off Constraint (T/W too high)</li> <li>-S&amp;C problems</li> <li>-Not presently CVN suitable</li> <li>-Not compatible with all diverts</li> </ul>

Abbreviations: S&C=Stability and Control T/W=Thrust to Wt  
CVN=Aircraft Carrier W/S=Wing loading  
Wt =Weight

## Basic Design Types -- Tradeoff Study

Table II.1

The "conventional" design was chosen, in large part because the other two designs--by virtue of requiring a T/W greater than 1.0--would be very inefficient in cruise flight. This would result in unacceptably short combat radii.

### III. WAVERIDER DESIGN

#### A. REQUIREMENTS

The RFP stipulated that the aircraft must incorporate waverider design techniques. It was hoped that waverider flow characteristics would increase the lift to drag (L/D) ratio in the supersonic cruise portion of the flight profile. The Kuchemann "barrier" value of  $L/D = 8$  for mach 3.0 flight was seen as a goal, and was required for the attainment of the 1500 nm combat radius within the weight constraints imposed by carrier suitability.

#### B. DESIGN CHOICES:

Due to the time consuming methods necessary for the design of a conic shock waverider, the NASA waverider design program was used to determine the Longbow body shape. The waverider program is capable of calculating the correct shape of any conic shock-derived vehicle, producing results for the lift, drag, and aircraft volume and weight. The dynamic pressure, Reynold's number per foot, body length, conic shock angle, and free stream mach number were the most significant inputs to the program, and were maintained at constant values while the shape of the waverider was iterated to find the best combination of aerodynamic and structural qualities.

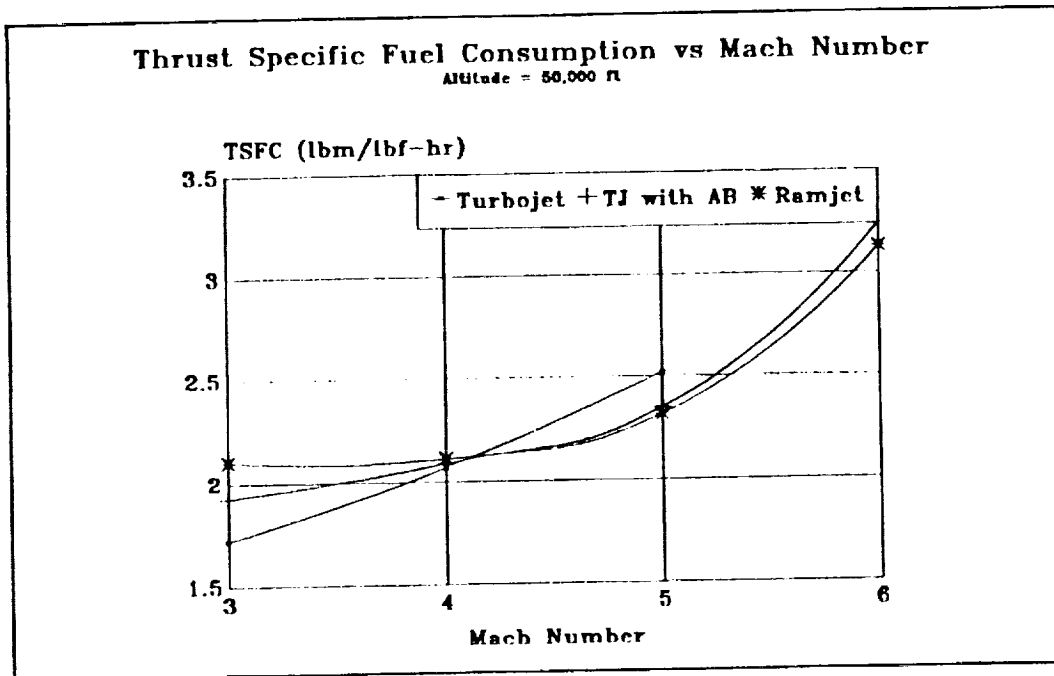
The final body shape needed to provide enough lift for the cruise condition, enough body volume for fuel storage, and the smallest amount of base drag possible within the other constraints. Increasing the shock angle provided more lift at the on-design

condition, but created a thicker body, increasing the base drag. The body shape and shock angle were chosen to provide 60,000 lbs of lift on design (initial cruise condition). Unless the body shape is altered in flight, the aircraft must be operated at a slightly off design AOA to reduce the excess lift after fuel is burned in the cruise configuration.

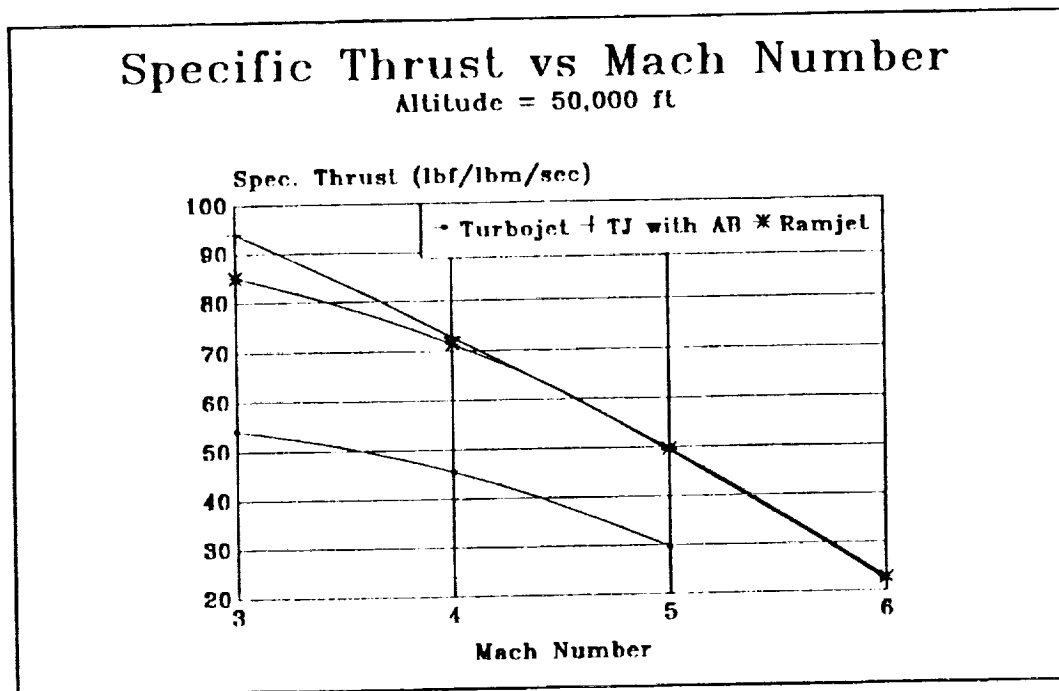
### C. PROPULSION CONSIDERATIONS FOR CRUISE MACH NUMBER

The choice of cruise mach number hinged on the theoretical capabilities of the propulsion system and affects of aerodynamic heating at high mach numbers. The performance of the engine was analyzed with cycle analysis of a turbojet, an afterburning turbojet, and a ramjet over a flight regime from mach 3 to 6, as shown in Figures III.1 and III.2. The turbojet ceased to operate approaching mach 5, and the afterburning turbojet required a reduction in compressor pressure ratio to 1.1 or less for optimum performance past mach 4. The afterburning turbojet displayed a 72% decrease in specific thrust, and a 71% increase in specific fuel consumption between mach 3 and 6. These problems greatly limited the efficiency of all three cycles operating at mach numbers higher than 3.

Aerodynamic heating was analyzed using the data produced by the waverider program. The code calculated the steady state surface temperatures for a given free-stream mach number, dynamic pressure, and Reynold's number (per foot). Figure III.3 shows these temperatures plotted for mach numbers from 3 to 6 and shock angles from 21 deg. to 50 deg. It was apparent from the initial



Thrust Specific Fuel Consumption vs Mach Number  
Figure III.1



Specific Thrust vs Mach Number  
Figure III.2



results that active cooling of the leading edge and lower surface of the body was required for free-stream Mach numbers of 4 and higher.

Due to the severe reductions in the engine performance and the aggravated aerodynamic heating problems, it was decided to design the vehicle for a cruise mach number to 3.

High and low aspect ratio designs are possible using the conic shock design, and both were considered in the initial stages of the design process. The high aspect ratio design had the advantages of improved body thickness, better visibility over the nose, and better fixed geometry low speed performance, though these were outweighed by significant disadvantages. The difficulty of providing adequate stability and control in the transonic and supersonic regions, along with the excessive wingspan needed for the required takeoff weight made this design unattractive, and the lower aspect ratio waverider design was chosen for further development.

#### **D. CRUISE ALTITUDE OPTIMIZATION**

The determination of an optimum cruise altitude was based on the required engine volume and the aerodynamic heating considerations of high speed, high altitude flight. Once the basic configuration was chosen, initial calculations could be made for both the vehicle drag and heat transfer at the cruise condition.

In order to make a weighted comparison of these factors, and to simplify the analysis, both the total required engine volume

(calculated from the vehicle drag) and heat transfer to the aircraft were non-dimensionalized with respect to the values at 30,000 ft and mach 3. This greatly simplified the heat transfer analysis, and allowed the effects of heating and loss of total fuel volume (due to increasing required engine size) to be combined and optimized for the best cruise altitude.

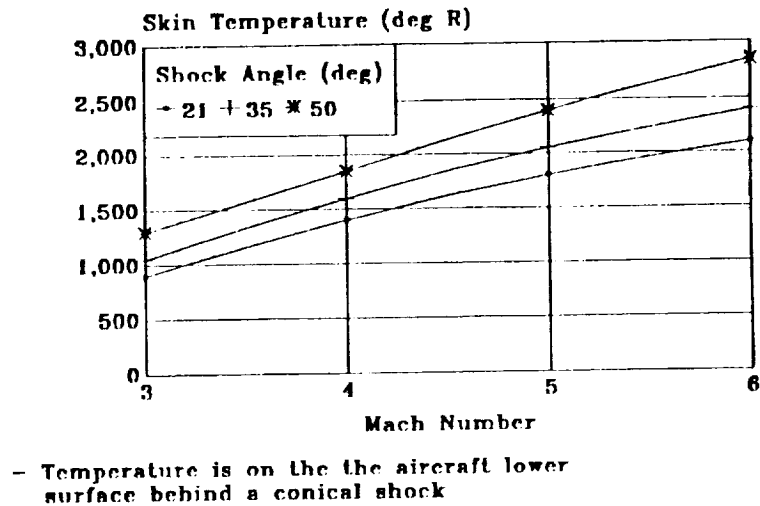
The early results for the aircraft skin temperature showed that it was unlikely to require any active cooling in the reasonable range of cruise altitudes as shown in Figure III.3. This suggested that the engine volume would be the dominant force in the analysis (see Figure III.4), and was taken into account by squaring the engine volume ratio before multiplying it with the heat flux ratio. As shown in Figure III.5, this combined parameter was plotted against altitude at mach 3, and displayed a flat region from 45 to 60 thousand feet with a minimum at 55 thousand feet. The restriction to a cruise altitude of 50000 feet allowed for the elimination of a pilot's pressure suit and associated hardware without a significant loss in aircraft fuel storage volume, and was therefore chosen for the cruise altitude.

#### **E. FINAL WAVERIDER DESIGN**

With constraints imposed by the preceding discussion of optimum altitude, basic propulsion type and volume, aerodynamic heating, optimum cruise Mach number, and aspect ratio the numerous runs of NASA Waverider code were run to select a Mach 3 shape optimized for lift to drag ratio. The result is shown Figure III.6.

## Aerodynamic Heating vs Mach

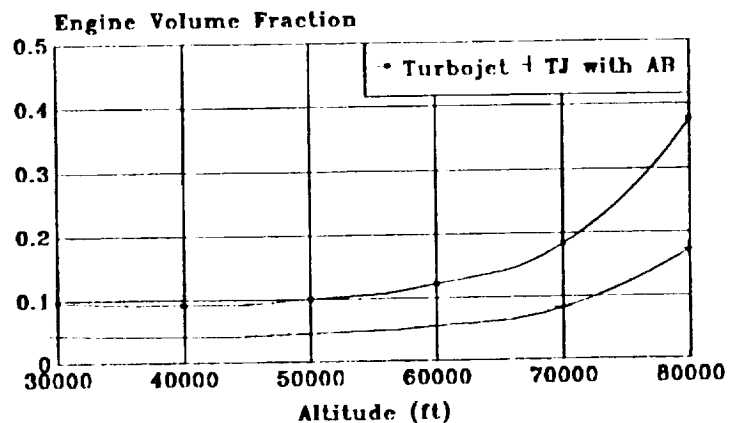
Altitude = 50,000 ft



Aerodynamic Heating vs Mach Number  
Figure III.3

## Engine Volume vs Altitude

(Based on 2 engines)



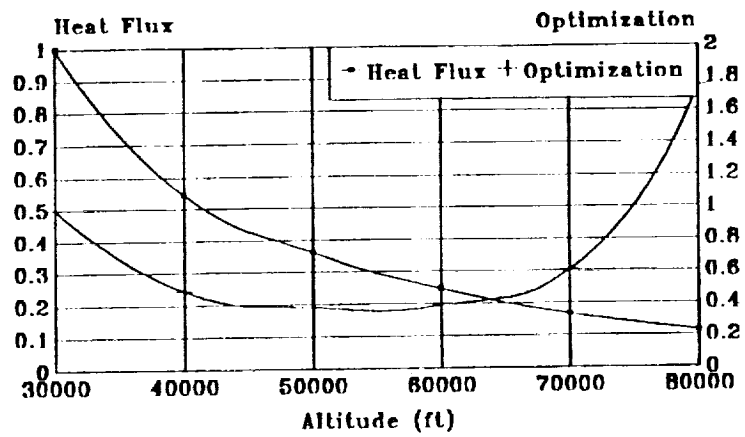
Cruise Mach = 3.0

Eng. Vol. Fraction = Total Engine Vol. / Aircraft Vol.

Engine Size vs Altitude  
Figure III.4

# Cruise Altitude Optimization

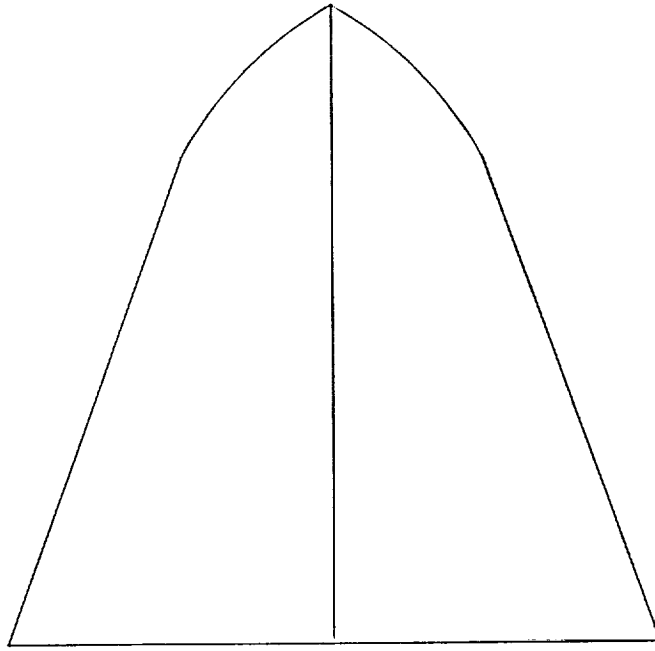
(Based on 2 engines)



The optimization curve is the square of the engine volume \* the non-dimensionalized heat flux

Cruise Altitude Optimization  
Figure III.5

# Final Waverider Body Design



Top View



Side View



Front View

Figure III-6

## IV. SUBSONIC CONFIGURATION

### A. BASIC:

The requirement that the Longbow be carrier-based presents many low speed obstacles. A tradeoff study was conducted to determine the most effective and efficient method of allowing the waverider design to fly at the required low speeds. Considerations for this flight regime included:

- \*Utilize the pre-determined waverider design (Figure III.6)

- \*The look-down angle over the nose at approach speed must allow for good field of view in the carrier environment. Zero pitch attitude was chosen as the goal based upon the flat upper fuselage surface, and to maintain the nose landing strut length within reasonable limits.

- \*The chosen wing design must conform to the basic waverider design in thickness, leading edge radius, and planform shape when swept.

- \*A wing loading of  $120 \text{ lb/ft}^2$ , determined from the constraint analysis.

Several alternatives were studied. An aircraft with no low speed lift devices was discounted due to the excessive AOA required to obtain the necessary lift in the approach configuration. A forward swept/canard combination (Figure IV.1) was appealing due to the estimated aft center of gravity (CG) of the waverider shape.

This design was not selected, however, as there were many concerns over the added weight of the canard, and the structural/ flutter problems present as the wings faired forward into the body.

The swing-aft alternative was judged to be the most feasible (Figure IV.2 and IV.3).

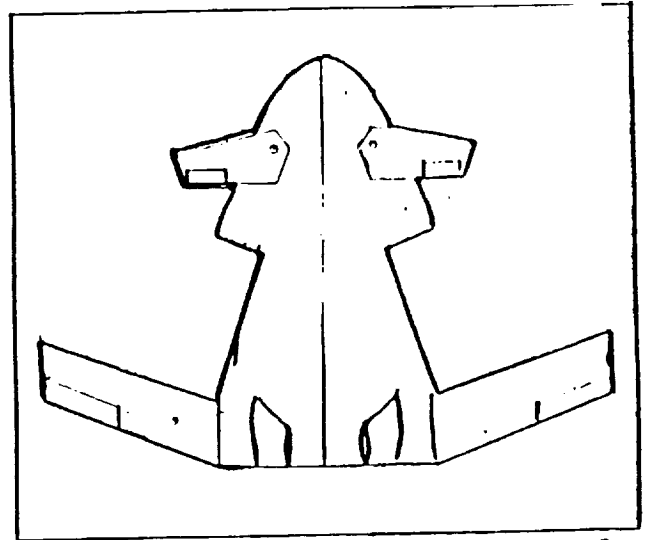


Figure IV.1: Swing Forward

The conventional swing wing technology helped reduce the risk in utilizing the unproven waverider design. The drawback to this selection was the apparent stability concerns with an aft CG/mean aerodynamic center (MAC) relationship. It was determined at this juncture that a reference area of  $S_{ref} = 1800 \text{ ft}^2$  would be used in all configurations to alleviate any confusion amongst the aerodynamic coefficients between the forward and aft swept wing flight regimes.

## B. WING PLANFORM AND AIRFOIL SELECTION:

### 1. SIZE/SHAPE

The Longbow wing planform was designed to fulfill its primary purpose of allowing the waverider design to operate in the carrier environment. The W/S of  $120 \text{ lb/ft}^2$ , as selected from the constraint analysis, Section II, resulted in a required lifting area of approximately  $525 \text{ ft}^2$  at maximum takeoff weight. The shape of the waverider restricted the flexibility of choosing various

wing positions and, along with the structural requirements for a pivot point placement, was crucial in determining the ultimate wing shape. The longitudinal stability requirement for a horizontal tail further constrained the wing design.

A subsonic Vortex-Lattice analysis was conducted on the swing-aft wing designs in Figs. IV.2 and IV.3 to determine the lift, drag, and stability characteristics of each, and their ability to achieve the desired results. Based upon this study, the wing-body shape in Figs. IV.4 and IV.5 was selected. The resulting geometric properties were a maximum spread wingspan of 76

ft, an aspect ratio (AR) of 3.21, and a taper ratio ( $\lambda$ ) of 0.62. The available leading edge wing sweep angle ( $\Lambda$ ) ranged from  $0^\circ$  to  $67^\circ$ .

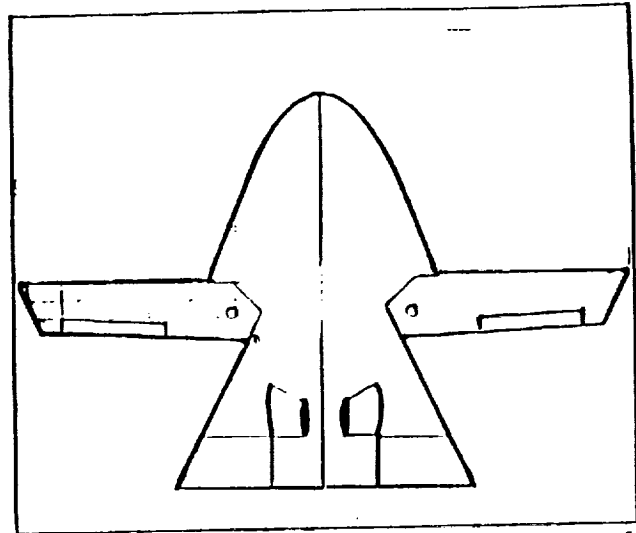


Figure IV.2: Swing Aft No. 1

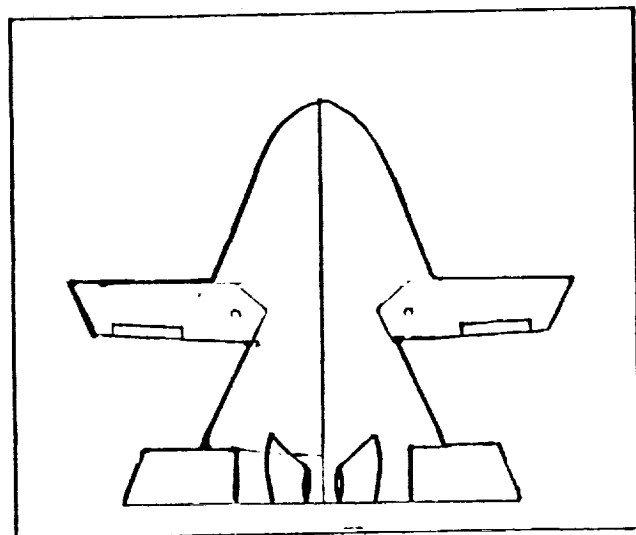


Figure IV.3: Swing Aft No. 2



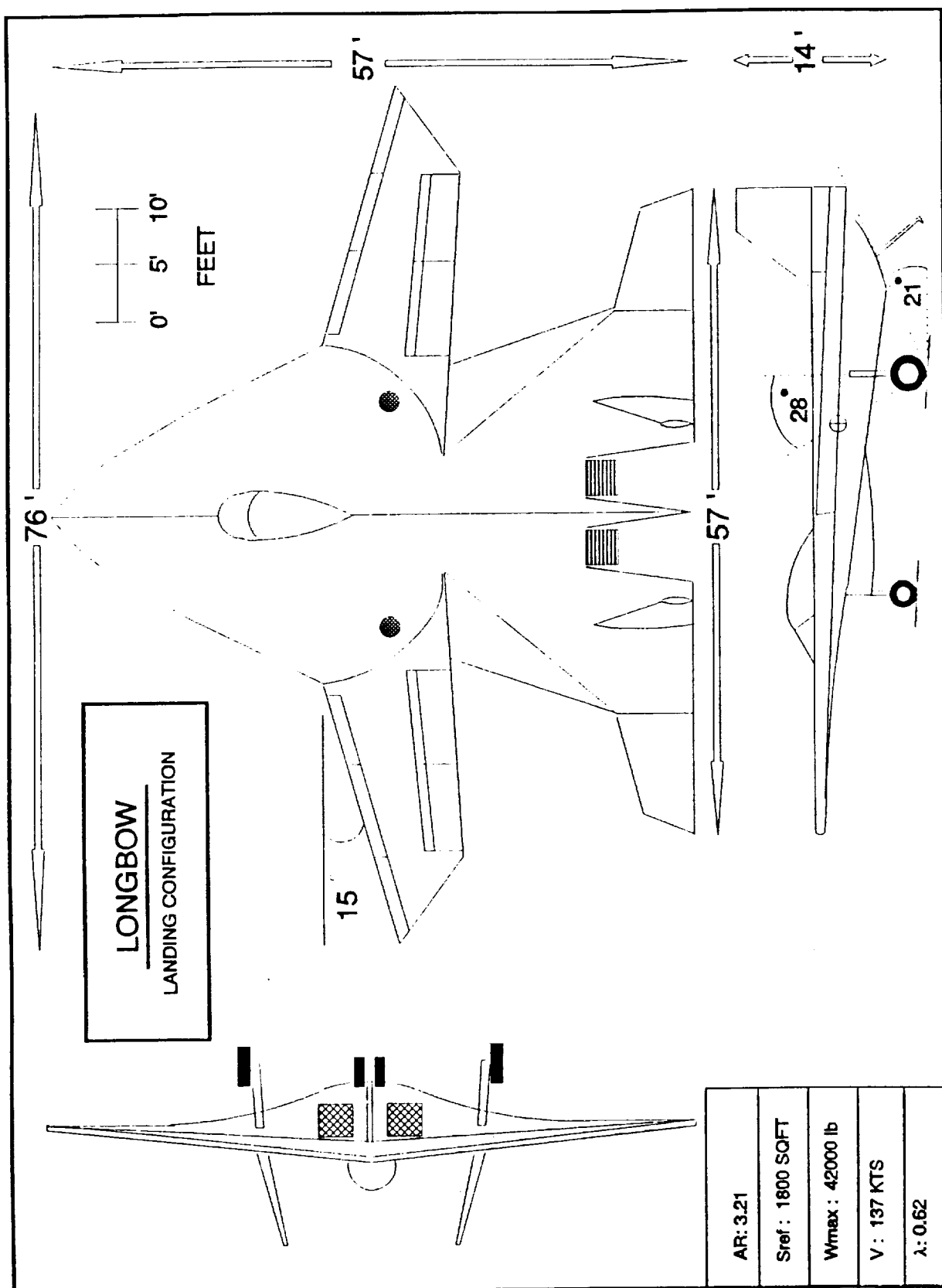


FIGURE IV.4: Longbow Landing Configuration View

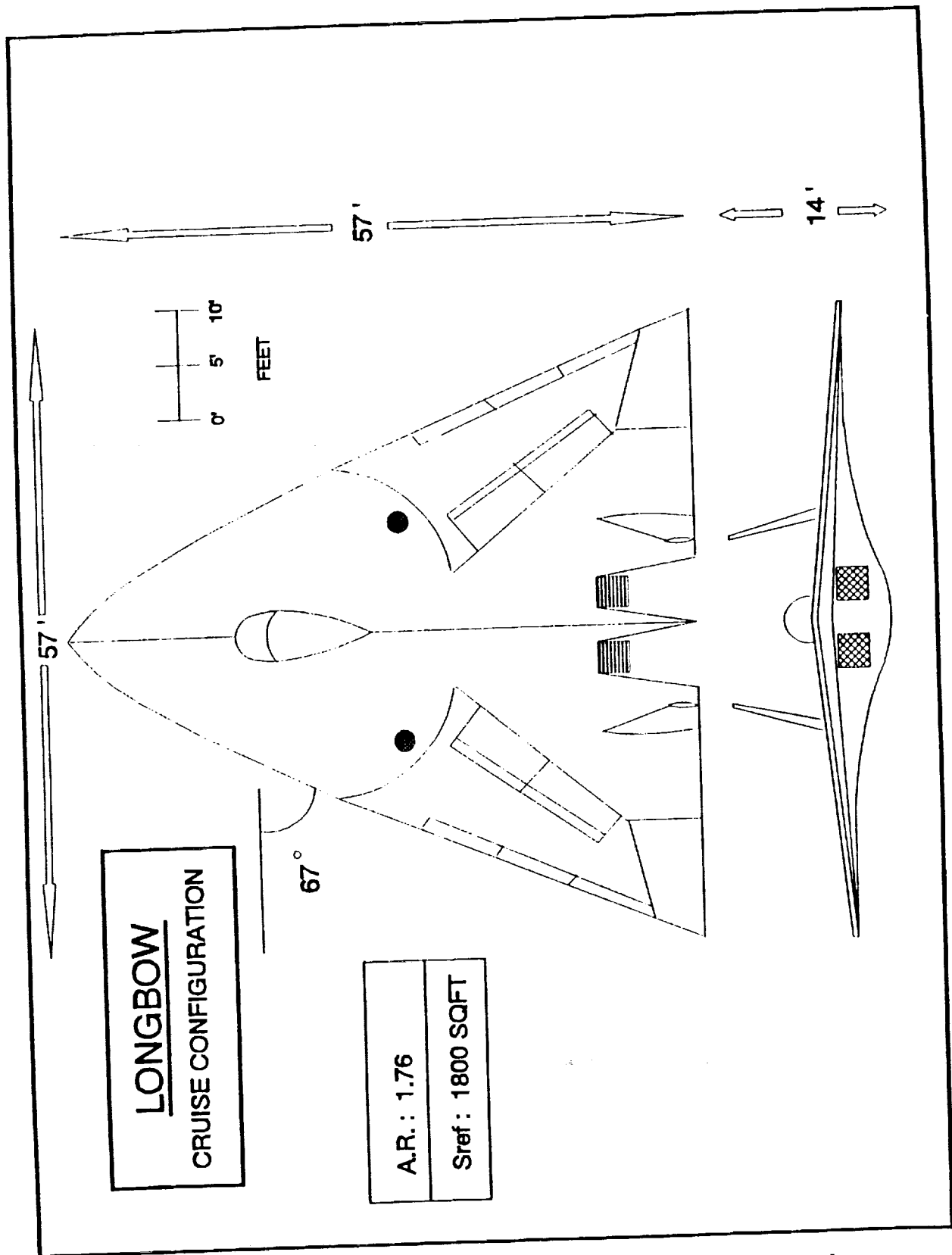


FIGURE IV.5: Longbow Cruise Configuration View

## 2. AIRFOIL

The airfoil selected for the Longbow was the NACA 66-006 section. This airfoil was chosen not only for its good transonic/supersonic aerodynamic qualities, but for its physical conformity to the waverider design as well. The airfoil had to minimize disruptions to the waverider aerodynamics when the wing was swept to its maximum aft sweep of 67', yet also provide sufficient lift when spread forward.

The 66-006 was determined to be sufficiently thin to closely match the upper waverider surface, yet still provide thickness to house fuel tanks and the necessary flight control equipment. A cambered section would aggravate the disturbances compared to the symmetric 66-006, and was therefore not selected. The waverider body design contained a 0.25 inch leading edge radius, which was matched by the 66-006's 0.27 inch radius (at MAC).

In addition to the geometric similarities of this airfoil, it also exhibited excellent high speed aerodynamics. The maximum thickness of the 66-006 was at 45% chord, which moved the minimum pressure point aft, decreasing the supersonic drag penalty. The symmetrical design also helped reduce wave drag losses, and was selected for use in the tail surfaces for similar drag reduction.

The use of this thin airfoil section resulted in poor low speed lifting ability, which was overcome by the use of high lift devices discussed in the next section. A study suggested by Nicolai comparing the empty weight of the design to the thickness

ratio of the wing was completed as shown in Figure IV.6, which verified the selection of this airfoil.

### **t/C TRADEOFF STUDY**

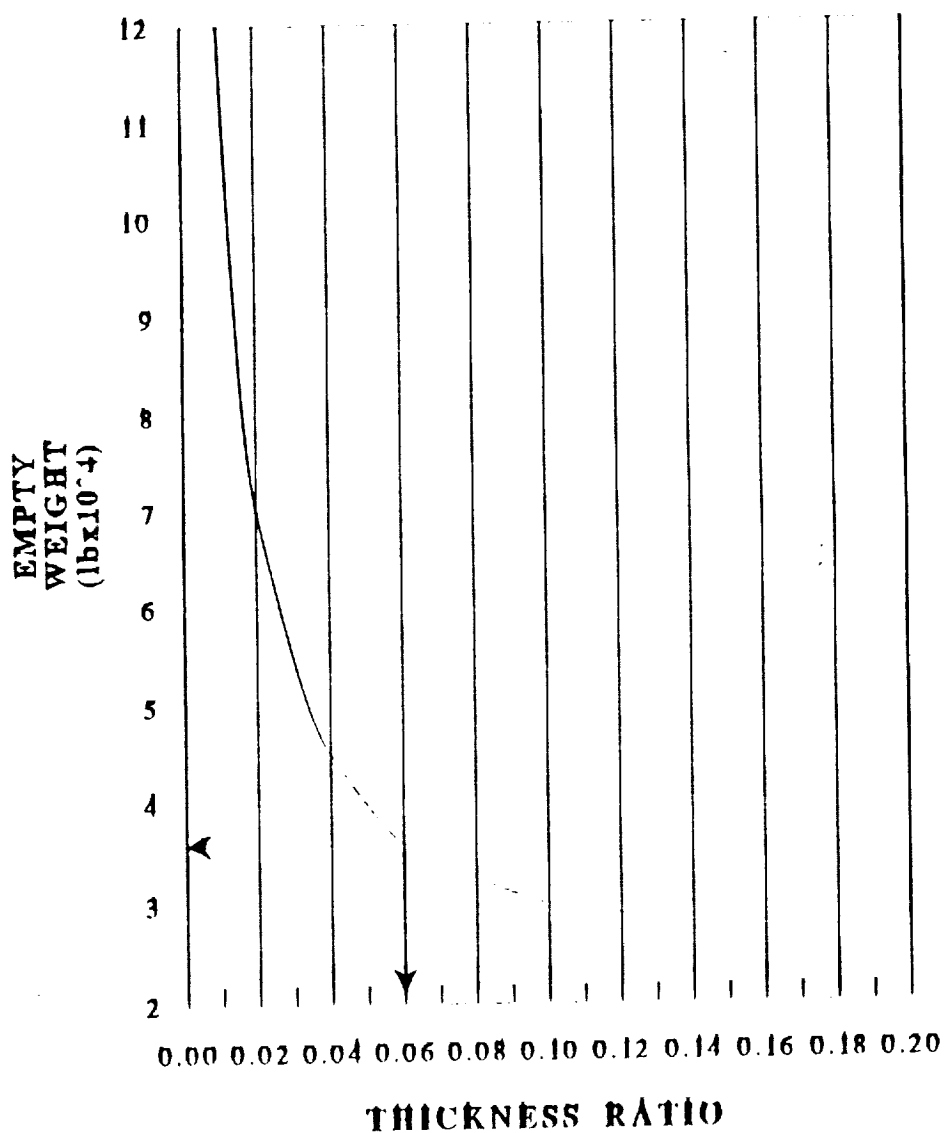


**FIGURE IV.6: Empty Weight vs Thickness Ratio**

### C. HIGH LIFT DEVICES

Plain flaps versus the more exotic devices were initially studied to examine their lifting effectiveness. The plain flaps were attractive due to their simplicity in design and lower structural requirements. A tradeoff study was completed comparing various trailing edge (TE) and leading edge (LE) plain flap combinations. The flap chords selected were 20% chord for the TE, and 10% for the LE, since Vortex-Lattice results showed that little advantage would be gained by larger flaps.

The Vortex-Lattice method was utilized to determine the resulting AOA at the maximum trap landing weight  $C_L$  of 0.369, and the best wing sweep to achieve that lift. Based upon this study, a flap configuration of 35' TE and 15' LE was determined to allow the Longbow to remain at near-zero AOA at the maximum landing weight of 42000 pounds and an approach speed of 137 knots. Therefore, no further flap types were studied since the plain flaps effectively met the design criteria by the simplest method. The LE flap deflection was small by industry standards, because larger angles would encourage flow separation at the desired zero AOA attitude. The corresponding wing sweep for this chosen configuration was  $\Lambda=15'$ . Figure IV.7 displays the 66-006 airfoil, its characteristics, and the high lift devices selected. The  $C_{L_{max}}$  available for this aircraft configuration was 0.64 as seen in Figure IV.8.

# AIRFOIL SELECTION

## NACA 66-006

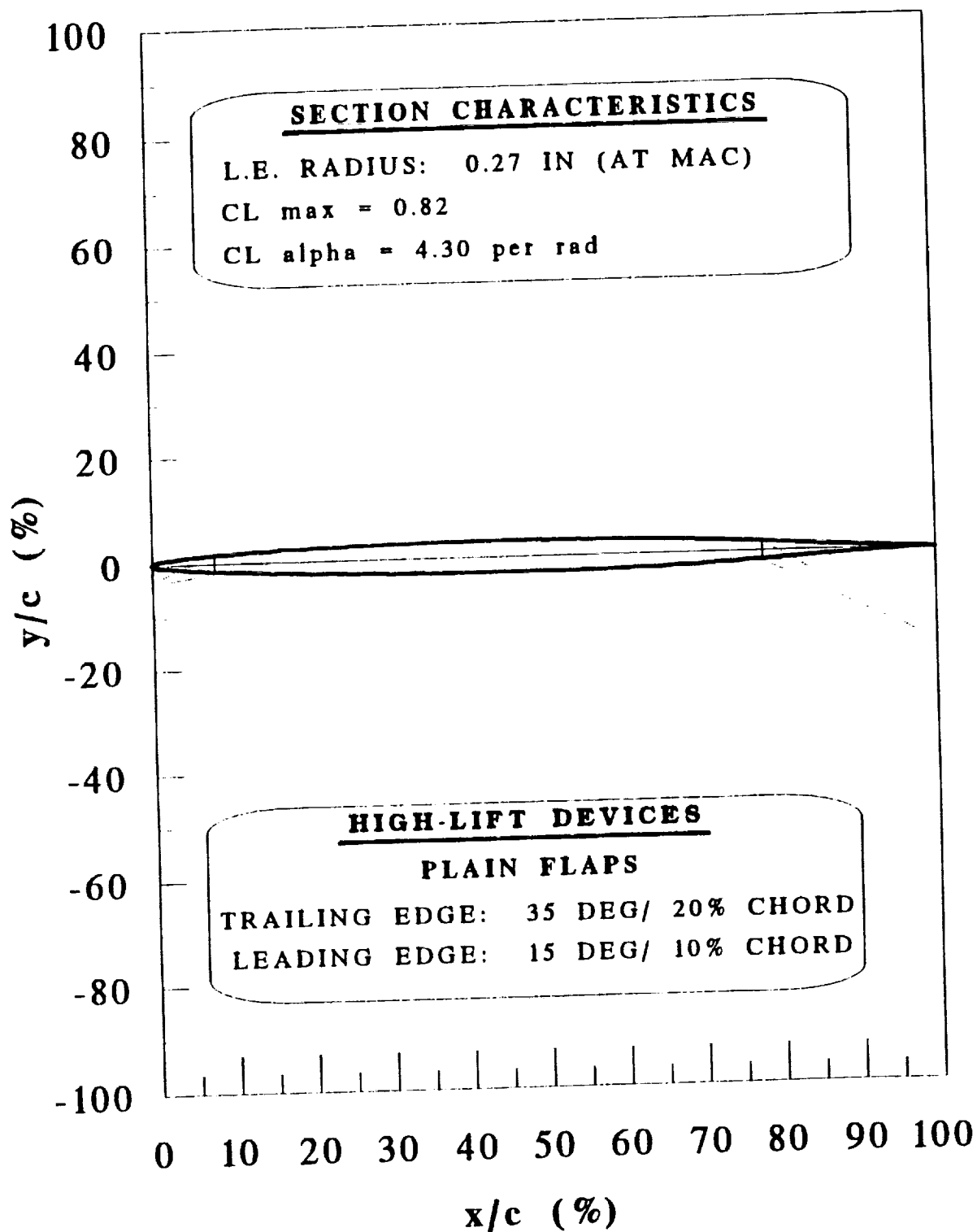


FIGURE IV.7: Airfoil Selection- NACA 66-006

# AIRCRAFT LIFT CURVE SLOPE

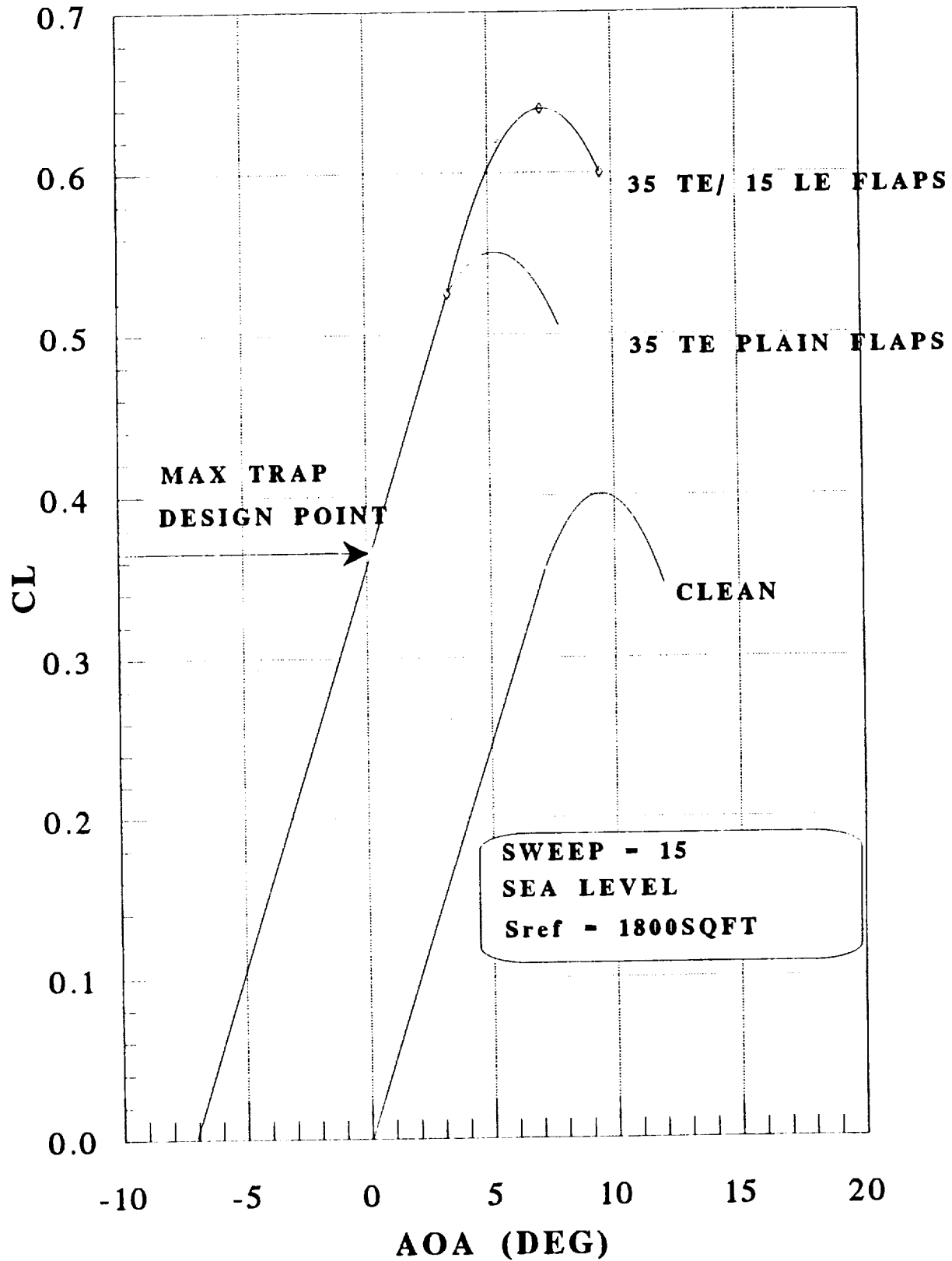


FIGURE IV.8: Aircraft Lift Curve Slope

#### D. WING SWEEP SCHEDULING

The wing sweep scheduling for the Longbow was selected to maintain as level as feasible the transition from slow speed,  $\Lambda=15^\circ$  sweep to the fully swept  $67^\circ$  waverider. Figure IV.9 displays the AOA perturbations as the wing is swept aft. The AOA excursions were limited to 5 degrees for the transition. The wing sweep schedule was integrated into the flight control system to enable optimum selection of sweep for the given flight condition.

The effect of this wing sweep on the wing-body lift curve slope is shown in Figure IV.10. The wing sweep began when the flaps were fully retracted and 0.35 Mach was achieved. The Longbow's wings were fully swept by 0.8 Mach. The  $C_{L\alpha}$  variations with respect to Mach for the scheduled sweep versus the waverider design demonstrates the smooth transition from the high lift configuration to the fully swept Longbow.



# WINGSWEEP SCHEDULE

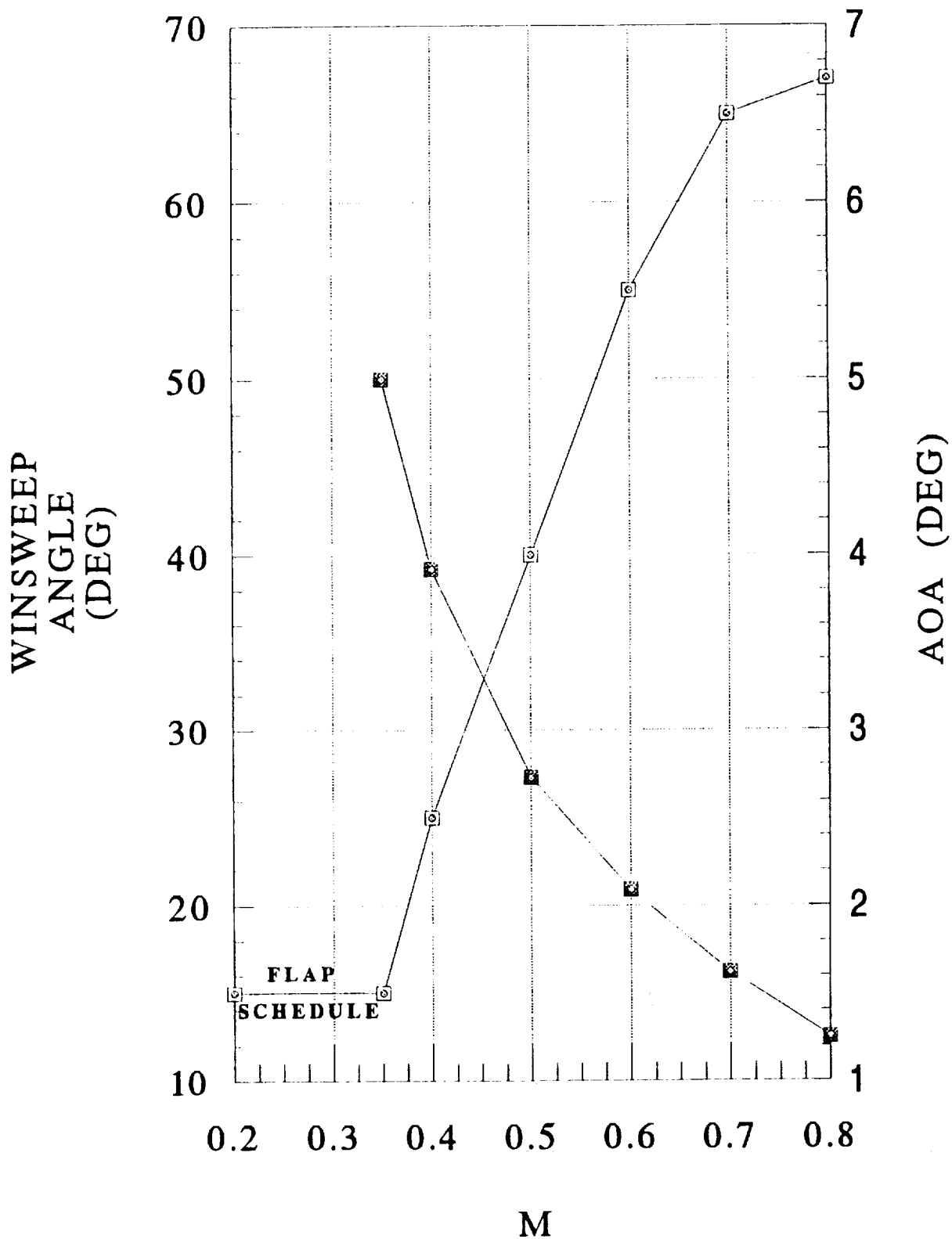


FIGURE IV.9: Wingsweep Schedule

# WING-BODY LIFT CURVE SLOPE

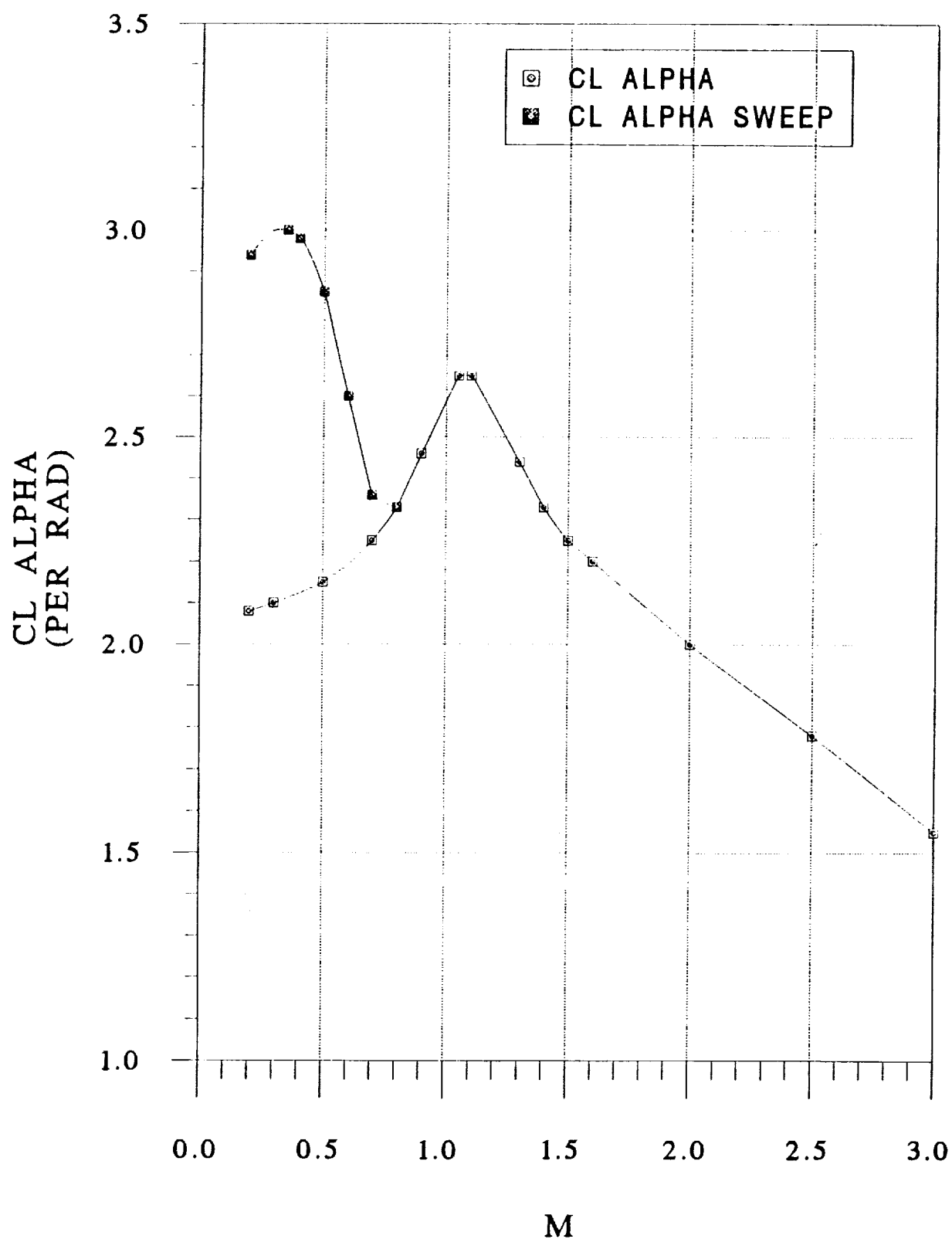


FIGURE IV.10:  $C_{L\alpha}$  vs Mach Aerodynamics

## V. AERODYNAMICS

### A. ZERO LIFT DRAG

The aerodynamic drag on the Longbow was calculated utilizing the methods outlined in Nicolai (chapter 11) and Roskam (chapter 4). The  $CD_0$  computation was broken down into Subsonic, Transonic to the drag divergence Mach number  $M_{DD}=1.27$ , and Supersonic regions. The results are displayed in Figure V.1 for the initial and final design configurations. Subsonic  $CD_0$  remains relatively constant at 0.0065, and the component contribution to this value is shown in Table V.1. The major contributors to subsonic zero-lift drag consisted of skin friction and parasite drag.

COMPONENT	$CD_0$ CONTRIBUTION
Wing	0.003014
Fuselage	0.002992
Tail (Horizontal and Vertical)	0.000335
Canopy	0.000159
<b>TOTAL</b>	<b>0.006500</b>
<b>ADDITIONAL COMPONENTS</b>	
Flaps	0.008980
Landing Gear	0.053333

TABLE V.1: Subsonic  $CD_0$  Component Breakdown

# CD<sub>0</sub> vs MACH NUMBER

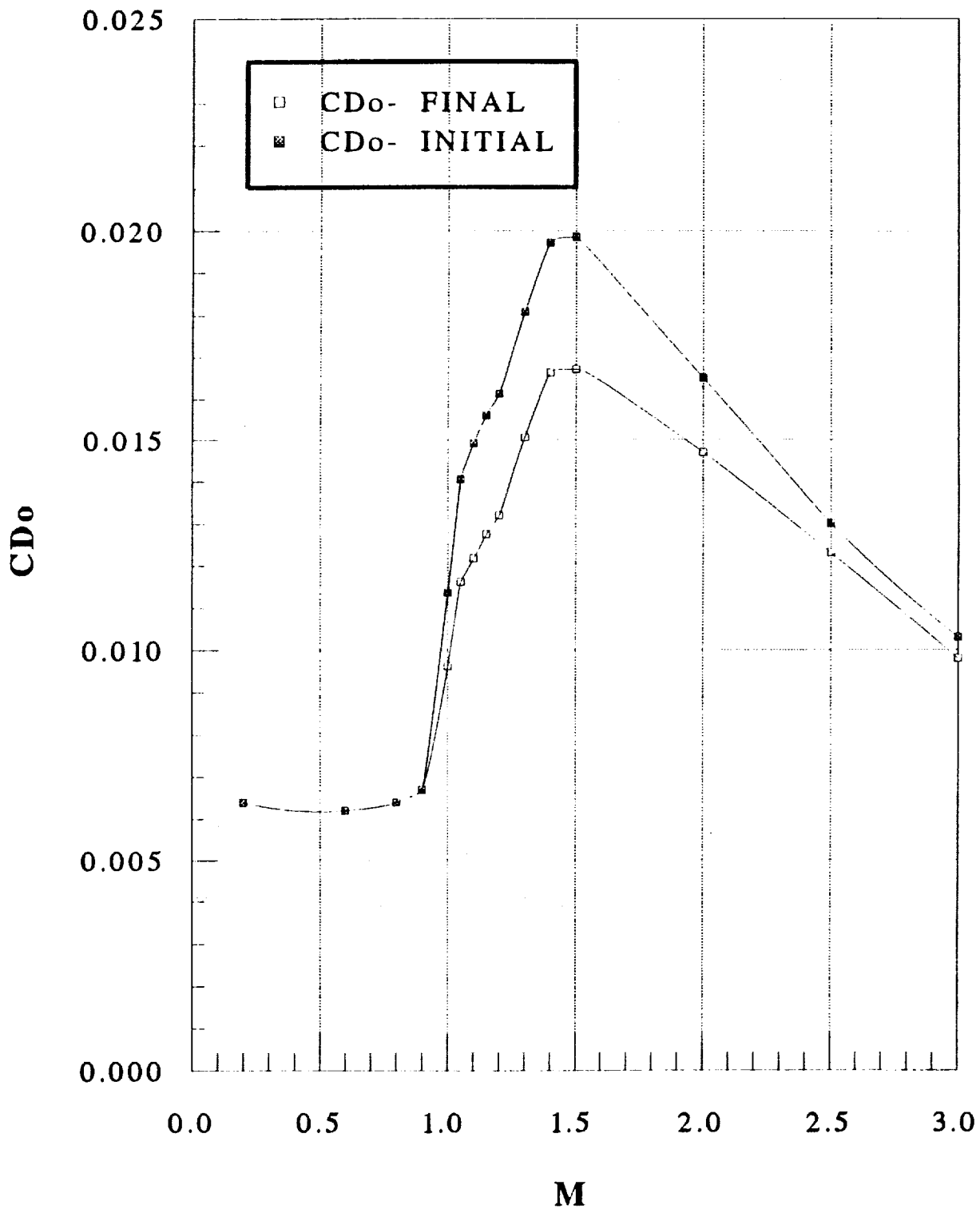


FIGURE V.1: Zero Lift Drag vs Mach Number

Transonic  $CD_0$  consisted primarily of skin friction and wave drag, the wave drag of the wing and fuselage being the dominant terms in the zero-lift drag magnitude. The sharp LE wing sweep of 67 degrees helped reduce the severity of the wave drag compared to a straight wing, but shifted the peak drag Mach number from 1.13M to 1.53M. The fuselage wave drag values were based upon its fineness ratio, which was constrained to a value of 4.52 due to utilizing the pre-determined waverider configuration. The  $CD_0$  values displayed a rapid increase as the Longbow transitioned through 1.0M, and reached a peak drag value of 0.0166 at 1.5M as shown in Figure V.1.

Supersonic  $CD_0$  characteristics consisted of a steady decline from the peak transonic drag to a value of 0.0098 at the desired cruise speed of 3.0M. Once again, the main contributor to the zero-lift drag was the wave drag caused by the wing and fuselage. The wing wave drag term was a strong function of Mach number, thickness to chord, and LE radius, which was the rationale behind utilizing the NACA 66-006 airfoil shape to help reduce the magnitude of this wave drag.

## **B. INDUCED DRAG**

The drag due to lift for the Longbow was primarily due to the wing, and to a much lesser extent, the fuselage. Subsonically, this added drag was modelled using the conventional function of  $C_L^2$ . The lift drag at transonic and supersonic speeds was determined using the parameters of the free-stream Mach, planform area, and

slenderness ratios as per Roskam (chapter 4).

The very nature of the waverider configuration operating at the design Mach number reduced the drag due to lift. The lower surface of the wing was effectively "sealed off" from the upper by the attached shock along the LE of the wing. Though the zero lift drag was unaffected, the elimination of the wing tip flow from the high pressure lower surface to the upper surface produced a lower induced drag. The drag coefficient due to lift was correspondingly reduced as the on-design Mach number was reached.

#### C. DRAG POLAR:

Drag Polar curves are presented in Figure V.2 for three flight regimes: subsonic- 0.2M/Sea Level (clean and dirty); subsonic- 0.8M/20000 ft; and supersonic- various Mach/50000 ft. Due to the small nature of the Longbow's aerodynamic coefficients (from using  $S_{ref}=1800 \text{ ft}^2$ ), the supersonic drag polar has been expanded to highlight the  $C_L$  range of interest. This portion of the drag polar clearly shows the efficiency of the Longbow at the higher Mach numbers, a direct result of utilizing the waverider design.

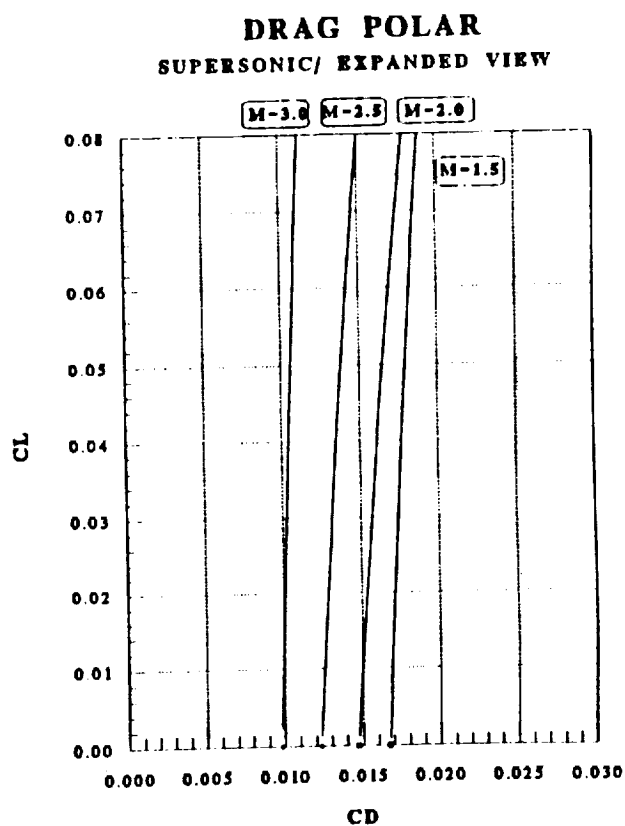
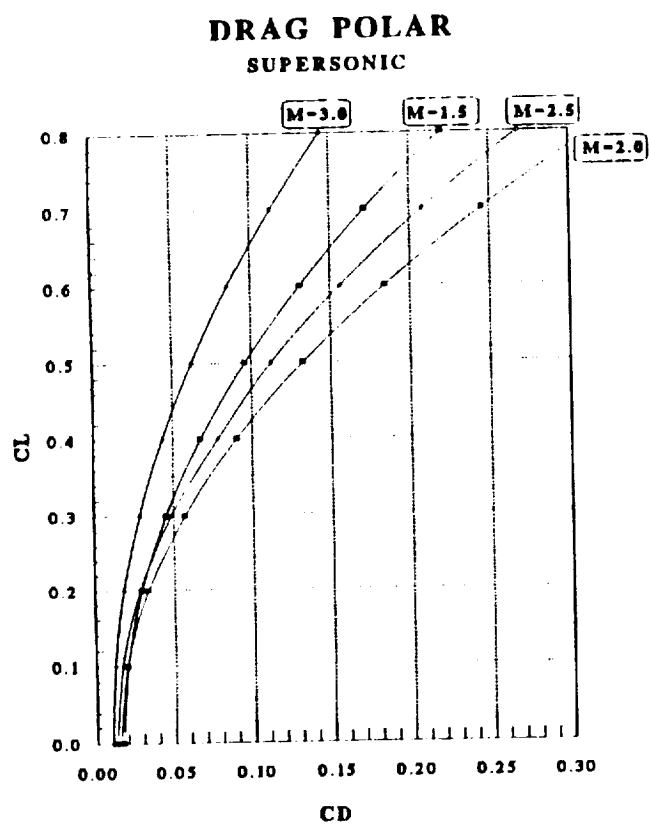
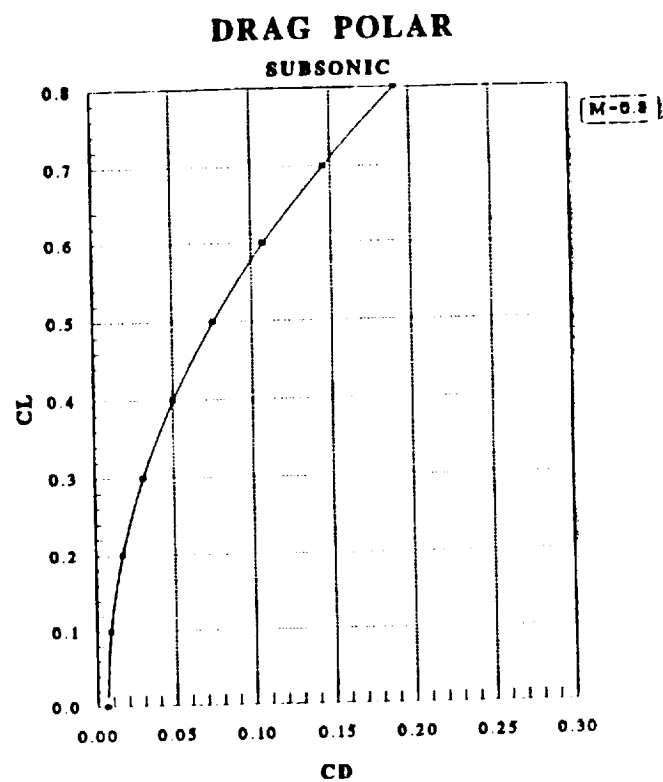
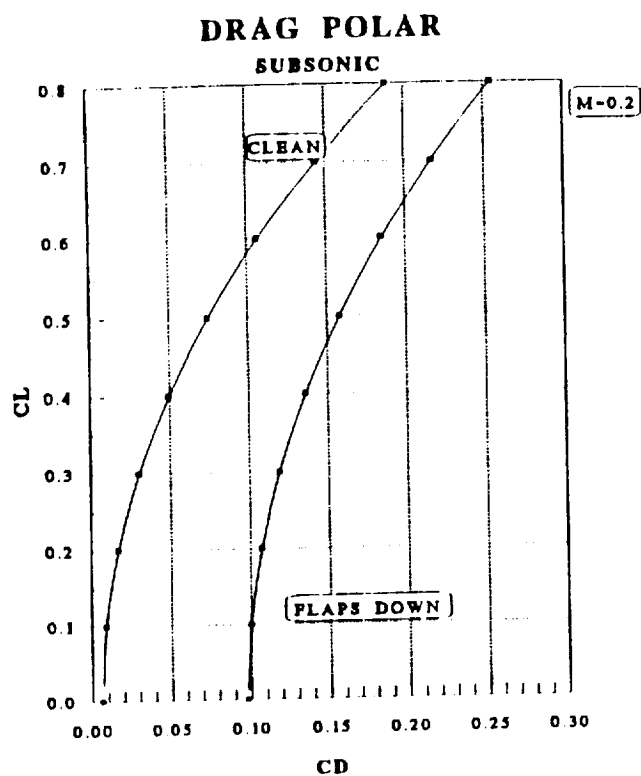


**FIGURE V.2: Longbow Drag Polars**

#### D. AREA RULING

The cross-sectional area of the Longbow was plotted to determine its similarity to the ideal Sears-Haack curves presented in Roskam (chapter 4) and Nelson. The initial comparison indicated the aft area of the Longbow should be reduced, yet the idealized waverider design did not lend itself to simple modification. A closer fit to the Sears-Haack type 2 curve was possible by locating the engine intake ducts and exhaust nozzles further forward, and by varying the taper of the aft underbelly. This, in turn, helped reduce the fuselage wave drag.  $CD_0$  was reduced by 16 percent at 1.5M, and 9 percent at 3.0M. Figure V.3 displays this comparison of the ideal area curve to the initial and final Longbow configurations.

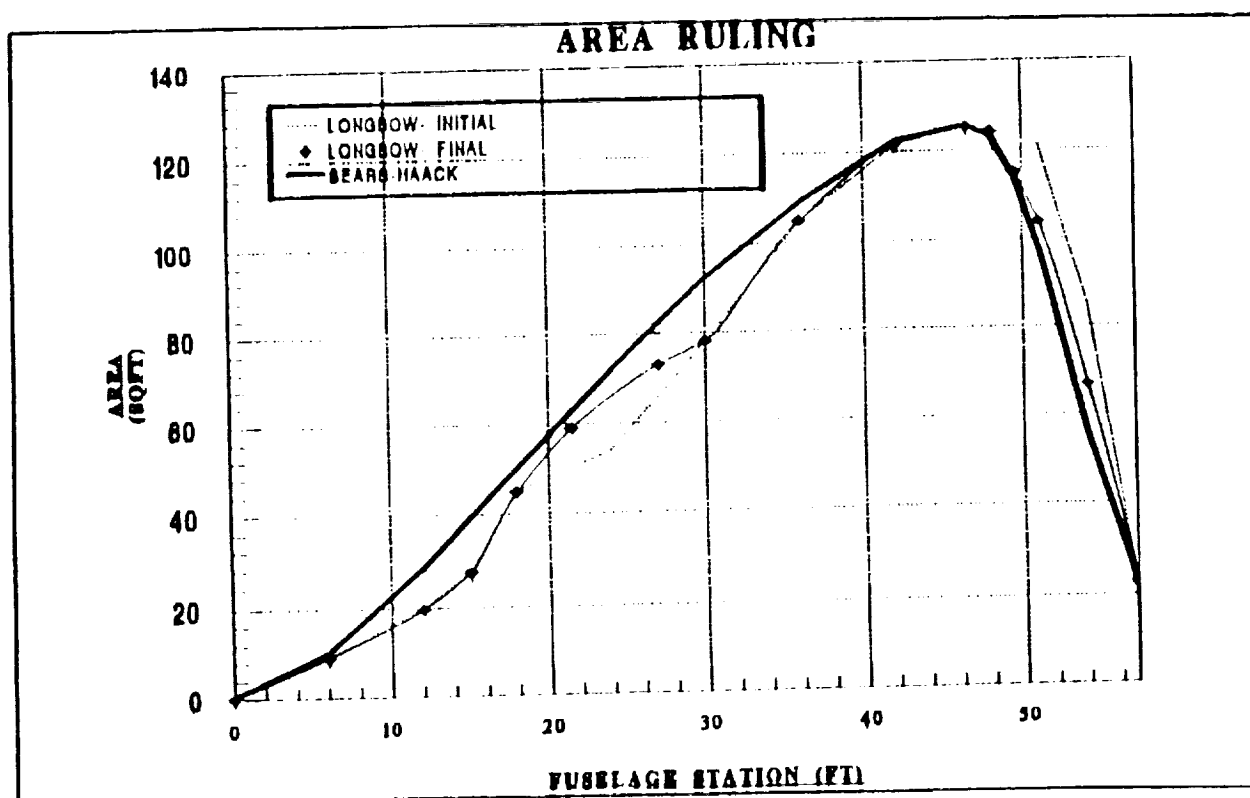


FIGURE V.3: Area Ruling Comparison



## E. SONIC BOOM CHARACTERISTICS

Sonic boom Characteristics for the Longbow were estimated utilizing procedures contained in NASA Technical Paper 1122, "Simplified Sonic-Boom Prediction". As shown on Figure V.4, the analysis was done for Mach numbers ranging from 1.5 to 3.0 and altitudes from 4 to 20 km (approximately 13000 to 65000 ft). Pressure at ground level was assumed to be sea level standard day and the weight used in the analysis was maximum gross weight, to give the worst case. Results were compared with an RFP limit of 1 psf ( $\approx 48\text{Pa}$ ), and showed that at a cruise Mach number of 3 or below at the expected cruise altitude of 50,000 ft, the Longbow will meet the sonic boom requirements.

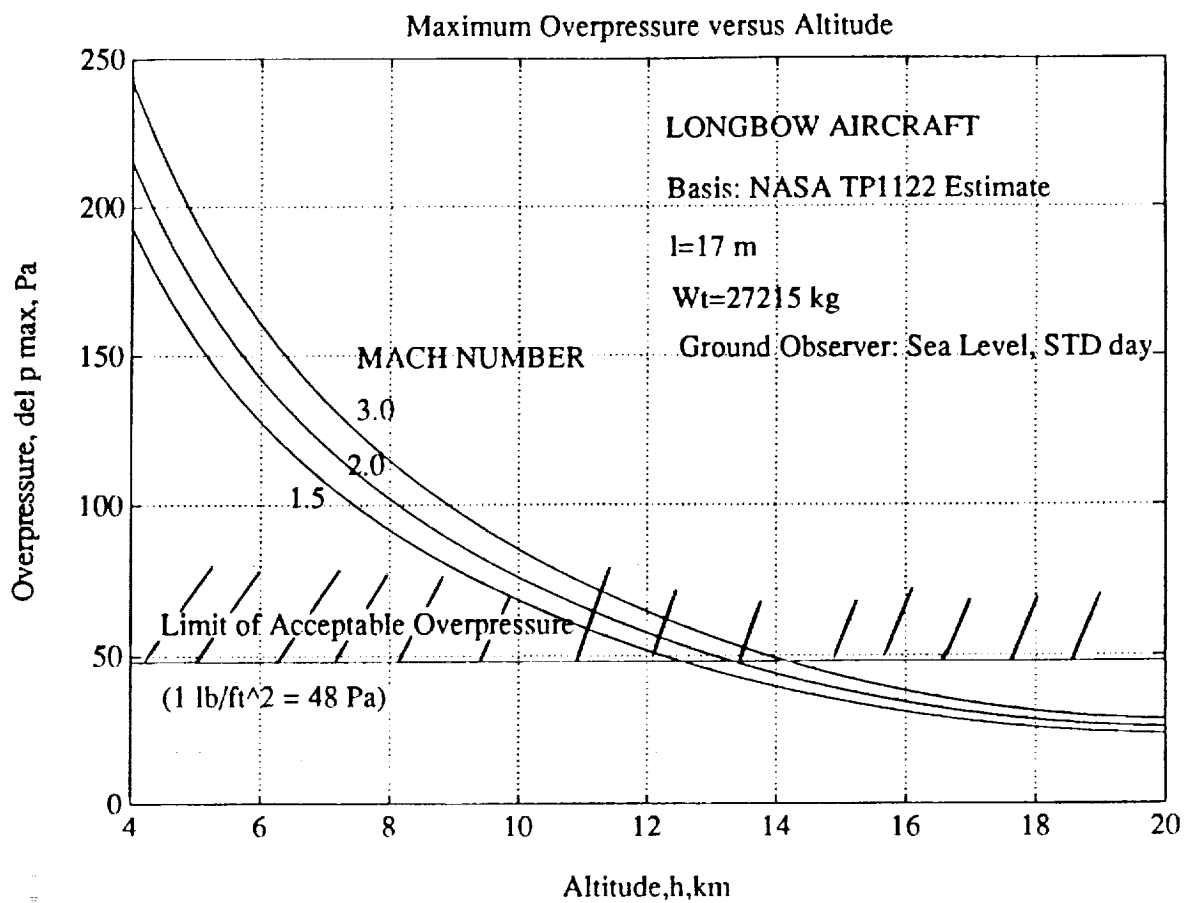


Figure V.4

LONGBOW Sonic Boom Characteristics

## VI. PROPULSION

### A. REQUIREMENTS

- 1500 nm mission radius
- 1+45 airborne cycle time
- Single engine wave off capability
- Mach 3 cruise capability (preferably without afterburner)

### B. CYCLE DESIGN

A current technology level was chosen for the engine design study. Current capabilities in high temperature-high strength materials, engine controls, and transonic compressor design were used in the analysis. The specific capabilities assumed were a turbine inlet temperature of 3200 deg. R, an afterburner temperature of 3700 deg. R, a maximum compressor polytropic efficiency of 0.9, a maximum total pressure ratio per compressor stage of 1.8, and a maximum uncooled compressor blade temperature of 1700 deg. R.

Most design compromises were dictated by the requirement for a single engine type to operate both in the low altitude, slow speed, and the high altitude, high mach regimes. The first choice was the engine cycle to be employed. Specific fuel consumption and specific thrust were compared for turbojet, turbojet with afterburner, and ramjet cycles as shown in Figures III.1 and III.2. The pure ramjet cycle was discarded due to the lack of slow speed

capability. The large disparity in specific thrust between the turbojet and turbojet with afterburner favored the afterburner. The size requirement for the non-afterburning turbojet was prohibitive in the high supersonic flight regime.

A variable cycle engine was considered for the high supersonic region of the envelope. A variable bypass cycle could allow (in theory) higher compressor pressure ratios to be used for lower altitude and mach number operation, with a corresponding increase in efficiency. The bypass ratio would be increased at cruise conditions, and the core pressure ratio reduced due to the material limitations. It would operate in essence as a ramjet in the cruise configuration.

Problems were found in attempting to mix the core and bypass air at the afterburner inlet however. The viscous losses due to mixing induced turbulence, along with large differences in the core and bypass air total pressure created a very restricted operating regime. These factors forced the abandonment of this configuration in favor of the afterburning turbojet. The small loss of efficiency in the low altitude/airspeed regime due to a low compressor pressure ratio was offset by a simpler and lighter design for the simple turbojet.

The gas turbine cycle analysis program ONX/OFFX (Mattingly) was used to optimize the cycle pressure ratio. As the aircraft must fly at mach numbers as high as 3, the total pressure ratio in the compressor must be low enough to prevent temperatures higher than 1700 deg R from occurring in the last stages. This restricts the compressor pressure ratio at mach 3 cruise from being higher

than 5. The optimum pressure ratio of 6 (at mach 3 and 50000 ft) yields an unacceptable temperature in the compressor, and must be reduced with a slight loss in specific fuel consumption. Using the drag coefficients determined for the subsonic, transonic, and supersonic regimes, the thrust required was calculated for the flight envelope of the proposed aircraft. Different design points were chosen, with the thrust available then being calculated off design over the aircraft's envelope. These engine choices were then compared to determine the point of smallest excess thrust in the operating range. The design point was chosen to minimize the engine size and weight while maintaining the required operational capability. A design point of 40,000 ft and Mach 2.0 was used for the final engine sizing. The region of supersonic acceleration from mach 1.5 to cruise speed at 50,000 ft provided the smallest margin of excess thrust in the flight envelope. The engine size was then determined to provide the required amount of excess thrust for this situation (see Figure V.1)

With the available thrust known, single engine climb rates were calculated to ensure an adequate waveoff capability (see Figure V.2).

Thrust specific fuel consumption and specific thrust were also determined for use in the final performance calculations (see Figures V.3 and V.4)

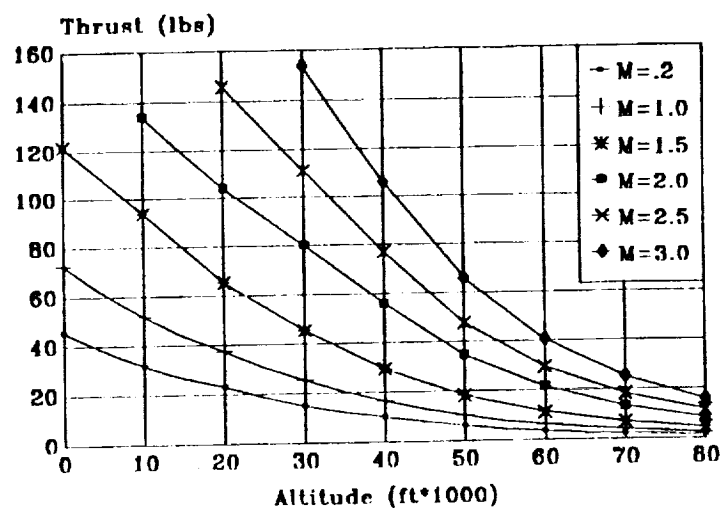
## **C. COMPONENT DESIGN**

### **1. INLET DESIGN**

The strict requirement for high total pressure recovery while cruising at mach three immediately ruled out any type of fixed

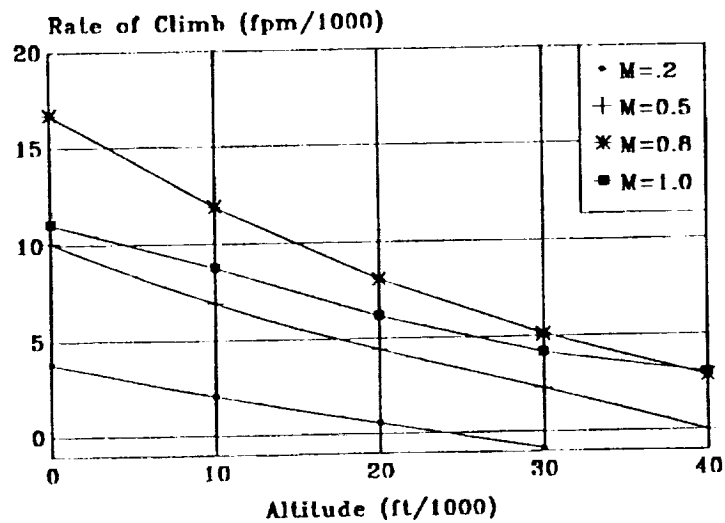
## Thrust vs Altitude and Mach Number

(Based on 2 engines)



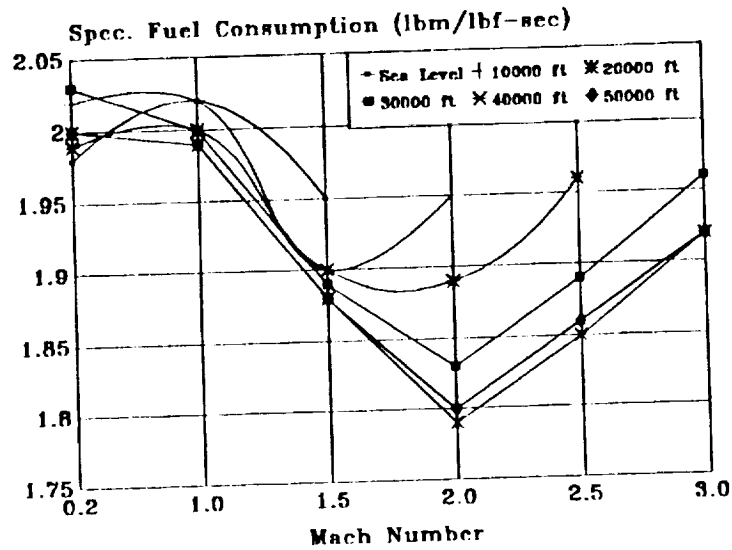
Thrust Available vs Altitude/Mach Number  
Figure V.1

## Single Engine Rate of Climb



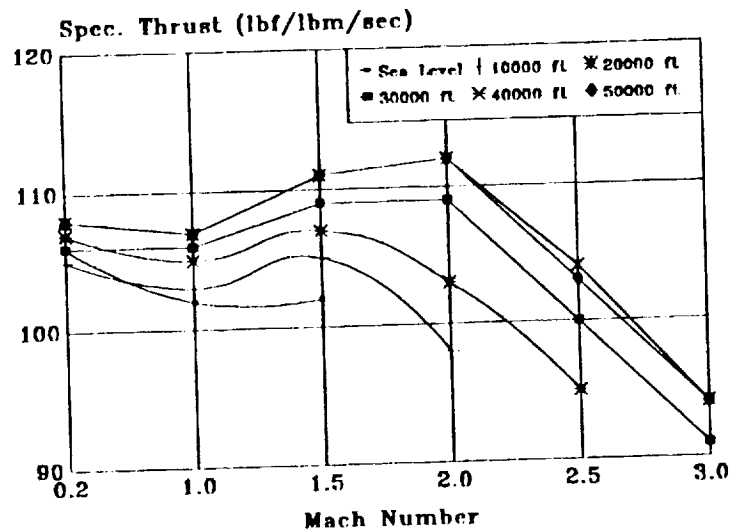
Single Engine Climb Capability  
Figure V.2

### Specific Fuel Consumption vs Mach Number/Altitude



Specific Fuel Consumption vs Mach and Altitude  
Figure V.3

### Specific Thrust vs Mach Number/Altitude



Specific Thrust vs Mach/Altitude  
Figure V.4

geometry inlet. A high priority for the inlet design was to minimize the disruption of the flow on the waveriders lower surface. The military requirement for total pressure recovery at mach 3 dictated no less than a four shock inlet system as shown in Figure V.6. A four shock external compression inlet would intrude a great distance into the flow both to turn the flow the required amount outside of the cowl for compression, and to turn it back towards the axial direction in the subsonic diffuser. This left only the options of planar or axisymmetric mixed compression inlets. Though the pressure recovery through a conical shock inlet is slightly greater than a planar inlet, the added mechanical complexity for independently movable conical ramps (required for good performance over a wide range of mach numbers), in addition to greater difficulty to matching half-cone inlets to a largely planar waverider lower surface forced the choice of planar inlets.

The final configuration--Figure V.8--of the inlet system consists of two external movable ramps against the aircraft's lower surface, and a movable cowl lip. The inlet ramps schedule according to both altitude and mach number, maximizing pressure recovery and placing the shocks on the cowl lip (mach number permitting). The cowl lip will move vertically, also scheduling according to both altitude and mach number, adjusting the inlet capture area to provide the required engine mass flow for that condition. The ramp schedules for 40,000 and 50,000 feet are shown in Figures V.5 and V.6. The inlet is designed to operate slightly supercritically in supersonic flight, providing a small buffer to prevent unstating the inlet. Since the inlet is mixed



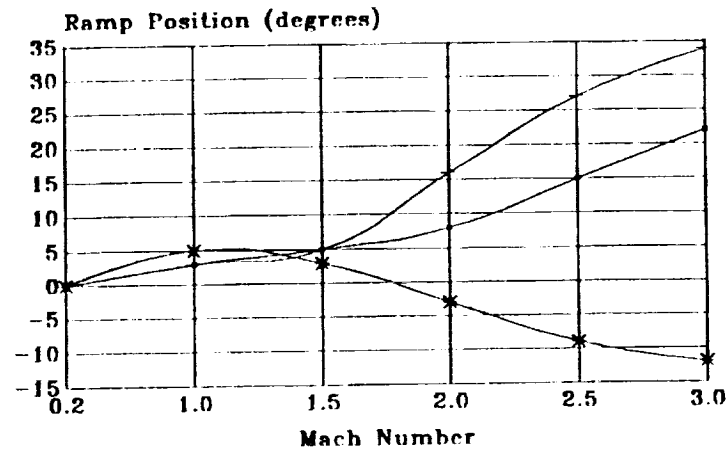
compression, with the normal shock inside the cowl, bypass air ducts will be provided in the subsonic diffuser. These doors will program with altitude, mach number, and engine setting to remove the excess mass flow for lower power settings, and preventing the inlet from unstating. Boundary layer bleed will also be used (as shown on Figure V.8, preventing shock-induced boundary layer separation in the inlet. Both slot and porous wall methods will be employed to low energy boundary layer fluid in those regions.

## 2. COMPRESSOR DESIGN

A twin spool, 5 stage transonic axial compressor will be used to provide a maximum pressure ratio of 13 for low altitude, slow speed operations, as shown in Figure V.7. The twin spool design will allow the compressor to more easily adjust to the lower pressure ratios required by the high altitude, high mach flight regime. The low pressure compressor will consist of two stages, and be driven by a single stage turbine. These two stages will produce a maximum pressure ratio of 1.9, while the three stage high pressure compressor will only provide a stage pressure ratio of 1.6. This is due to larger expected tip losses in the smaller high pressure compressor stages. Inlet guide vanes will be used in advance of the low pressure compressor, and variable stators will be necessary for every stage of both the low and high pressure compressor. This will increase the engine's complexity, but is required for the large range of pressure ratios which must be delivered.

# Inlet Ramp Position vs Mach Number (50000 ft)

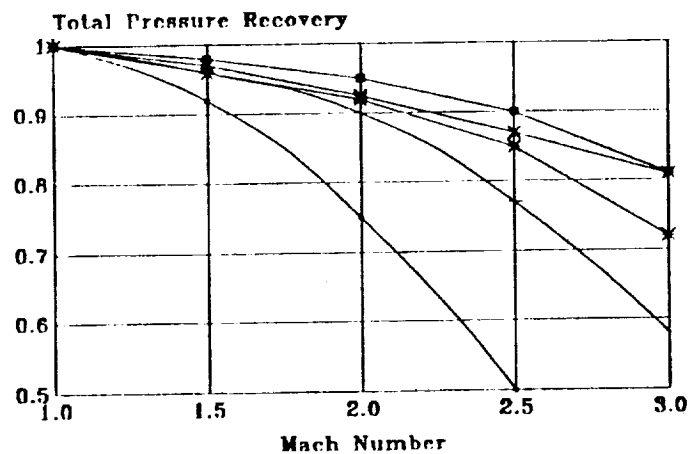
- Ramp 1 + Ramp 2 \* Cowl lip



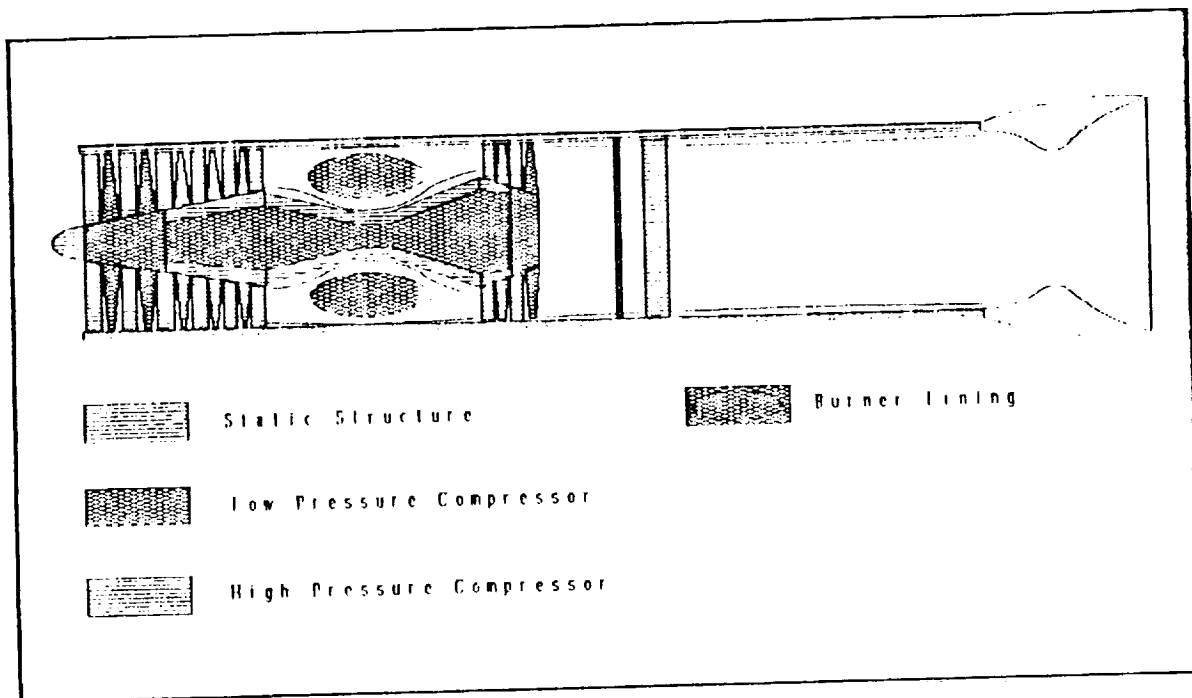
Inlet Ramp Position Schedule vs Mach - 50,000 ft.  
Figure V.5

# Total Pressure Recovery vs Mach Number

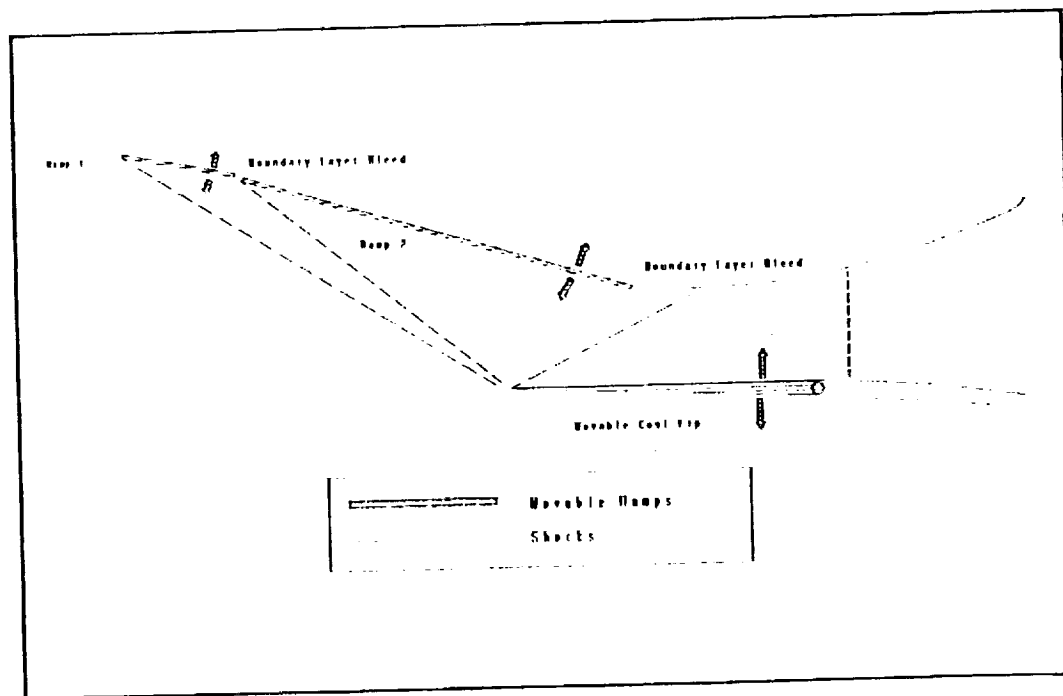
- Normal Shock + 2 Shock \* 3 Shock ■ 4 Shock × MIL Spec



Total Pressure Recovery vs Mach  
Figure V.6



Engine Schematic  
Figure V.7



Inlet Schematic  
Figure V.8

### **C. BURNER DESIGN**

The burner will consist of a annular combustion chamber, with both primary and secondary fuel injectors. This will both improve the efficiency of the combustor, but also lessen the severity of the cooling required for the combustor walls. The fuel injectors will be sized to provide the optimum atomization at the supersonic cruise condition, as approximately 70% of the aircraft fuel is burned in this flight regime.

### **D. TURBINE DESIGN**

A two stage turbine will be used, with one stage to power each compressor spool. 50% reaction turbines will be used, due to both the improved efficiency of the design (over impulse turbines) and the lower total power requirement of the compressor with the reasonably modest pressure ratios. The reaction turbine will have the added benefit of providing an opposing load to the forward thrust of the compressor, thereby reducing the bearing loads, and allowing smaller thrust bearings on the compressor spools. Both turbines will be fixed area designs, and will operate choked over the engine envelope.

### **E. AFTERBURNER**

The afterburner will be a reasonably standard design, with a separate afterburner fuel pump and throttle valve to meter the afterburner fuel. A spark igniter will be employed for light-off, and concentric flame holders will provide adequate flame stabilization during operation.

## **F. NOZZLE**

The nozzle will be a variable area axisymmetric configuration, with a maximum exit diameter of 4 feet. This will provide a loss of thrust at high altitude, but is necessary for the reduction of boattail drag in the cruise configuration. The nozzle will program during both afterburning and non-afterburning operation to maintain the highest allowable compressor pressure ratio for a given flight condition.

## VII. STABILITY AND CONTROL

### A. INTRODUCTION

#### 1. CONTROL SURFACES

As shown in Figures IV.4 and IV.5, the aircraft is controlled in pitch at all speeds by a pair of all-moving stabilators located at the outboard trailing edge of the waverider body. Roll control at slow speeds (wings forward) is accomplished through a combination of conventional 25% span ailerons, 85% span spoilers (to reduce adverse yaw) and the above mentioned stabilators. At high speeds with the wings swept, the stabilators alone provide roll control at all speeds. Yaw is controlled by a pair of all-moving vertical surfaces canted inward to reduce roll due to rudder. Pilot inputs to these surfaces are implemented through stick and rudder pedal inputs through a quad-redundant flight control computer.

#### 2. GENERAL

A detailed static and dynamic stability analysis was conducted on the LONGBOW both in the Mach 0.2 powered approach (PA) configuration (wings forward, gear and flaps extended) and the Mach 3.0 cruise (CR) configuration (wings swept, clean) conditions. The USAF Stability and Control DATCOM and Etkin's text were used to estimate nondimensional derivatives, which were then converted to dimensional derivatives for the dynamic analysis using MATLAB. Table VII.1 shows the derivatives. Stability augmentation was then applied when necessary to ensure satisfaction of requirements delineated in MIL-F-8785C. Through stability augmentation, LONGBOW met or exceeded all static and dynamic stability requirements.

VALUE	Longbow (M=0.2)	Longbow (M=3.0)
$X_u$ (1/sec)	-0.0617	-0.0028
$X_\alpha$ (ft/sec <sup>2</sup> )	-0.193	-0.011
$\theta_0$ (deg)	0	0
$Z_u$ (1/sec)	-0.234	-0.001
$Z_\alpha$ (ft/sec <sup>2</sup> )	-250.0	-105.0
$Z_{\dot{\alpha}}$ (ft/sec)	-0.0021	-0.22
$Z_q$ (ft/sec)	-2.44	0
$M_u$ (1/ft-sec)	0.0009	0.0002
$M_q$ (1/sec)	-0.25	-0.353
$M_\alpha$ (1/sec <sup>2</sup> )	1.05	-4.23
$M_{\dot{\alpha}}$ (1/sec)	0.0007	-0.00009
$X_{\delta e}$ (ft/sec <sup>2</sup> )	0	0
$Z_{\delta e}$ (ft/sec <sup>2</sup> )	-16.32	-20.6
$M_{\delta e}$ (1/sec <sup>2</sup> )	-1.478	-2.51
$U$ (ft/sec)	236.0	2903.8
$Y_\beta$ (ft/sec <sup>2</sup> )	-1.522	-2.01
$Y_p$ (ft/sec)	0	0
$Y_r$ (ft/sec)	0	0
$L_\beta$ (1/sec <sup>2</sup> )	-5.72	-60.5
$L_p$ (1/sec)	-1.57	-0.98
$L_r$ (1/sec)	0.564	0.0839
$N_\beta$ (1/sec <sup>2</sup> )	1.76	3.02
$N_p$ (1/sec)	0.036	0.0098
$N_r$ (1/sec)	-0.255	-0.182
$I_{xx}$ (slug-ft <sup>2</sup> )	149576	100966
$I_{zz}$ (slug-ft <sup>2</sup> )	363117	286729
$I_{xz}$ (slug-ft <sup>2</sup> )	15945	11660
$Y_{\delta r}$ (ft/sec <sup>2</sup> )	9.8	17.2
$L_{\delta r}$ (1/sec <sup>2</sup> )	5.23	6.01
$N_{\delta r}$ (1/sec <sup>2</sup> )	-4.89	-5.2
$Y_{\delta a}$ (ft/sec <sup>2</sup> )	-0.97	-0.087
$L_{\delta a}$ (1/sec <sup>2</sup> )	10.5	11.3
$N_{\delta a}$ (1/sec <sup>2</sup> )	0.416	0.28

Table VII.1  
Longbow Stability and Control Values

## B. STATIC STABILITY

Dimensional derivatives from Table VII.1 were converted to nondimensional derivatives for longitudinal static stability analysis. This analysis revealed that, through constraints brought about by the waverider shape, the aircraft never achieves a positive static margin in the PA configuration. Both during takeoff and landing, the center of gravity remains behind the neutral point, yielding a positive  $Cm_0$  and a positive  $Cm_q$ . As fuel is burned, the slope of the  $Cm$  versus  $\alpha$  flattens out but never goes negative, making the aircraft statically unstable longitudinally as seen in Figure VII.1. In the CR configuration, LONGBOW has a negative  $Cm_0$ , but has a  $Cm_q$  of zero. This is due to it being considered a tailless delta wing during analysis. Figure VII.2 shows the effect of upward (negative) stabilator deflection on moving  $Cm_0$  into the positive range and thus accomplishing the required "reflex" needed for tailless aircraft and making it trimmable. In the wings aft, delta configuration the aircraft maintained a positive static margin throughout the range of possible centers of gravity.

Laterally, the aircraft produced stable derivatives for both configurations and speeds. The required negative values of  $L_\beta$  and positive values of  $N_\beta$  are shown in Table VII.1.

## C. DYNAMIC STABILITY

### 1. INTRODUCTION

Dynamic simulation and analysis was completed using MATLAB and assumes small perturbation theory. Additional assumptions included: rigid body motion (no aeroelastic effects), linearized



# **Cm vs. Alpha (Wings Forward) Effect of CG Travel**

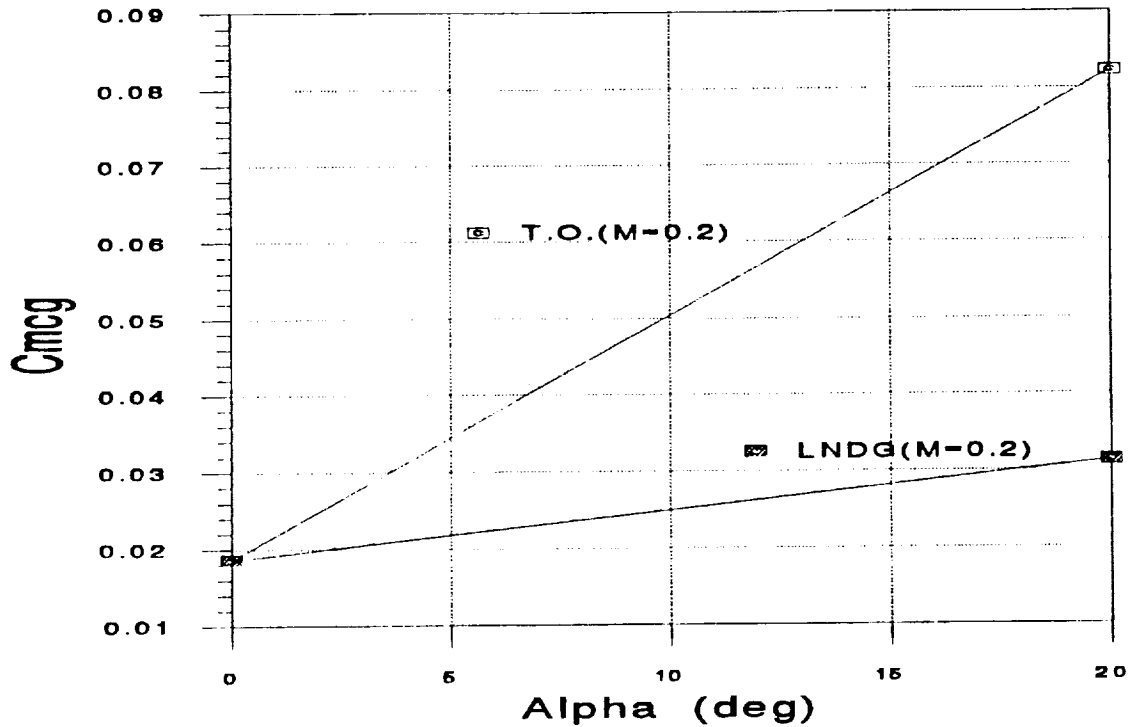


Figure VII.1  
 LONGBOW Static Longitudinal Stability CONFIGURATION PA

# **$C_{m\alpha}$ Curve Shift due to Elevon Deflection (Mach=3.0)**

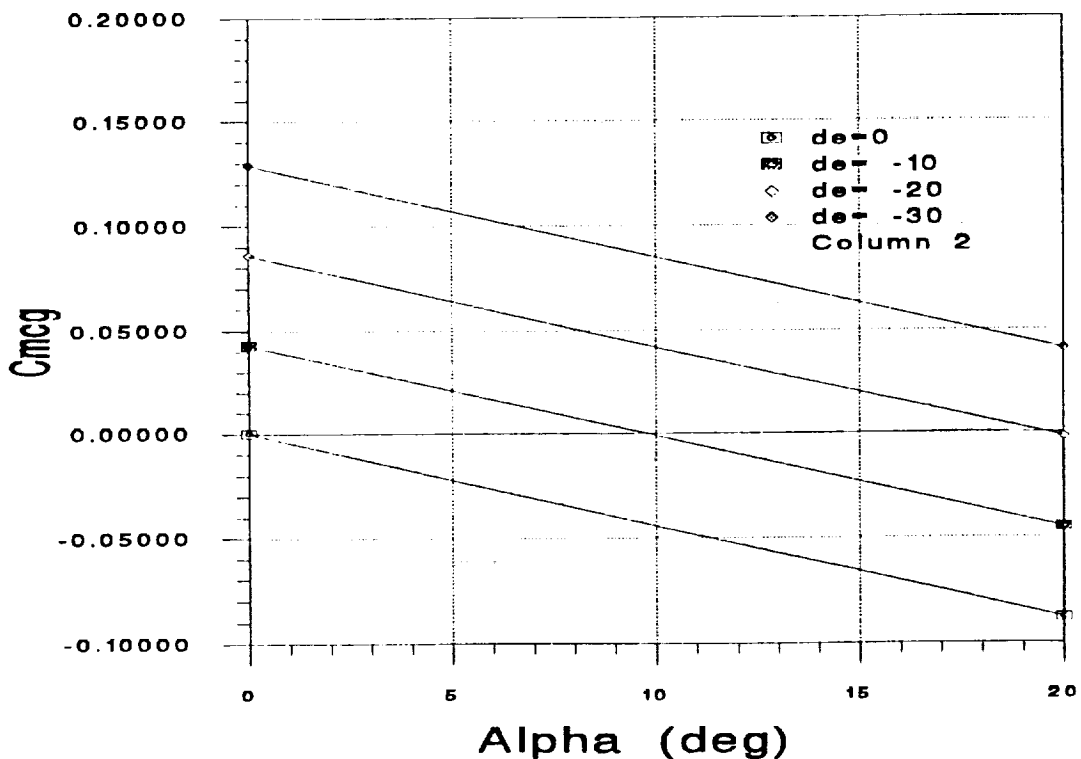


Figure VII.  
 LONGBOW Static Longitudinal Stability CONFIGURATION CR

equations of motion, time-invariant transfer functions, second order dynamics, and no coupling between the longitudinal and lateral/directional equations of motion. Controllability was checked and in each case the dynamic response of the airplane was found to be controllable. Eigenvalues from the unaugmented equations of motion were analyzed for compliance with MIL-F-8785C (Flying Qualities of Piloted Airplanes), whose paragraphs will be referred to in this section of the report. Augmentation was performed when necessary to satisfactorily place eigenvalues and control was implemented using state-variable feedback techniques. The dimensional derivatives and other constants used in the dynamic analysis are listed in Table VII.1.

## **2. LONGITUDINAL--MACH=0.2, PA CONFIGURATION**

Analysis of the longitudinal "plant" using state-variable analysis and evaluation of the resulting open loop poles showed a failure of paragraphs 3.2.2.1.1 and 3.2.2.1.2 in that the open loop behavior was divergent. The classical pole placement technique was utilized to make the system respond as a classic 4th order longitudinal plant--i.e. exhibit short period and phugoid modes. Table VII.2 delineates open and closed loop poles, the gain required to achieve the closed loop poles, and closed loop specification compliance. Figure VII.3 shows the open and closed loop poles on the Argand plane. Figure VII.4 shows specification compliance for the augmented short period natural frequency. Figure VII.5 shows the phugoid response to a below trim airspeed input and release. Figure VII.6 shows the unaugmented and augmented short period response to a pitch doublet at about the

Table VII.2  
 LONGBOW LONGITUDINAL DYNAMIC STABILITY AND CONTROL SUMMARY

OPEN LOOP POLES FOR MACH=0.2 CONFIGURATION PA:					
MODE	POLES	DAMPING ( $\zeta$ )	FREQ ( $\omega_n$ )	$\zeta$ SPEC (1)	$\omega_n$ SPEC (2)
Short Period	-1.76 & +0.4207	Divergent	Divergent	Fail (divergent)	Fail (Divergent)
"Phugoid"	-0.0161±0.0596i	0.2601	0.0617 rad/sec	Pass	N/A
CLOSED LOOP POLES FOR MACH=0.2 CONFIGURATION PA (F=[-0.508 -4.217 -2.163 -0.0111])					
Short Period	-2.4+1.8i	0.8	3.0 rad/sec	Pass	Pass
Phugoid	-0.0298±0.1859i	0.1583	0.1882 "	Pass	N/A
OPEN LOOP POLES FOR MACH=3.0 CONFIGURATION CR:					
MODE	POLES	DAMPING ( $\zeta$ )	FREQ ( $\omega_n$ )	$\zeta$ SPEC (1)	$\omega_n$ SPEC (2)
Short Period	-0.1939+2.0504i	0.0941	2.0596 rad/sec	Fail (73%)	Fail (54%)
Phugoid	-0.0022±0.0078i	0.2656	0.0081 "	Pass	N/A
CLOSED LOOP POLES FOR MACH=3.0 CONFIGURATION CR (F=[1.5427 -11.2135 -1.4871 -0.0007])					
Short Period	-2.1+5.3i	0.3684	5.7 rad/sec	Pass	Pass
Phugoid ( same)	-0.0022±0.0078i	0.2656	0.0081 "	Pass	N/A

Notes: (1)  $\zeta$  specifications: Phugoid--para 3.2.1.2; Short period--3.2.2.1.2  
 (2)  $\omega_n$  specifications: Phugoid--n/a; Short period: 3.2.2.1.1 (plots of  $\omega_n$  vs.  $n/\alpha$ )

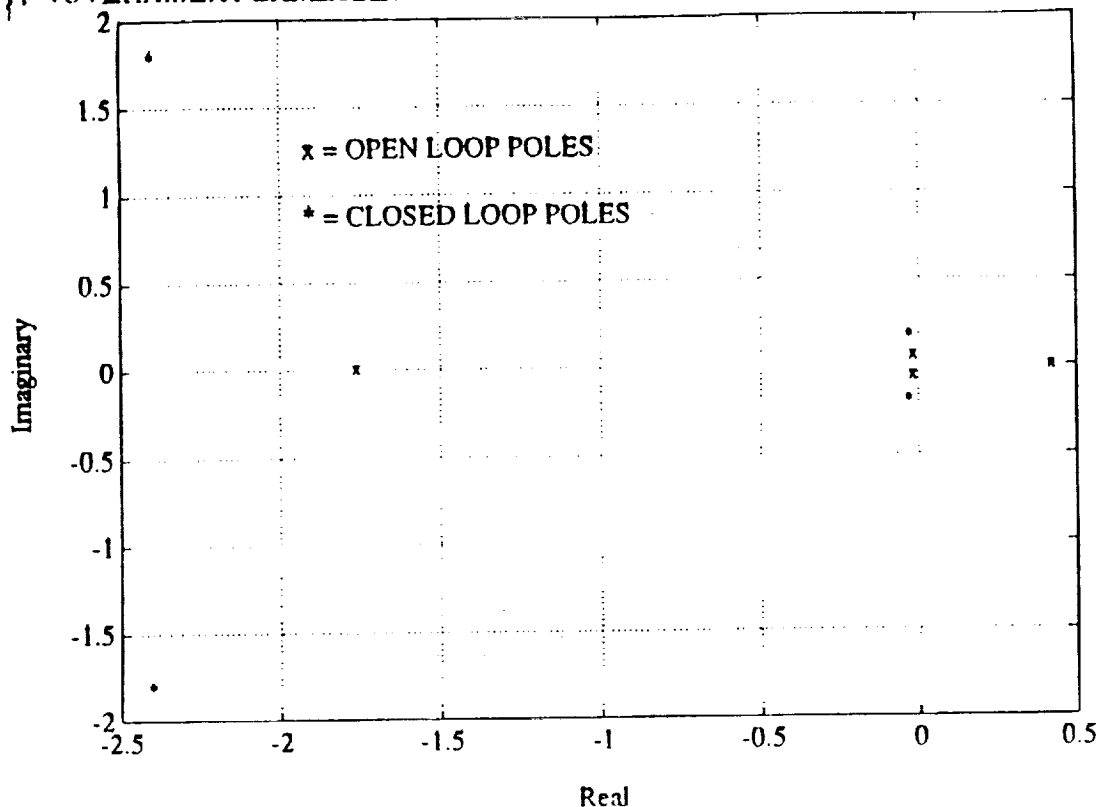


Figure VII.3  
 LONGBOW Longitudinal Pole Locations,  $M=0.2$ , CONFIGURATION PA

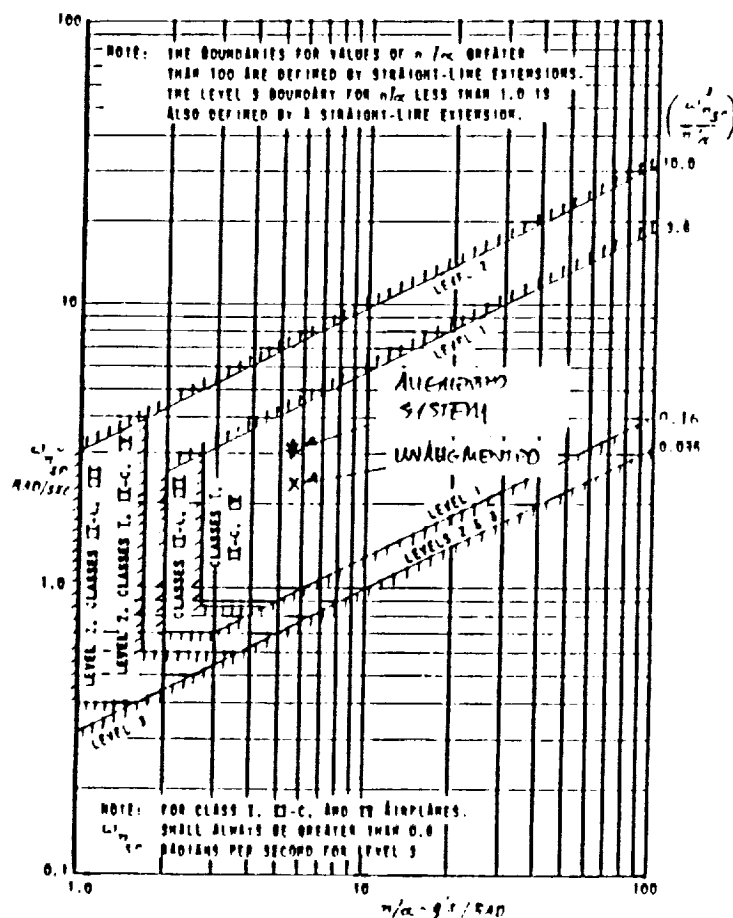


Figure VII.4

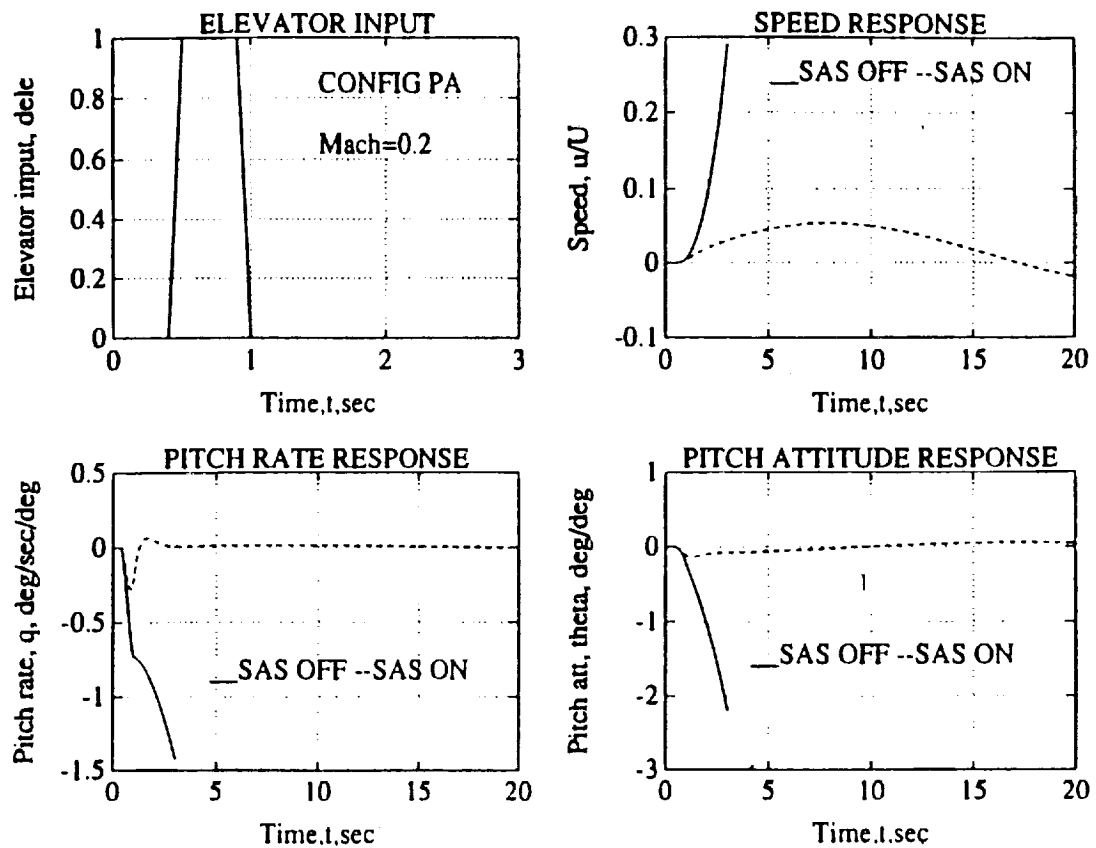


Figure VII.5  
 LONGBOW CONFIGURATION PA Phugoid Response

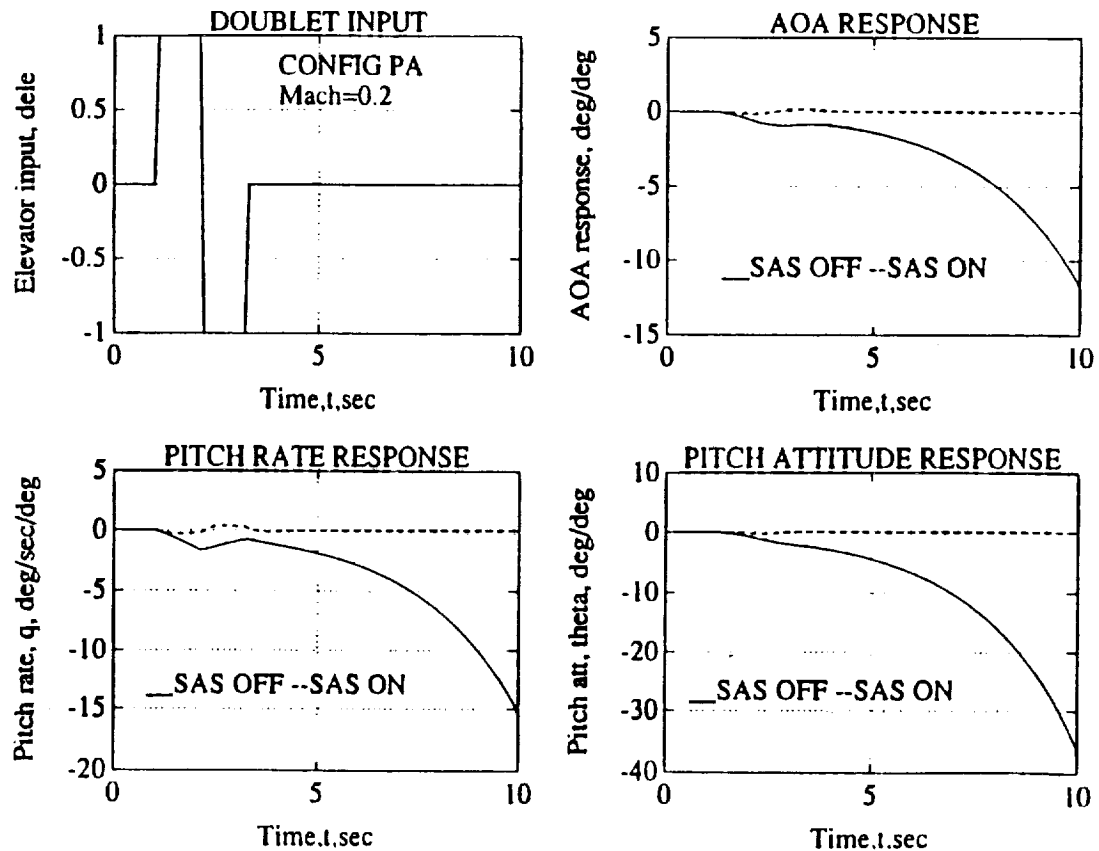


Figure VII.6  
 LONGBOW CONFIGURATION PA Short Period Response

natural frequency.

### 3. LONGITUDINAL--MACH=3.0, CONFIGURATION

Analysis of the longitudinal "plant" at a Mach Number of 3 showed a failure of paragraph 3.2.2.1.2 in that the unaugmented short period damping ratio of 0.094 was 73% below the minimum allowable. In addition, the unaugmented natural frequency was 54% below the minimum allowable, as specified in paragraph 3.2.2.1.1 and shown on Figure VII.7. Pole placement improved the short period damping and frequency, while leaving the long period mode unaffected. Table VII.2 delineates open and closed loop poles, the gain required to achieve the closed loop poles, and specification compliance. Figure VII.8 shows the open and closed loop poles on the Argand plane. Figure VII.9 shows the phugoid response to a below trim airspeed input and release. Figure VII.10 shows the unaugmented and augmented short period response to a pitch doublet at about the natural frequency.

### 4. LATERAL/DIRECTION--GENERAL

The steps in the analysis of the airplane's lateral/directional behavior were as follows:

- 1) The eigenvalues (poles) of the unaugmented plant were calculated. In both cases ( $M=0.2$  and  $M=3.0$ ) the dutch roll damping was below the minimum specified in paragraph 3.3.1.1.

- 2) The open loop (unaugmented) spiral and roll mode poles were evaluated for specification compliance and in both cases were determined to be satisfactory.

- 3) Stability Augmentation System (SAS) gains were then

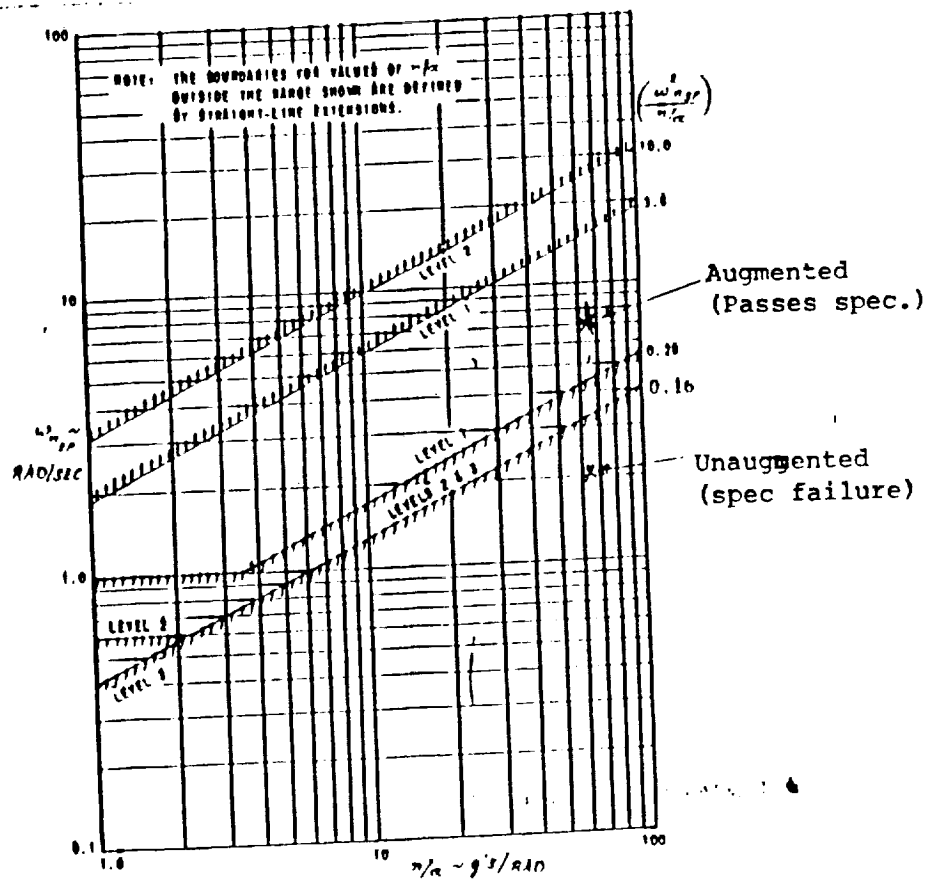


Figure VII.7  
LONGBOW CONFIG CR Short Period Spec Compliance

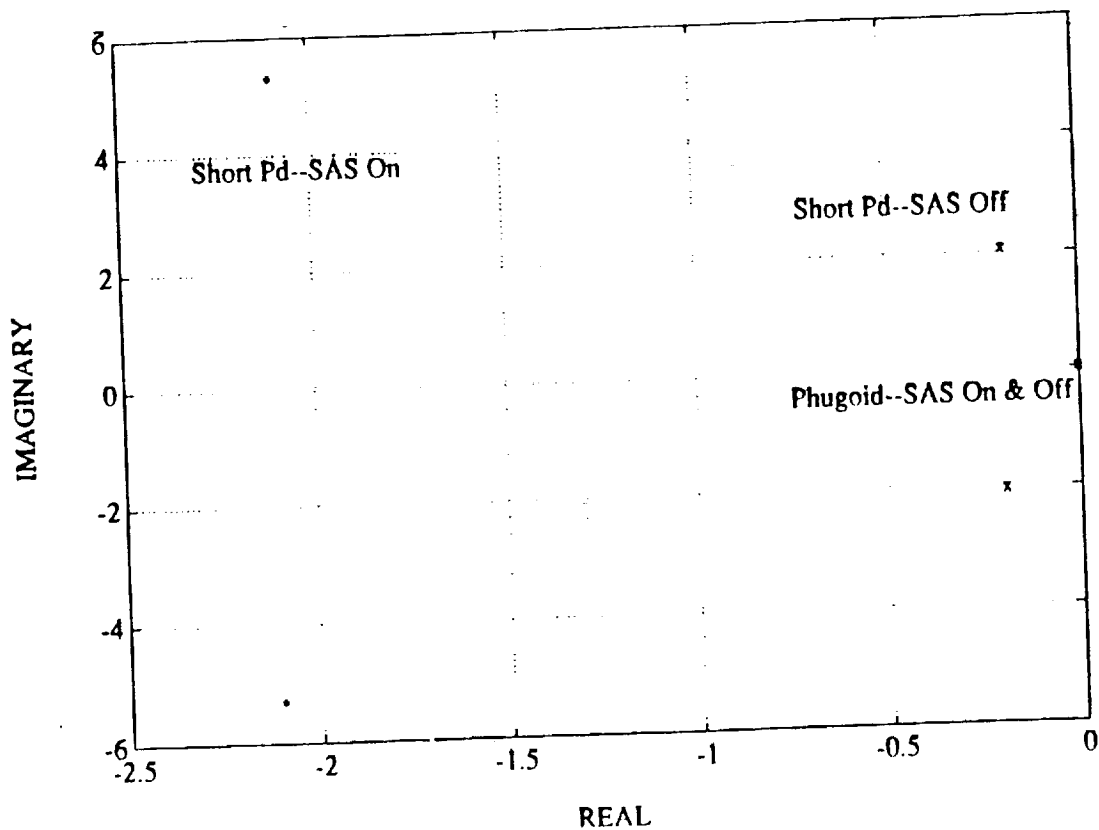


Figure VII.8  
LONGBOW Longitudinal Pole Locations, CONFIGURATION PA (M=3)

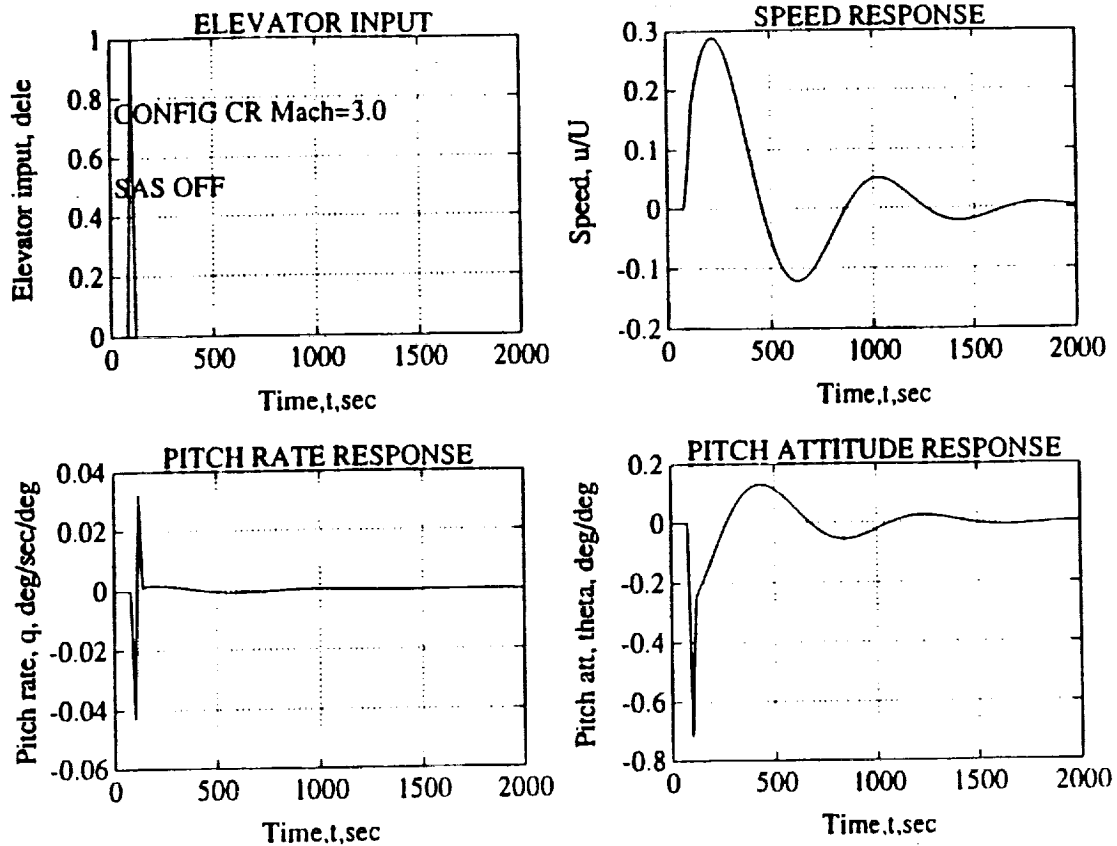


Figure VII.9  
 LONGBOW CONFIGURATION CR Phugoid Response to Step

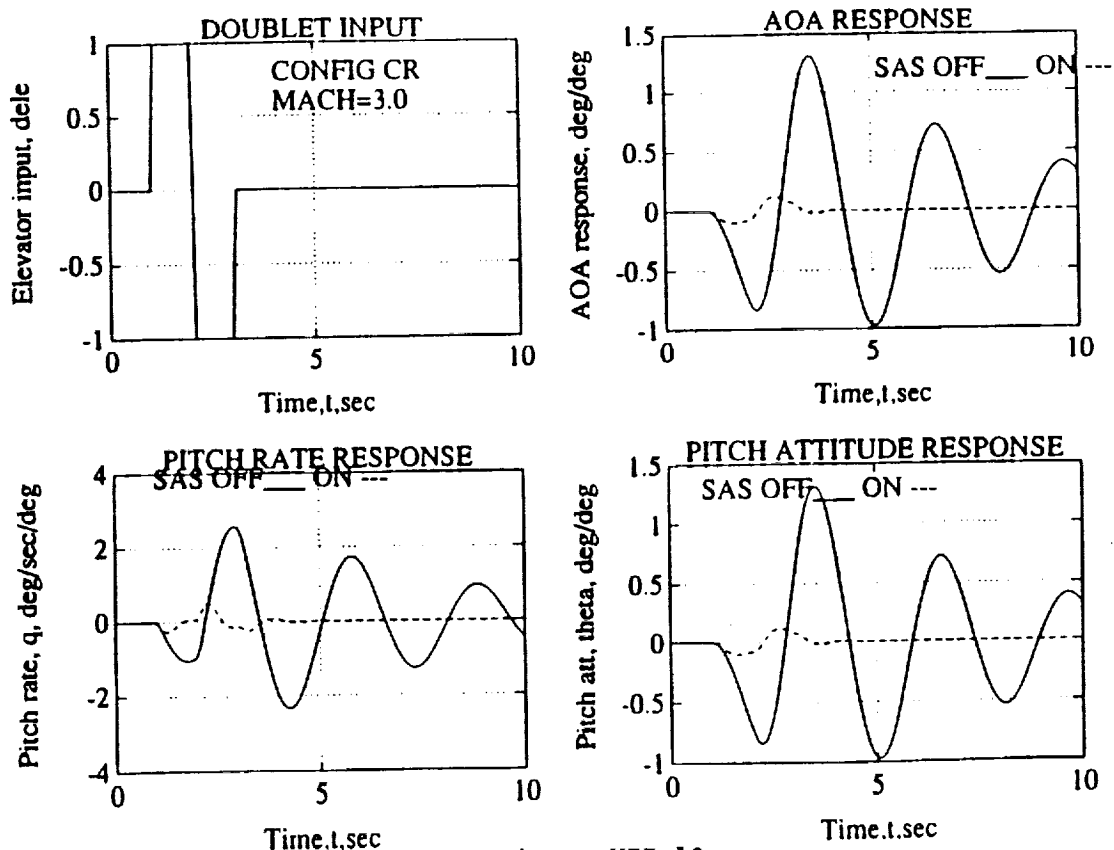


Figure VII.10  
 LONGBOW CONFIGURATION CR Short Period Response to Doublet



calculated for three different SAS implementations: Aileron only feedback; rudder only feedback; and combined aileron and rudder feedback.

4) The input voltage required for each of the above implementations was calculated to select the most efficient method of providing Dutch Roll damping. Figure VII.11 shows the results of this analysis for configurations PA and CR. In both cases the rudder only SAS was selected.

5) Once the rudder only SAS was selected, the response of the system was simulated and eigenvalues calculated to determine specification compliance.

Table VII.3 summarizes the results of the lateral/directional analysis. Plots of pole location, roll response and Dutch Roll response are discussed in the following paragraphs.

#### **5. LATERAL/DIRECTIONAL--MACH=0.2, CONFIGURATION PA**

The open loop poles revealed insufficient Dutch Roll damping. This was corrected using rudder feedback, as shown in Table VII.3. Both open and closed loop poles are displayed in Figure VII.12. Roll performance was estimated based on the roll control power, roll mode time constant and roll damping, and passed the specification, as shown on Figure VII.13. The response of the system to a rudder doublet at about the Dutch Roll natural frequency is shown for SAS off and on cases in Figure VII.14.

#### **6. LATERAL/DIRECTIONAL--MACH=3.0, CONFIGURATION CR**

As in configuration PA, the open loop poles for cruise flight revealed insufficient Dutch Roll damping. This was corrected using rudder feedback, as shown in Table VII.3. Both open and closed

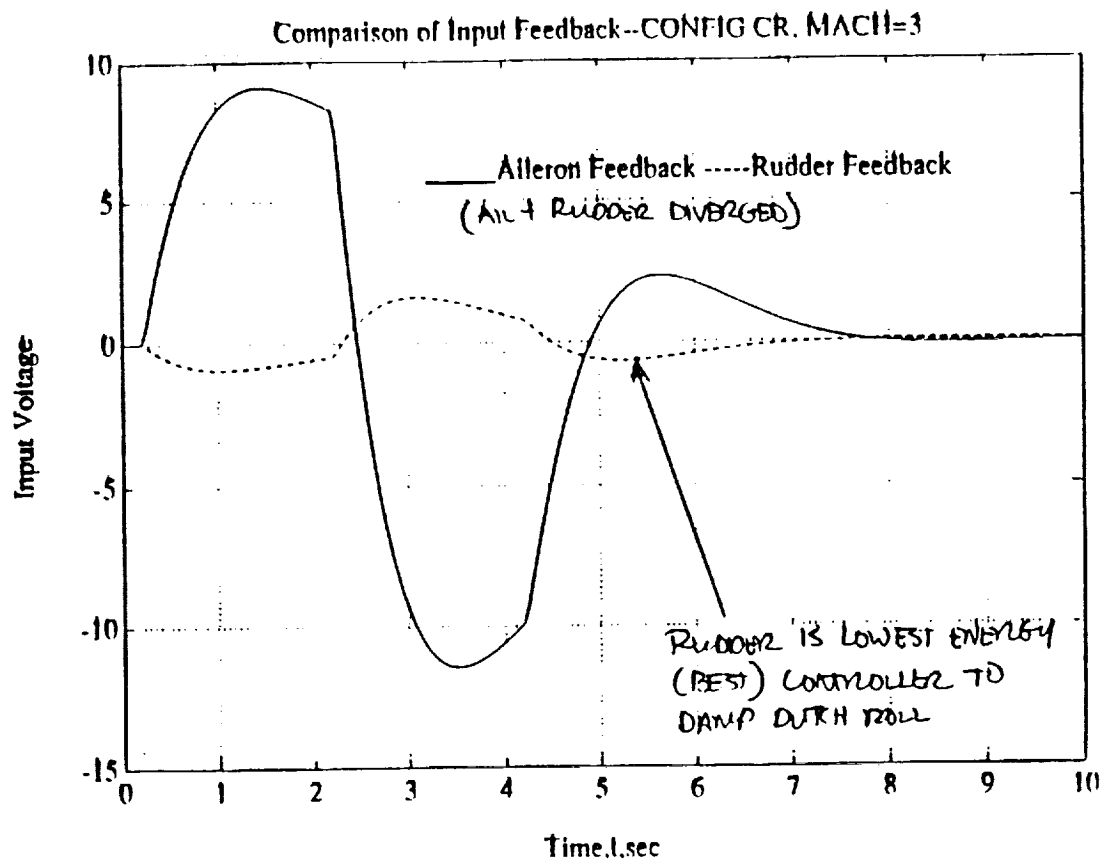
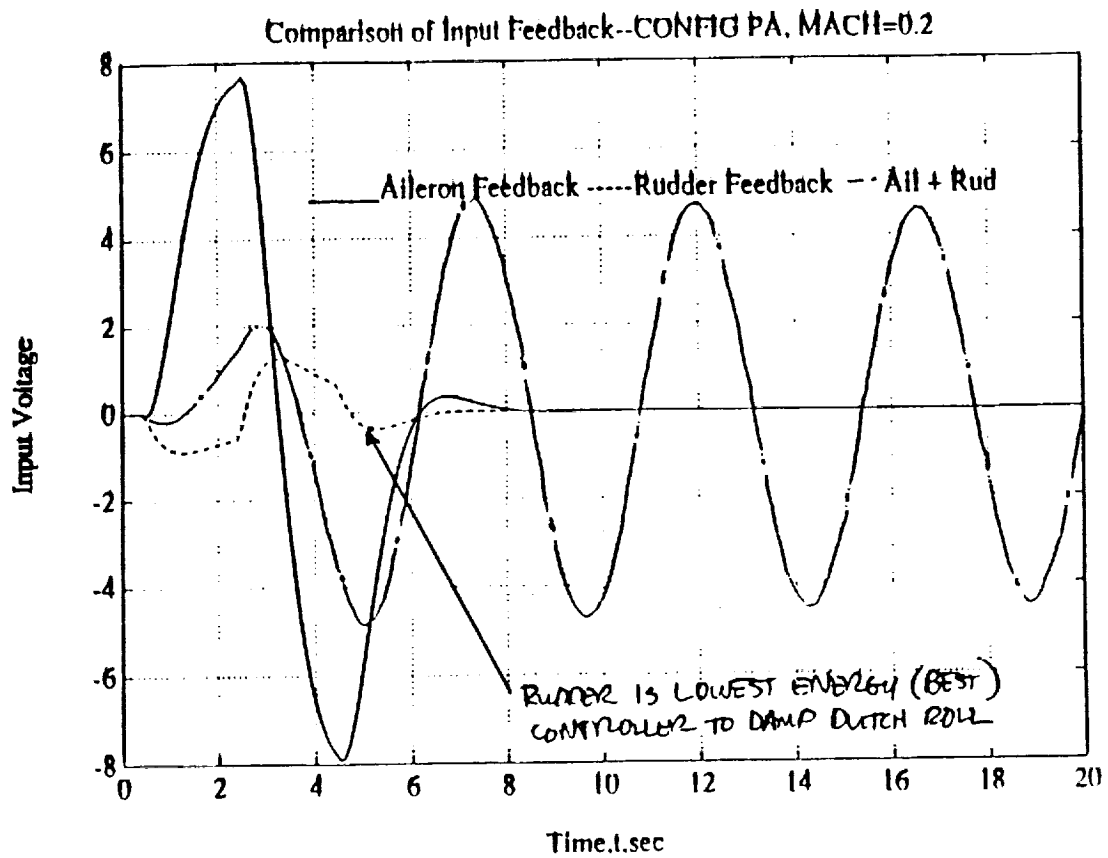


Figure VII.11  
Dutch Roll Augmentation Analysis for Configurations PA and CR

Table VII.3  
LONGBOW LATERAL/DIRECTIONAL DYNAMIC STABILITY AND CONTROL SUMMARY

MACH=0.2, CONFIGURATION PA, UNAUGMENTED SYSTEM		
Mode	RESULTS	SPECIFICATION
Dutch Roll	Poles: $-0.0066 \pm 1.3606i$ $\zeta = 0.0048$ $\omega_n = 1.3606$ rad/sec	$\zeta$ fails (94%) 3.3.1.1 $\omega_n$ passes
Spiral	Pole: $-0.0194$ (positive stability)	passes 3.3.1.3
Roll	Pole: $-1.7788$ $\tau = 0.5622$ sec	$\tau$ passes 3.3.1.2
MACH=0.2 RUDDER FEEDBACK AUGMENTED SYSTEM (F=[0.5308 0.0126 0.07 -0.5837])		
Mode	RESULTS	SPECIFICATION
Dutch Roll	Poles: $-1.414 \pm 1.414i$ $\zeta = 0.707$ $\omega_n = 2.0$ rad/sec	$\zeta$ passes 3.3.1.1 $\omega_n$ passes
Spiral (no change)	Pole: $-0.0194$ (positive stability)	passes 3.3.1.3
Roll (no change)	Pole: $-1.7788$ $\tau = 0.5622$ sec	$\tau$ passes 3.3.1.2
MACH=3.0, CONFIGURATION CR, UNAUGMENTED SYSTEM		
Mode	RESULTS	SPECIFICATION
Dutch Roll	Poles: $+0.3031 \pm 1.3212i$ $\zeta = -0.2294$ $\omega_n = 1.3212$ rad/sec	$\zeta$ fails (negative $\zeta$ ) 3.3.1.1 $\omega_n$ passes
Spiral	Pole: $-0.0397$ (positive stability)	passes 3.3.1.3
Roll	Pole: $-1.7301$ $\tau = 0.578$ sec	$\tau$ passes 3.3.1.2
MACH=3.0 RUDDER FEEDBACK AUGMENTED SYSTEM (F=[0.5121 0.0052 0.0059 -0.5413])		
Mode	RESULTS	SPECIFICATION
Dutch Roll	Poles: $-1.06 \pm 1.06i$ $\zeta = 0.707$ $\omega_n = 1.5$ rad/sec	$\zeta$ passes 3.3.1.1 $\omega_n$ passes
Spiral (no change)	Pole: $-0.0397$ (positive stability)	passes 3.3.1.3
Roll (no change)	Pole: $-1.7301$ $\tau = 0.578$ sec	$\tau$ passes 3.3.1.2

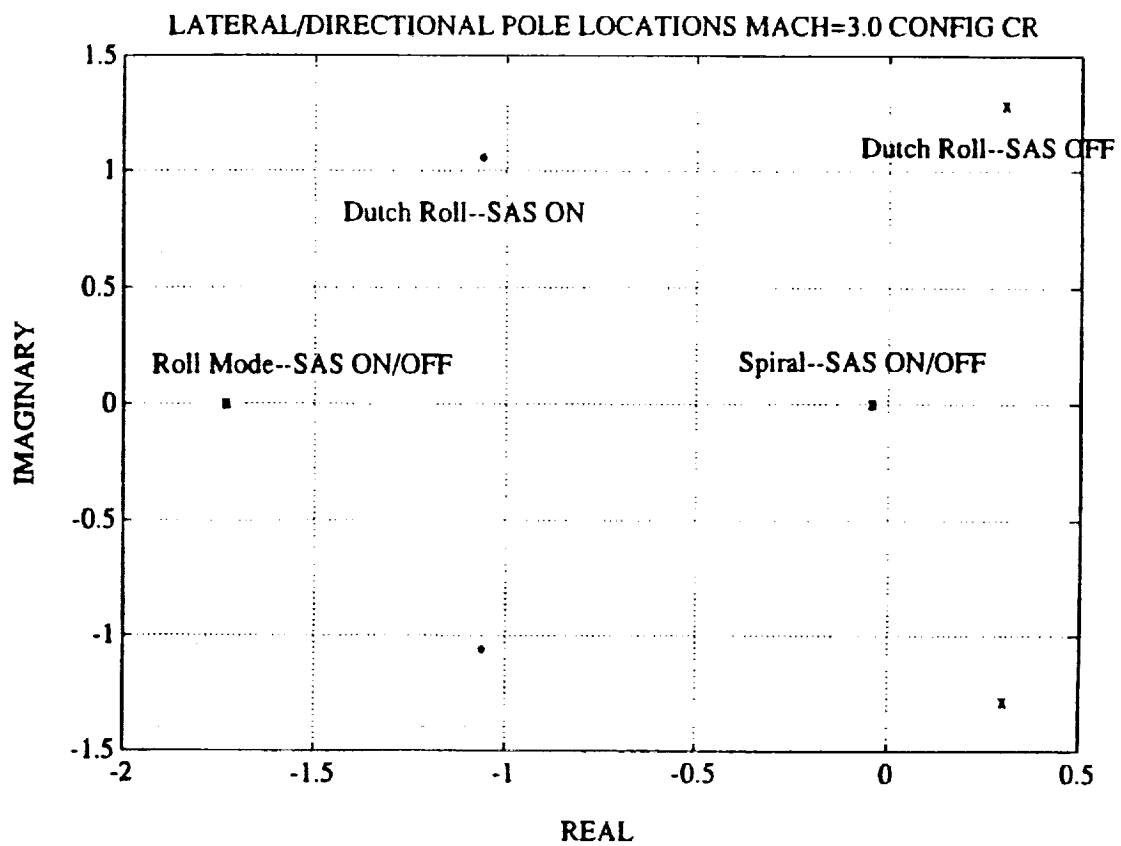
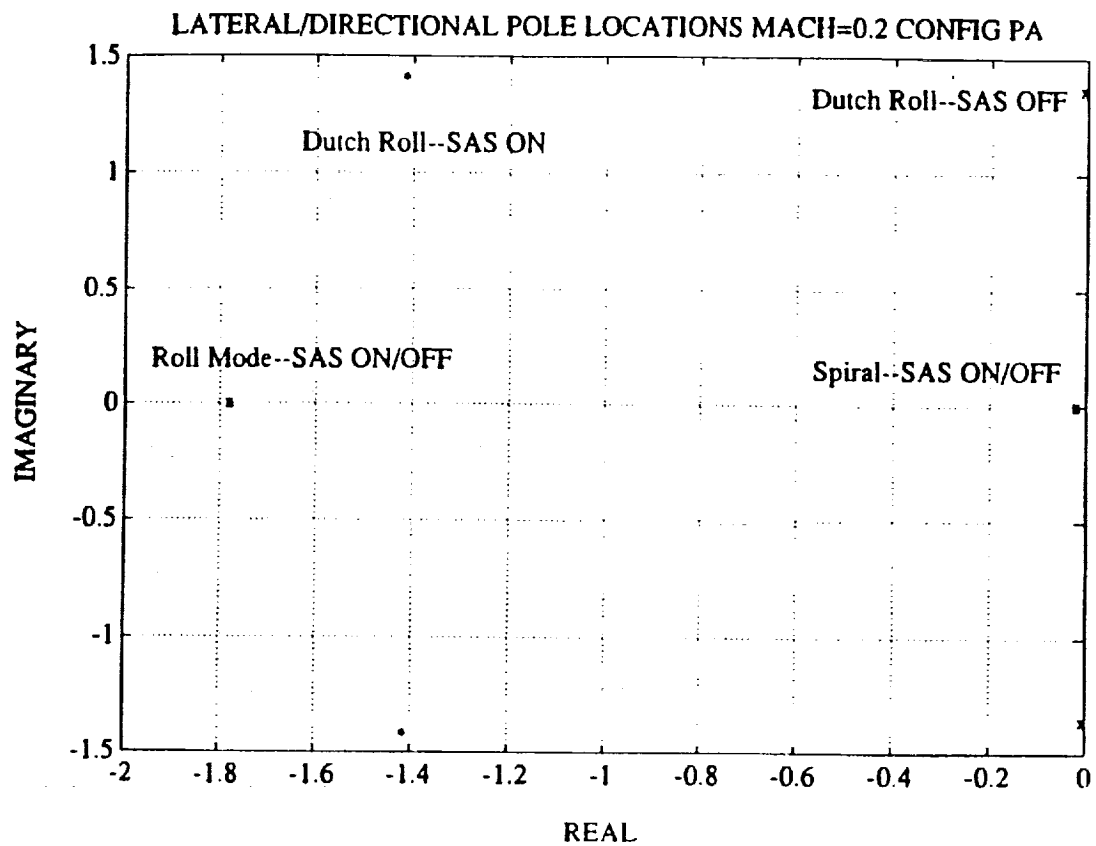


Figure VII.12  
 LONGBOW Lateral/Directional Pole Locations; CONFIGURATIONS PA & CR

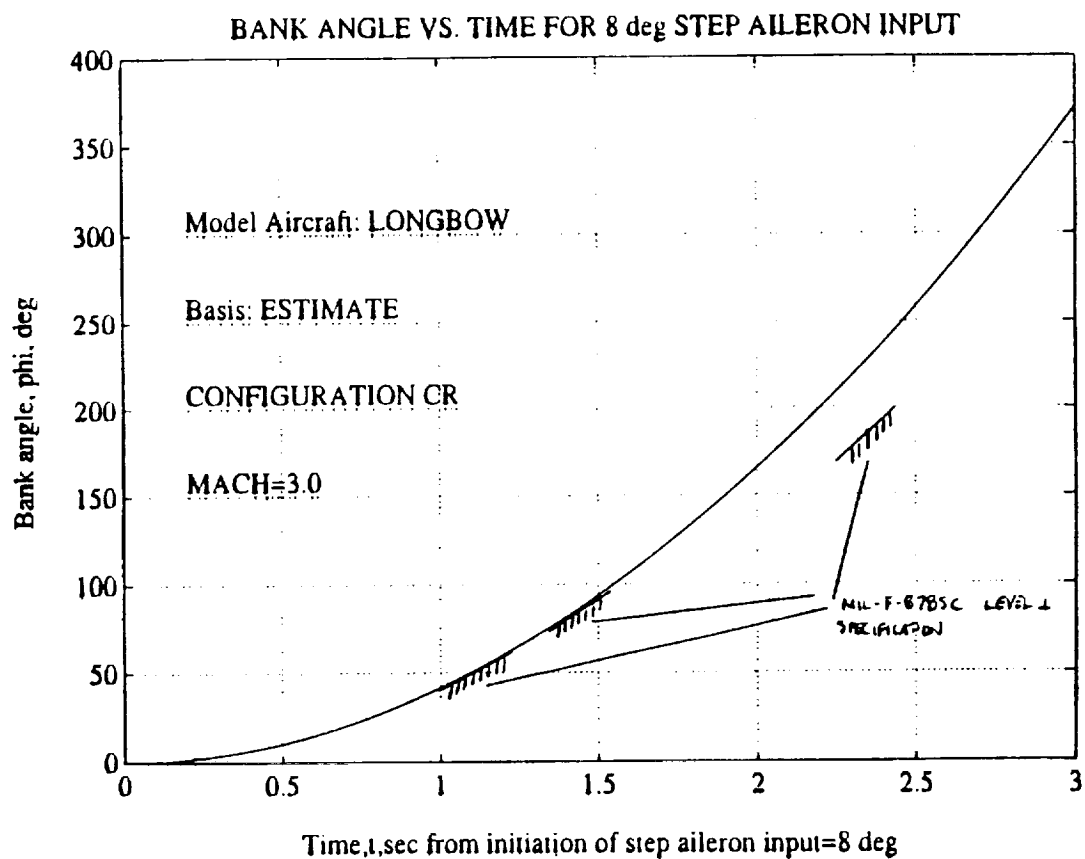
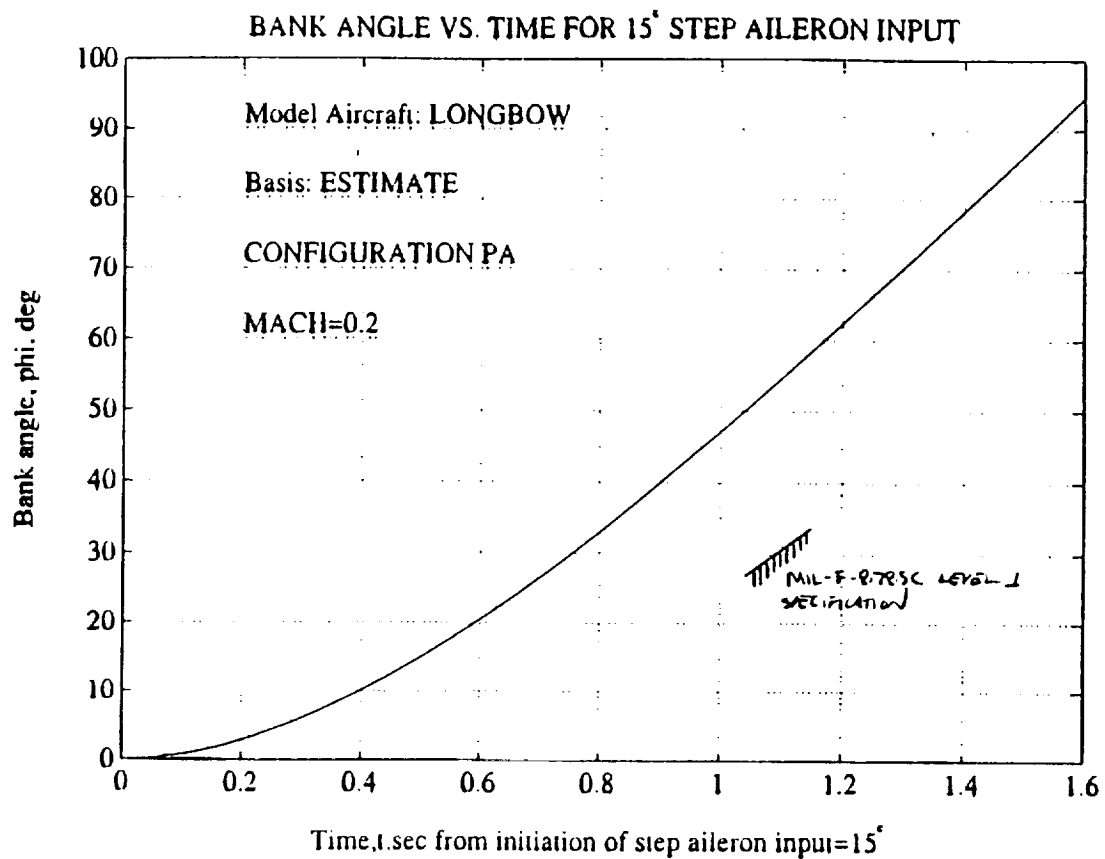


Figure VII.13  
 LONGBOW Roll Performance Spec: Compliance, Configurations PA & CR

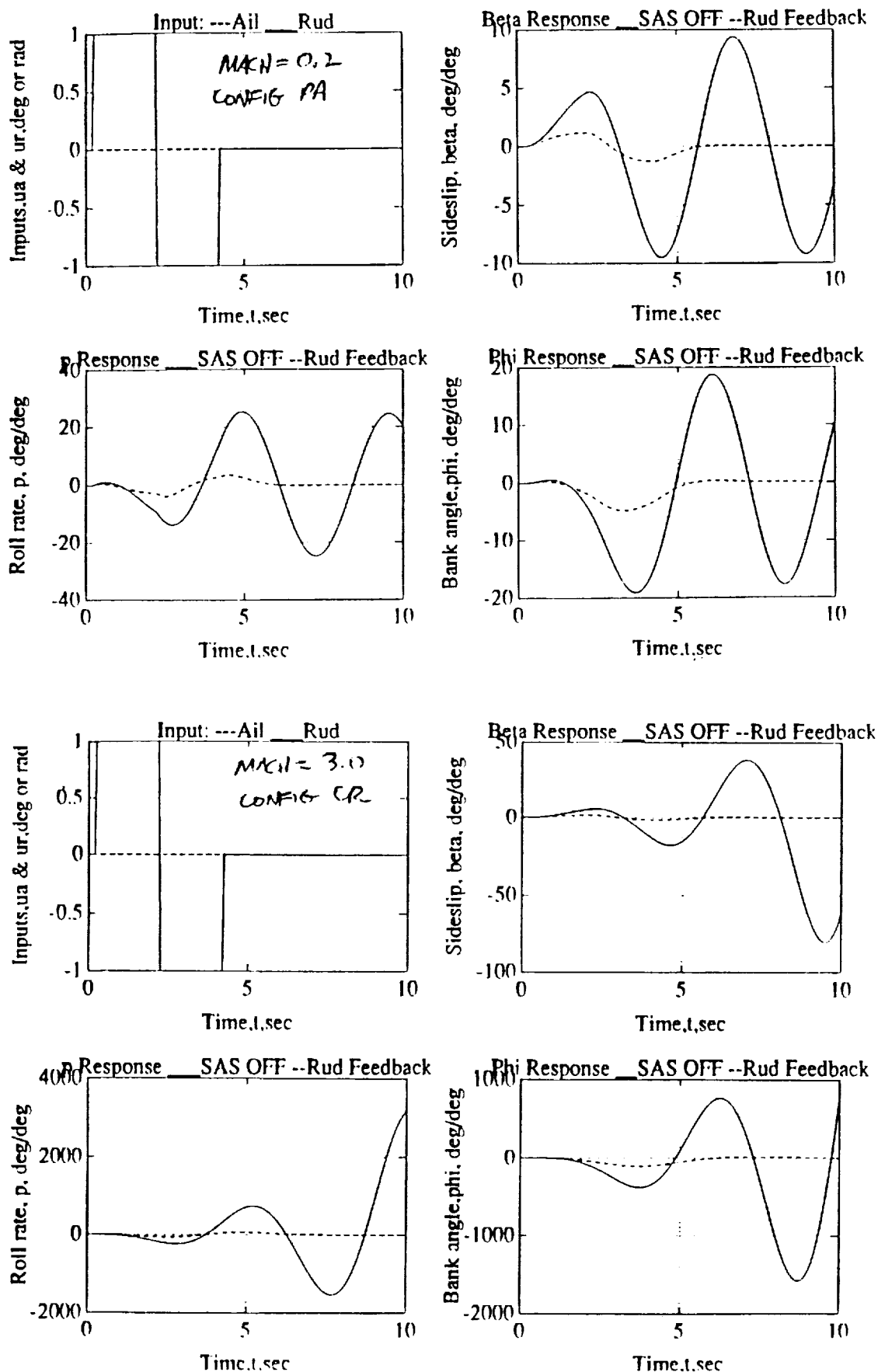


Figure VII.14  
 LONGBOW lateral/directional Response to Doublet; Configuration PA & CR

loop poles are displayed in Figure VII.12. Roll performance was estimated based on the roll control power, roll mode time constant and roll damping, and passed the specification, as shown on Figure VII.13. The response of the system to a rudder doublet at about the Dutch Roll natural frequency is shown for SAS off and on cases in Figure VII.14.

## **7. FLYING QUALITIES**

The flying qualities of the Longbow will be further investigated during detail design. High fidelity simulation of the vehicle and the cockpit controls will be used by the Stability and Control group to refine the stick force and displacement gradients, mechanical characteristics and airplane dynamics during applicable mission tasks.

## **IX. STRUCTURES**

### **A. DESIGN GOALS**

The structural design goal was to develop the lightest, most cost effective, aircraft structure which would support the required aerodynamic loads with the necessary safety factor. Many parameters were factored into the structural design including: strength, weight, thermodynamics, and cost. Material selection was limited to materials currently available to eliminate any technological delays and reduce the risk associated with future developmental speculation. However, with the fast pace of technological advances in structural material, particularly in the area of composites, it is anticipated that the structural weight of the aircraft could be significantly reduced as stronger, light weight, heat tolerant composites become available.

### **B. REQUIREMENTS**

The structural requirements were driven largely by the restriction of carrier suitability which limited the maximum gross weight to 65,000 lbs. A maximum load factor of 4g's was selected based on a constraint analysis conducted early in the design phase. The RFP required a minimum cruise speed of mach 3.0 which presented a major concern due to aerodynamic heating. The applicable military specifications for aircraft structures and carrier suitability are listed below.

- MIL-A-8860 - Strength and Rigidity
- MIL-A-8861 - Flight Loads
- MIL-A-8863 - Carrier Suitability
- MIL-A-8870 - Vibration and Flutter
- MIL-A-2066 - Carrier Launch and Arrestment



Some of the military specifications critical to the design were:

- A safety factor of 1.5 shall determine the ultimate load.
- The flight design weight is aircraft gross weight less 40% of the internal fuel.
- Arrestment weight is the empty weight plus fuel for 20 minutes of loiter, 5% of maximum internal fuel, 10 minutes at normal thrust, plus mission armament.

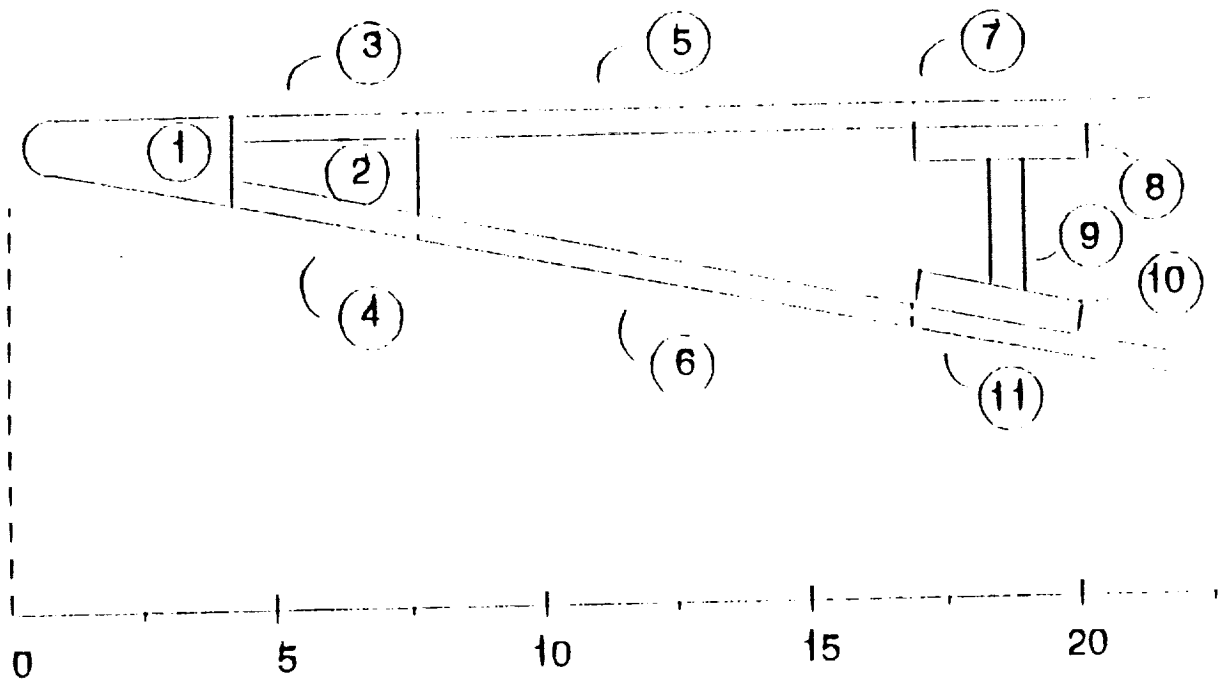
### C. THERMAL ANALYSIS

One of the primary goals in developing the Longbow was to accurately determine the aerodynamic heating. The aerodynamic heating was of major concern since it was the driving parameter in determining the mission profile. The mission profile in turn effected many other critical design areas, such as, cruise speed and altitude, engine design, and the necessity for an active leading edge cooling system. Structurally the thermal analysis determined the material selection.

The thermal analysis was conducted by using the basic heat equation and modelling the leading edge as shown in Figure IX.1. The heat equation is given below.

$$mC_p dT_a/dt = hA_{conv}(T_{aw}-T_a) + kA_{cond}(T_a-T_b)/(x_b-x_a) - \sigma \epsilon A_{conv} T_a^4$$

- m - mass of component(lbm)
- C<sub>p</sub> - specific heat(Btu/lbm-R)
- dT<sub>a</sub>/dt - time rate of change of component "a" temperature (R/sec)
- h - local convective heat transfer coefficient (Btu/sec-ft<sup>2</sup>-R)
- A<sub>conv</sub> - convective area of component(ft<sup>2</sup>)
- T<sub>aw</sub> - adiabatic wall temperature(R)
- T<sub>a</sub> - component "a" skin temperature(R)
- k - thermal conductivity(Btu/sec-ft-F)
- A<sub>cond</sub> - conductive area of component(ft<sup>2</sup>)
- x - distance from stagnation point(ft)
- σ - Stefan-Boltzman constant(Btu/sec-ft<sup>2</sup>-R<sup>4</sup>)
- ε - emissivity



DISTANCE FROM LEADING EDGE (INCHES)

FIGURE IX.1: Leading edge section model (1' depth)

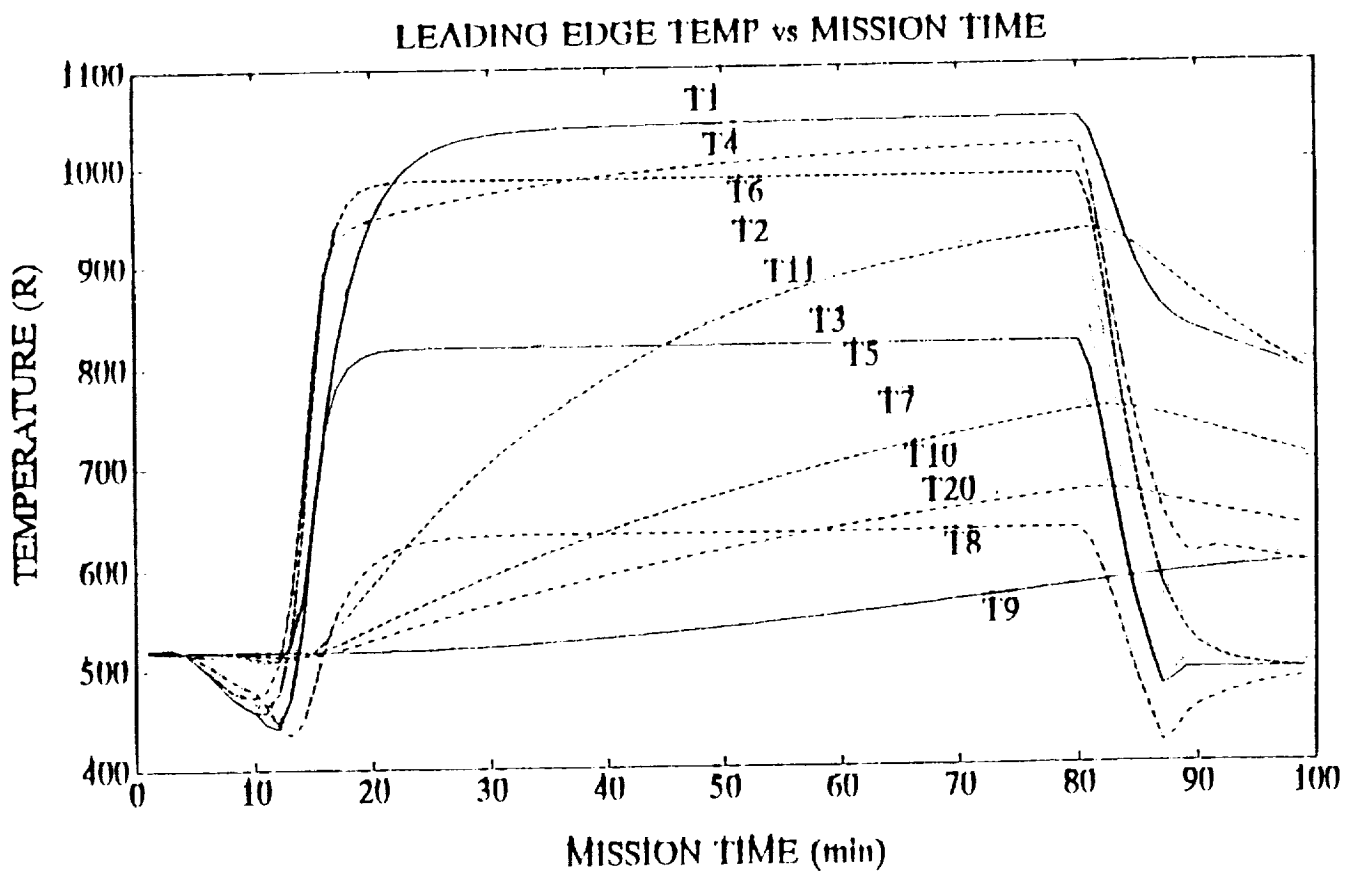


FIGURE IX.2: Transient temperature response  
(mach 3.0, 50,000 ft)

For the leading edge component, the convective heat transfer term was replaced by

$$qA_{cs} = 20800/R^{.5}(\rho/\rho_{sl})^{.5}(V/26000)^{3.25}(1-T_a/T_{stag})A_{cs}$$

- q - leading edge heat transfer rate(Btu/sec-ft<sup>2</sup>)
- A<sub>cs</sub> - equivalent cross sectional area of leading edge(ft<sup>2</sup>)
- R - leading edge radius(ft)
- ρ - freestream density(psf)
- ρ<sub>sl</sub> - sea level air density(psf)
- V - freestream velocity(ft/sec)
- T<sub>stag</sub> - stagnation temperature(R)

The leading edge section was divided into the 11 sections shown in Figure IX.1. A FORTRAN program was written to solve the heat equation for each section as the speed and altitude of the aircraft varied during a typical mission profile. The profile assumed a worst case scenario for aerodynamic heating with a climb to 50,000 ft and a mach 3.0 transit out and back followed by a descent to 10,000 feet and mach 0.3 loiter for 10 minutes. Figure IX.2 shows the transient temperature response for the individual components. As expected, component 1 located at the tip of the leading edge was the most heat critical, reaching 98% of the adiabatic wall temperature within 20 minutes at mach 3.0. The lower skin temperatures were higher than the upper surface due to increased pressure generated by the waverider design. T20 is a skin panel located 6 feet from the leading edge on the lower surface and represents the steady state skin temperature of 650 R.

Several parameters were varied to determine their influence on skin temperature. By painting the skin black to increase its emissivity, the maximum skin temperature was reduced by 35 degrees as shown in Figure IX.3. Skin thickness was found to have little

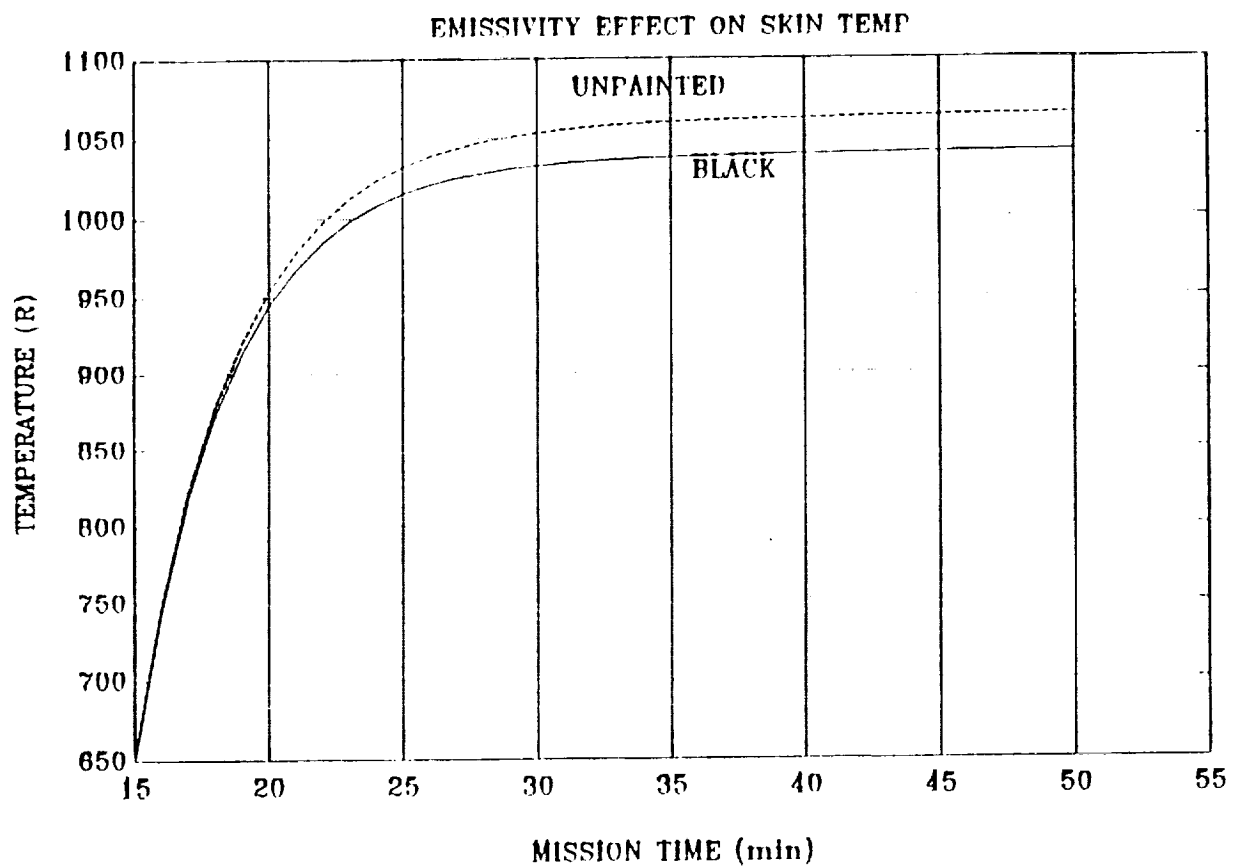


**FIGURE IX.3: Emissivity effect on leading edge temperature.  
(Component #1, titanium, mach 3.0, 50,000 ft)**

impact on the maximum skin temperature. Figure IX.4 shows only a 4% drop in temperature with a tripling of skin thickness. The weight penalty for increasing skin thickness renders this option impractical. The material selection varied the rate at which the adiabatic wall temperature was approached, but had little effect on the maximum skin temperature.

Altitude and mach number had the most significant impact on the aerodynamic heating of the structure. Specifically, altitudes below 40,000 ft created a sharp rise in skin temperature as depicted in fig. IX.5. This increase results from the combined impact of higher freestream temperature and higher density at lower altitudes. Figure IX.6 shows the effect of mach number on skin temperature. A cruise speed greater than mach 3.5 or an altitude below 40,000 ft sent temperatures into a realm where different materials or the weight penalty of an active cooling system would be required.

All configurations were variations of the base model which consisted of 100% titanium alloy (Ti-6A-4V), 1/6 inch skin thickness and black paint.

#### **D. MATERIALS**

Material selection was determined through a trade-off study which evaluated several available materials based on thermal properties, strength, weight, and cost. For the design of Mach 3.0 aircraft, Nicolai recommends using either steel, titanium, or graphite polyimide for a weight/cost effective design. Steel presented the best thermodynamics which enabled its use up to 1450 R. However, since the weight penalty is significantly larger

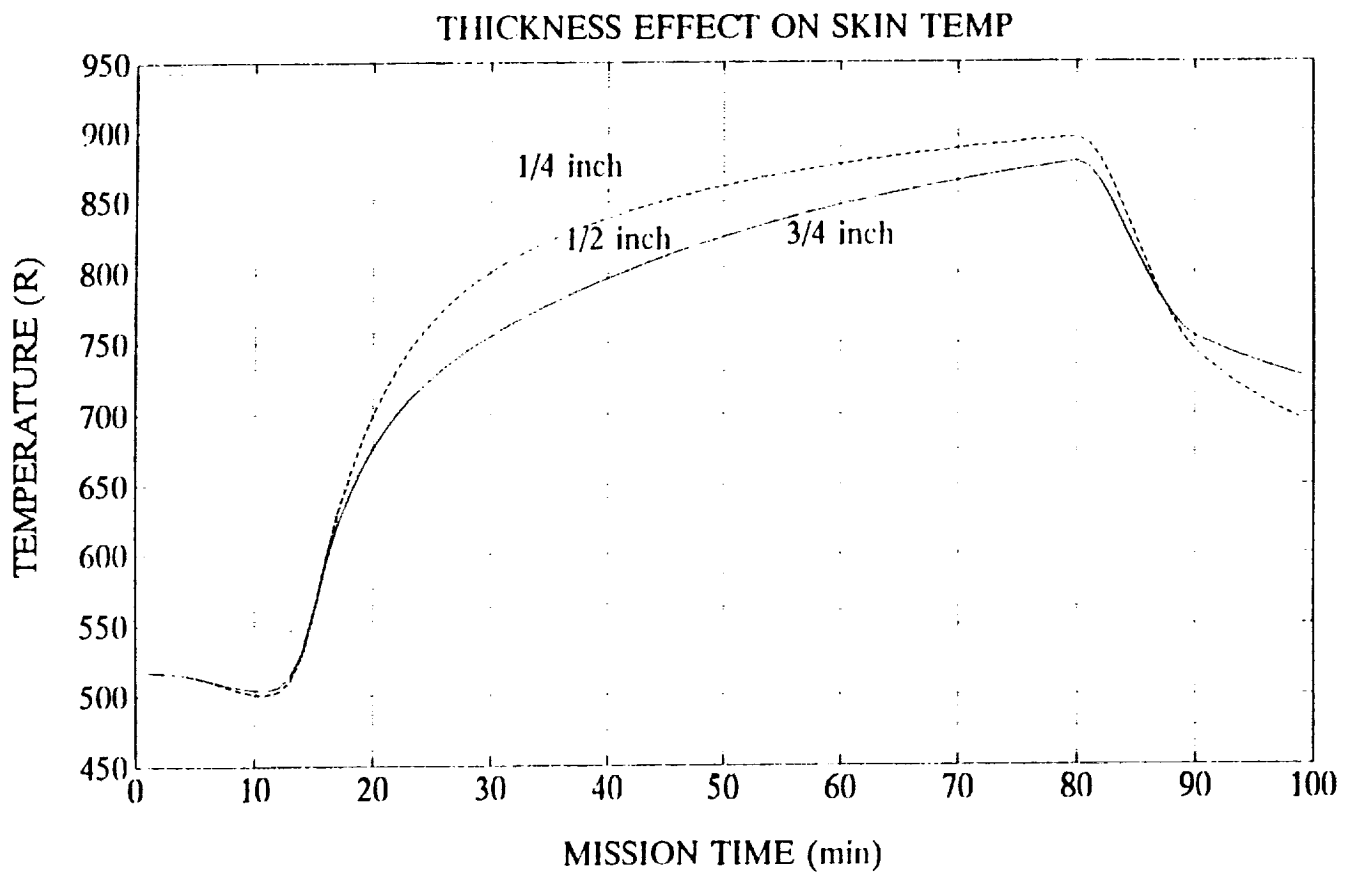


FIGURE IX.4: Skin thickness effect on skin temperature.  
(component #4, titanium, mach 3.0, 50,000 ft)

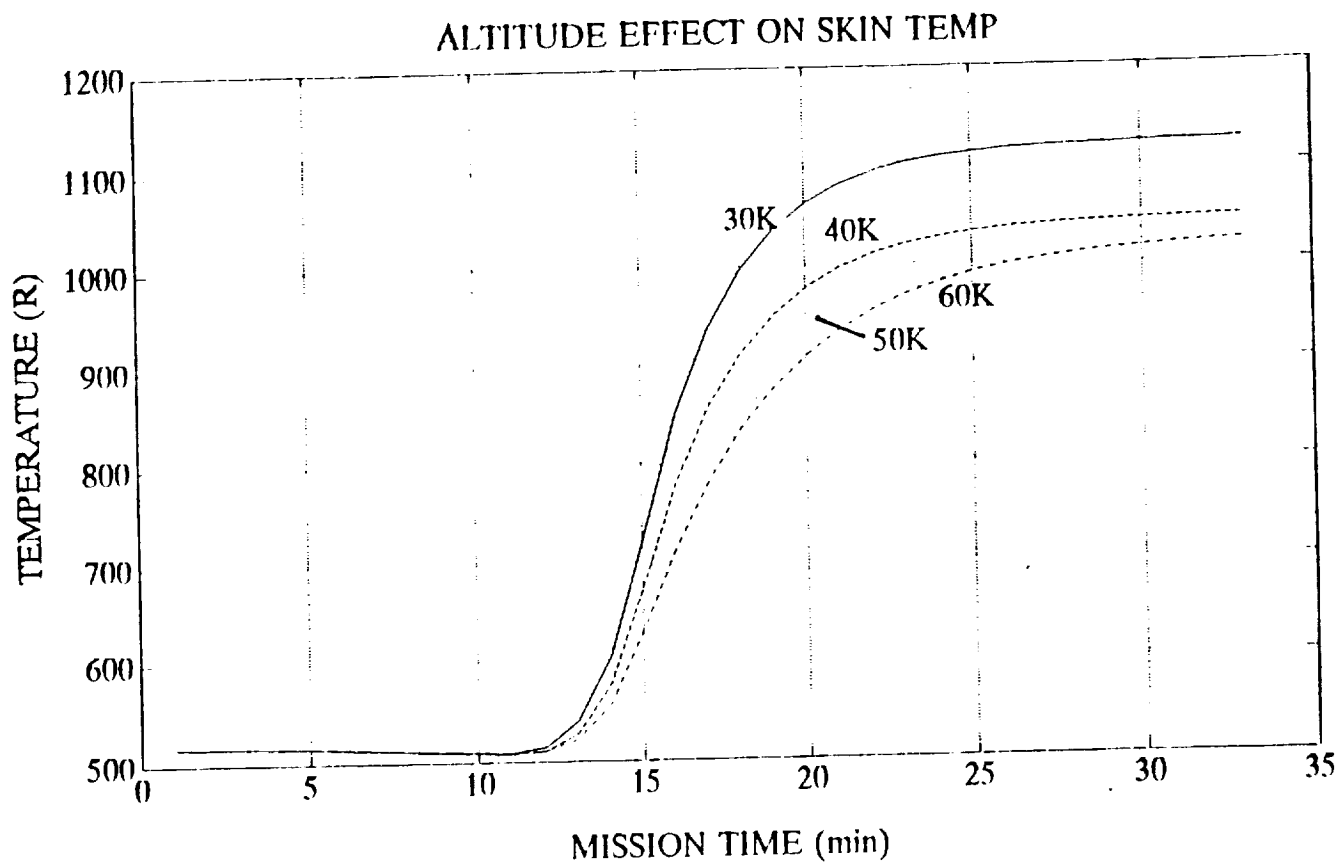


FIGURE IX.5: Altitude effect on leading edge temperature.  
(Component #1, titanium, mach 3.0)

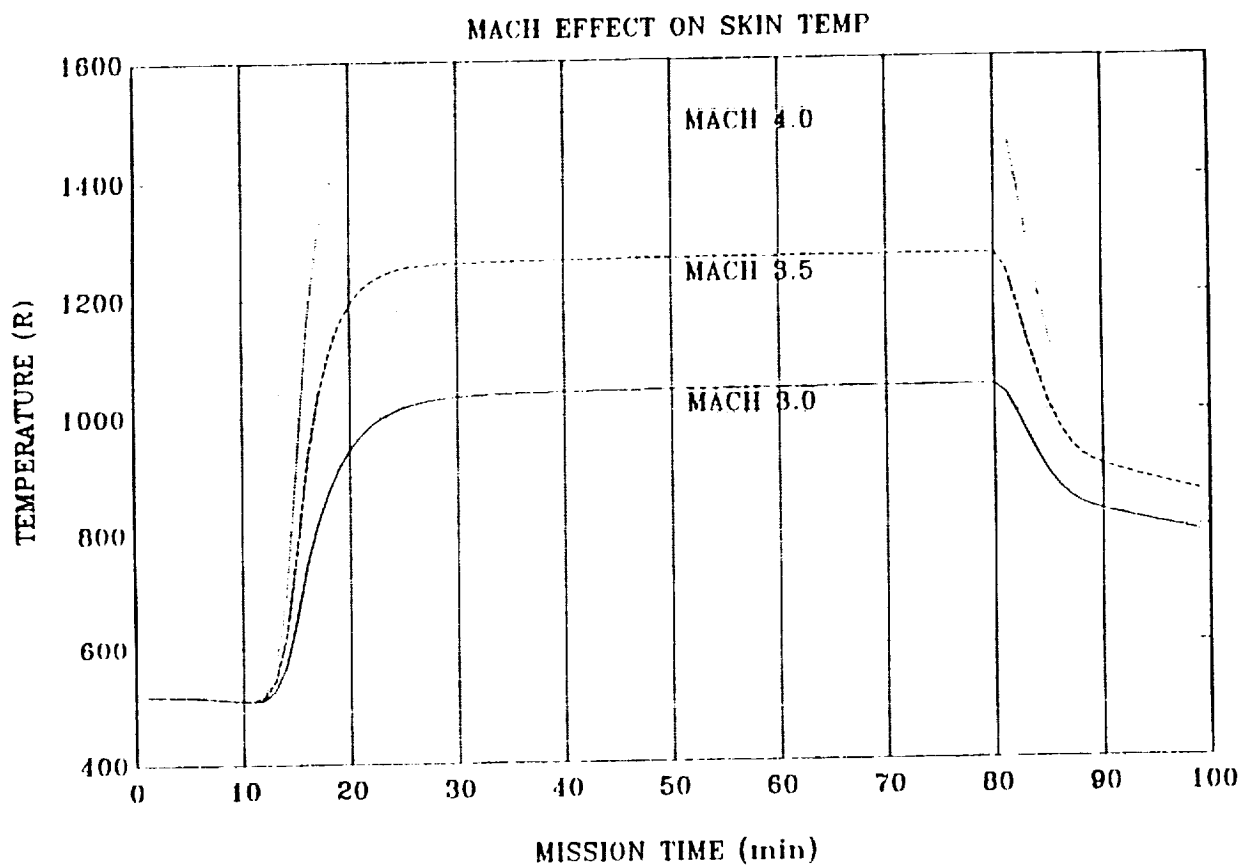


FIGURE IX.6: Mach effect on leading edge temperature.  
(Component #1, titanium, 50,000 ft)



than other materials, steel will only be used in high strength areas, such as, in the landing gear. Titanium offers excellent strength and heating characteristics and is only slightly heavier than aluminum. Titanium has a useful temperature limit of 1250 R and will form the leading edge sections. Boron aluminum is a lightweight material with outstanding thermal properties , but was too expensive to be cost effective. Boron polyimide was the composite selected for the majority of the upper skin and lower aft skin. Though somewhat expensive, its weight savings significantly reduce the life cycle cost while providing excellent structural strength up to 1060 R. Graphite epoxy is another popular composite which will only see limited interior use since its temperature limit is only 800 R. Figure IX.7 presents a graphical depiction of material cost and weight trade-offs.

#### **E. V-N DIAGRAM**

The structural design of the Longbow is defined by the operating envelope. Figure IX.8 shows two V-n diagrams, one for low altitude subsonic flight with wings swept forward and the other for high altitude supersonic flight with wings swept aft. The maximum load factor ranges from 4g's to -2g's. The ultimate load factor ranges from 6g's to -3g's based on a safety factor of 1.5. The V-n diagrams were constructed using the design weight of 51,000 lbs. All gust envelopes fell within the required limits and, therefore, did not alter the V-n diagrams.

#### **F. WING BOX DESIGN**

The maximum loads on the wing were determined using a 6g, Mach

# Material Tradeoff Study

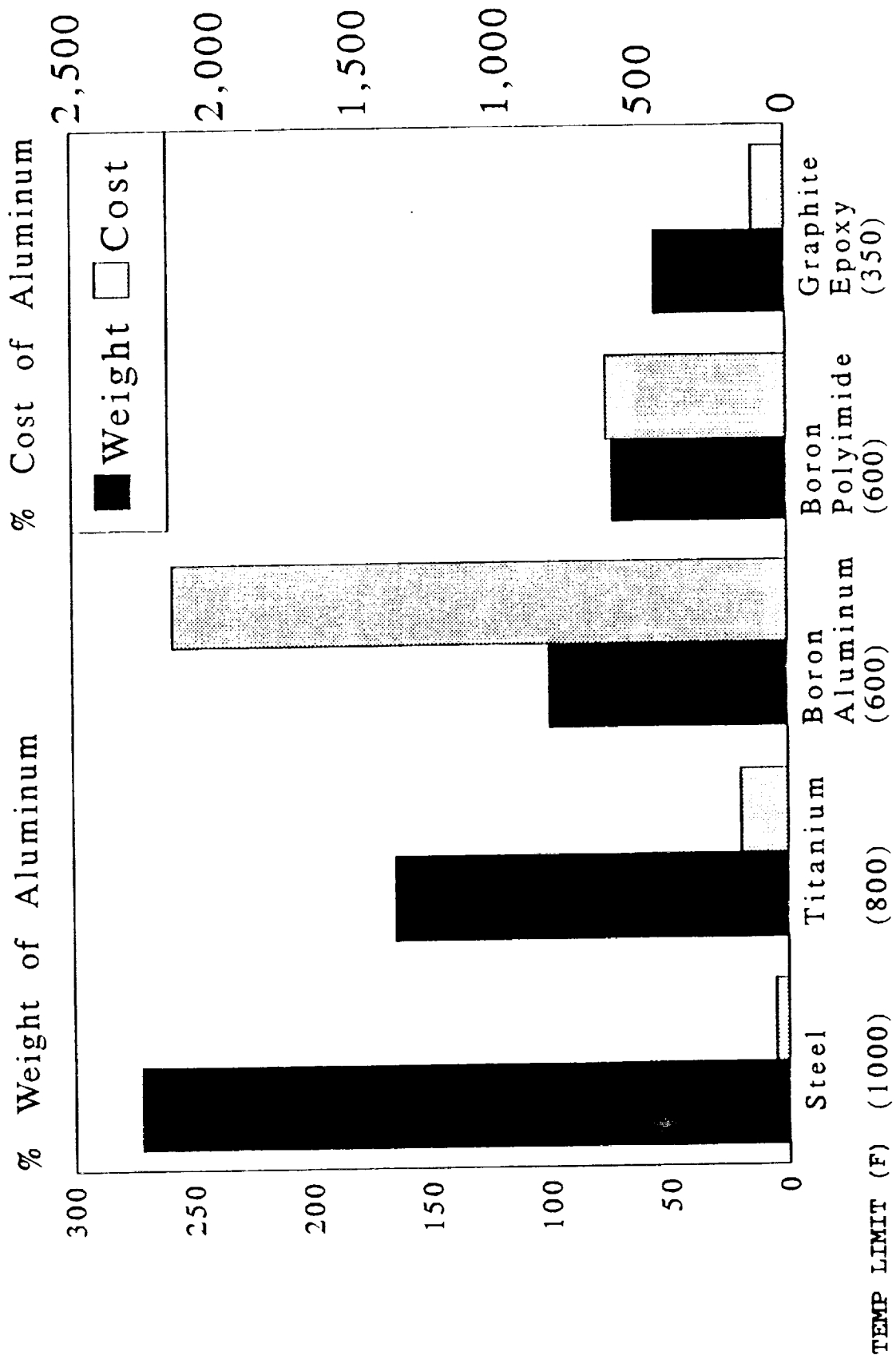


FIGURE IX.7: Material tradeoff study based on a 10,000lb block weight of aluminum

# V-N DIAGRAM

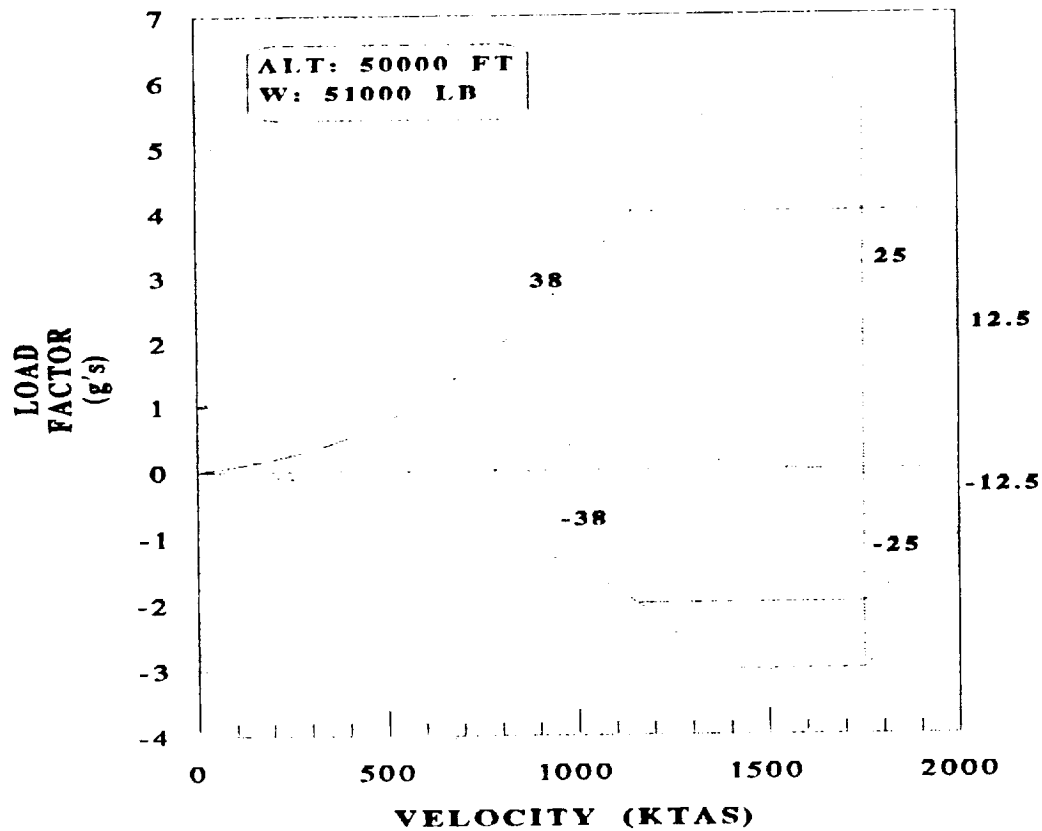
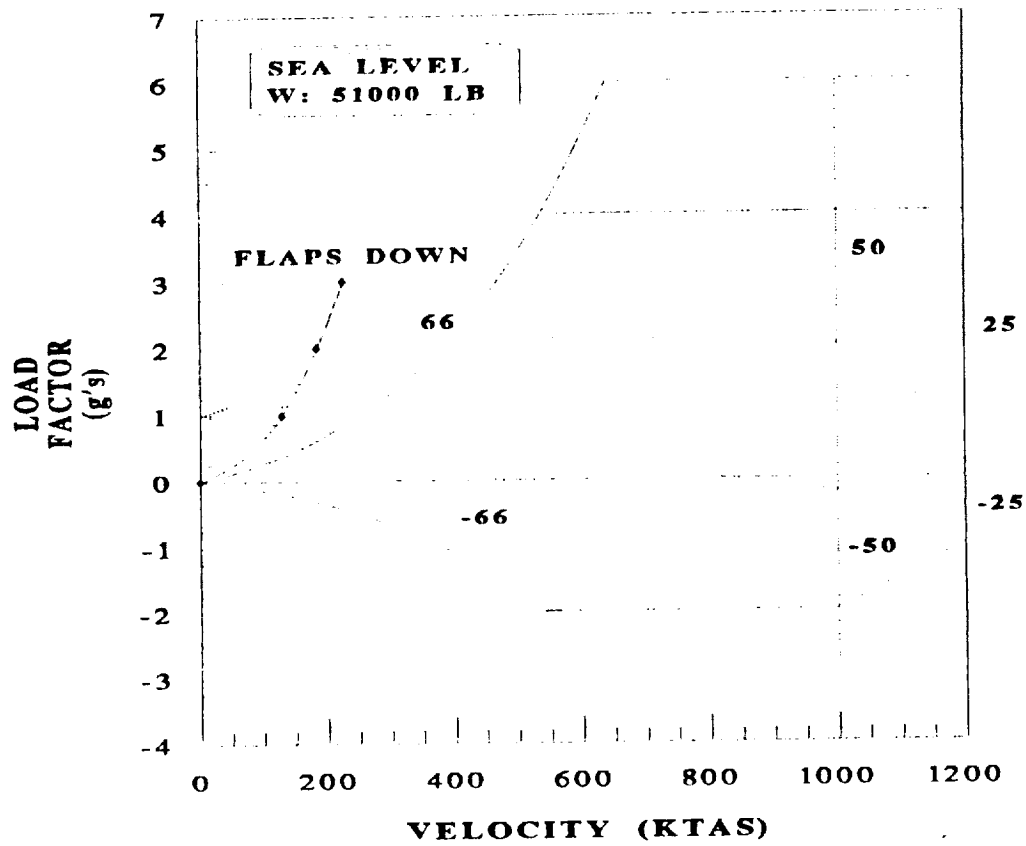


FIGURE IX.8: Subsonic and supersonic V-n diagram with gust load envelope.

3.0 turn at 50,000 ft and 65,000 lbs. The total lift required for the maneuver was 390,000 lbs. Using the lift distribution generated by the aeronautics group, the shear force, bending moment, and torsion diagrams were constructed as shown in Figs. IX.9, IX.10 and IX.11 respectively.

Two wing box designs were required. The wing box for the supersonic waverider design was modelled after a delta wing. Based on the design of previous delta wing interceptors, the wing skins will provide a large percentage of the bending support and torsional rigidity. Therefore, relatively thick skins will be required which will also provide improved thermal performance. The swing wing structure was designed to support the aerodynamic loads while remaining within the NACA 66-006 airfoil shape. The sweep schedule for the swing wing caused the wing to become fully swept aft by mach 0.8. (A review of the V-n diagram at mach 0.8 shows a maximum load factor of 3g's.) Therefore, the swing wing was designed to carry a 3g load at maximum gross weight.

A primary concern when designing variable swept wings is the pivot design. Four basic pivot designs were considered; track and shoe, moment bearing, track with roller bearing, and vertical pin. The vertical pin design offers the most simplicity and confidence in load path while minimizing weight. Pivot location presented another problem which was resolved using a trade-off study which compared pivot location to weight based on sizing the actuator, lugs, fixed wing glove, and outer wing box .

Using MSC/PAL2 software, a finite element analysis was

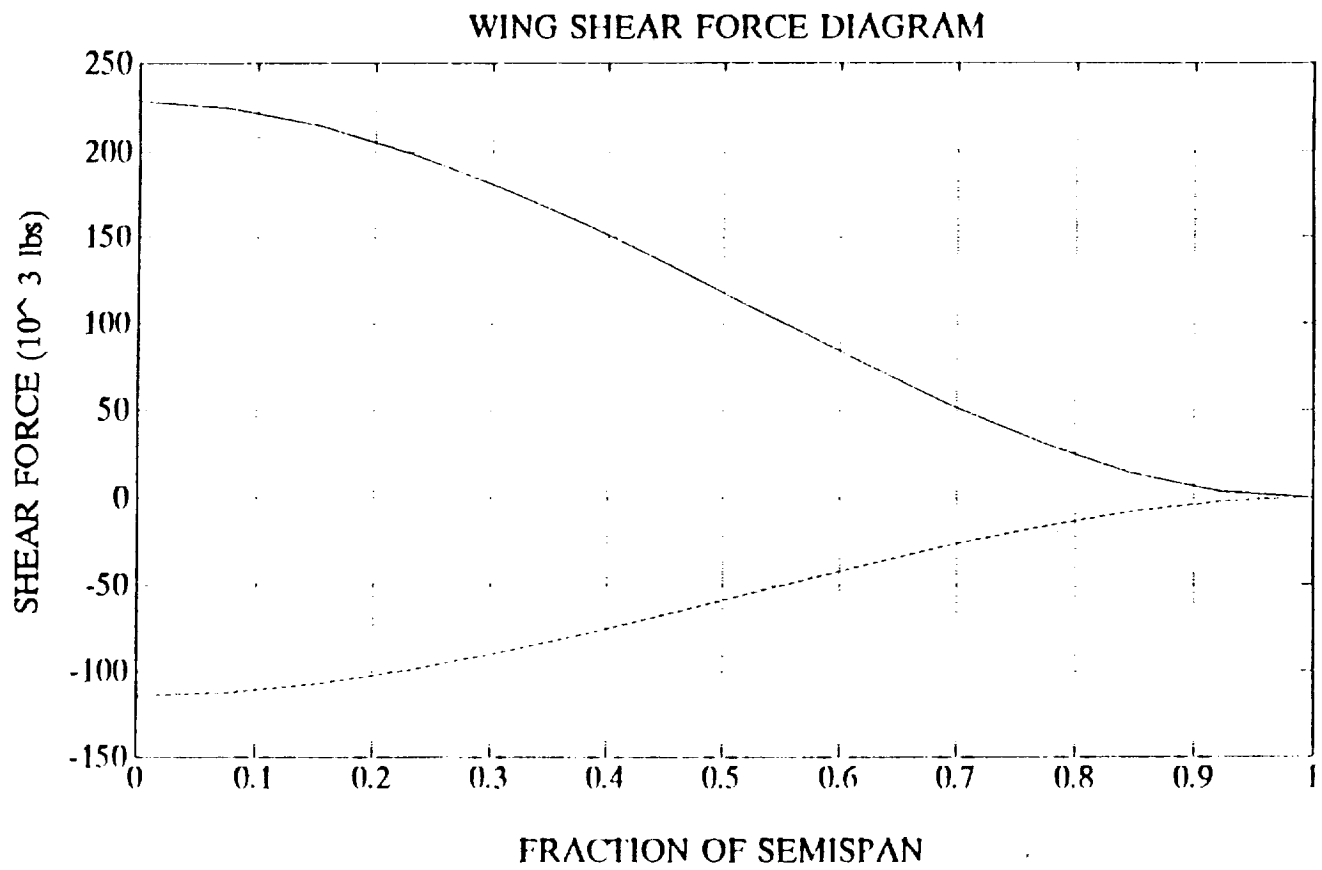


FIGURE IX.9: Wing shear force diagram  
(mach 3.0, 6g's, 65,000 lbs)

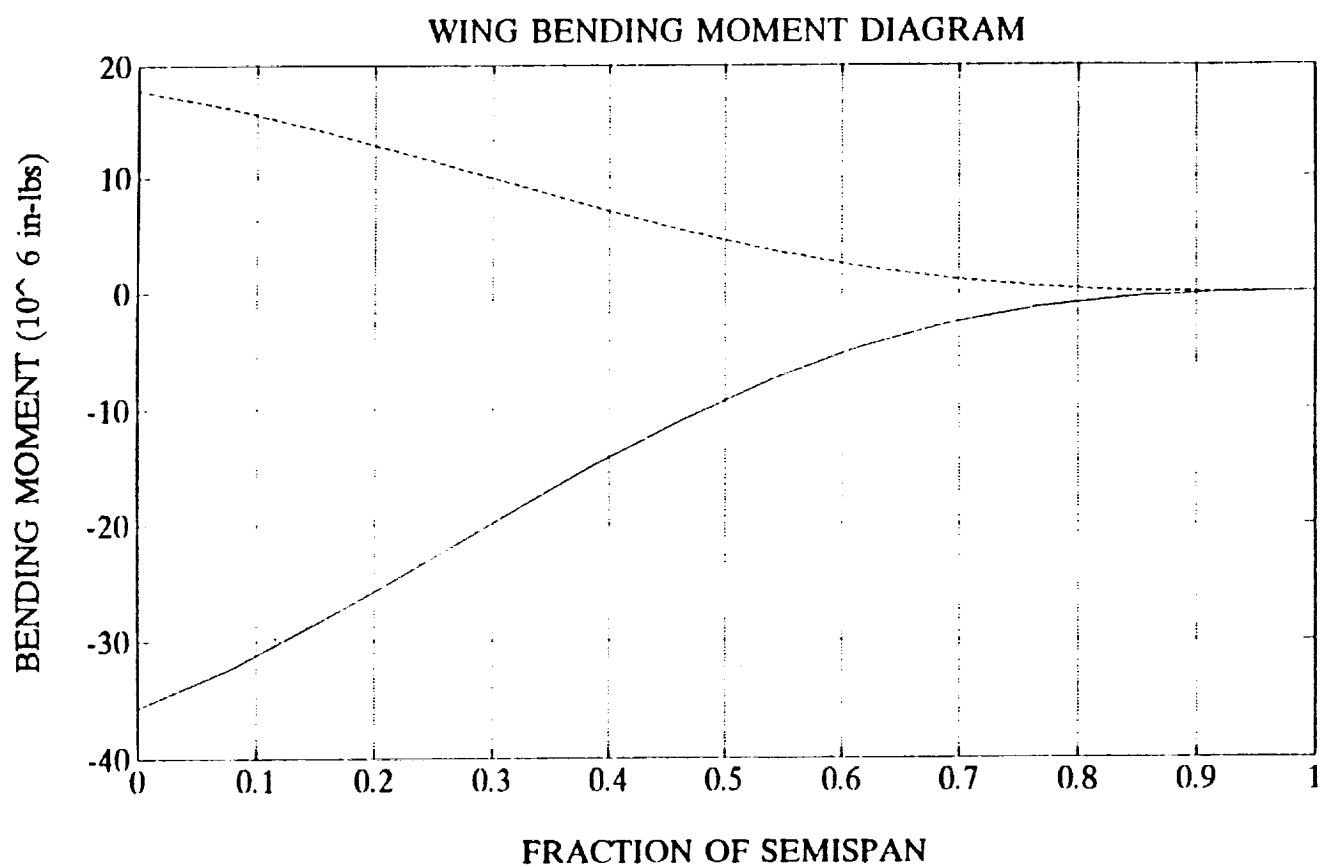


FIGURE IX.10: Wing bending moment diagram  
(mach 3.0, 6g's, 65,000 lbs)

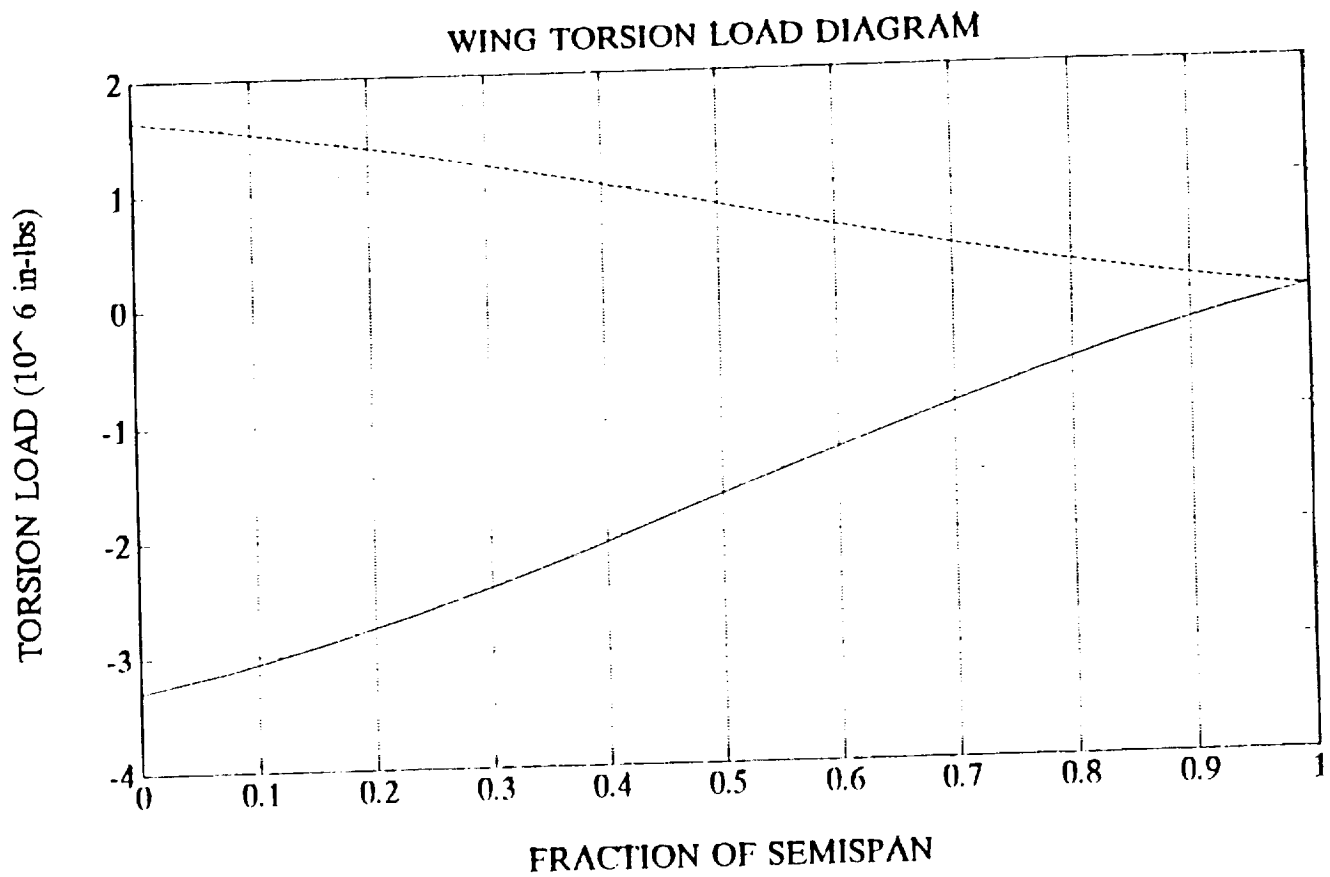


FIGURE IX.11: Wing torsion diagram  
(mach 3.0, 6g's, 65,000 lbs)

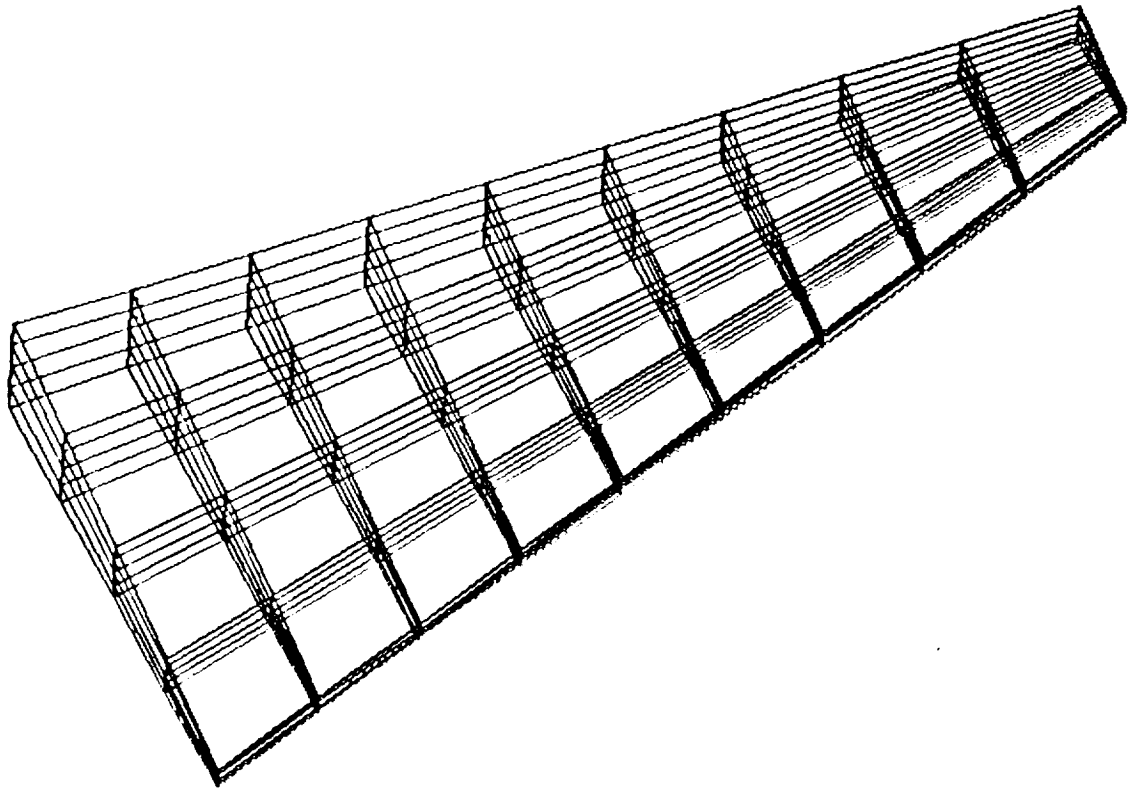
conducted. Figure IX.12 shows the finite element models for both the Longbow wing and the swing wing. As shown in Figure IX.13, the maximum normal and shear stress for the Longbow wing box occurs at the aft wing root. The same stress pattern is evident in the swing wing as shown in Figure IX.14. The initial wing skin thickness of 1/2 inch was selected based on historical fighter wing skin design. The initial material selection was titanium, however, the use of composites with the advantage of lighter weight and added strength will allow for an adjusted skin thickness in further iterations. The maximum stress for the swing wing skin while supporting 40% of a 3g load was 164 ksi which barely exceeds the ultimate structural limit of the material. The next iteration required either a thicker skin or a reduction in load percentage carried by the wing skin.

The initial swing wing spar design was conducted by modeling the spar as a rectangular cantilever beam. The stress along the beam caused by the bending moment was computed as a function of spar thickness. The height of the spar was constrained by the NACA 66-006 airfoil shape. The initial results showed that four, one inch thick spars spaced evenly from 15% to 70% chord would provide the remaining 60% of the bending support without failure.

By reducing the load percentage of the wing skin to 35% and increasing the spar load bearing percentage to 65%, the maximum stress was below the ultimate stress of the material. The goal was to minimize the structural weight of the wing by optimizing the load bearing capacity of the wing skin/spar combination.



Longbow Wing Box



Swing Wing Box

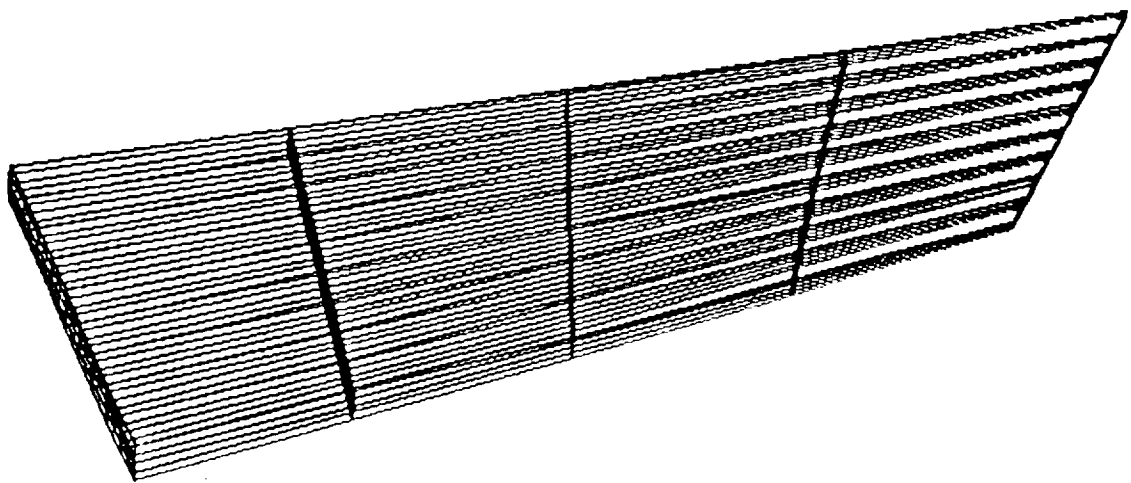
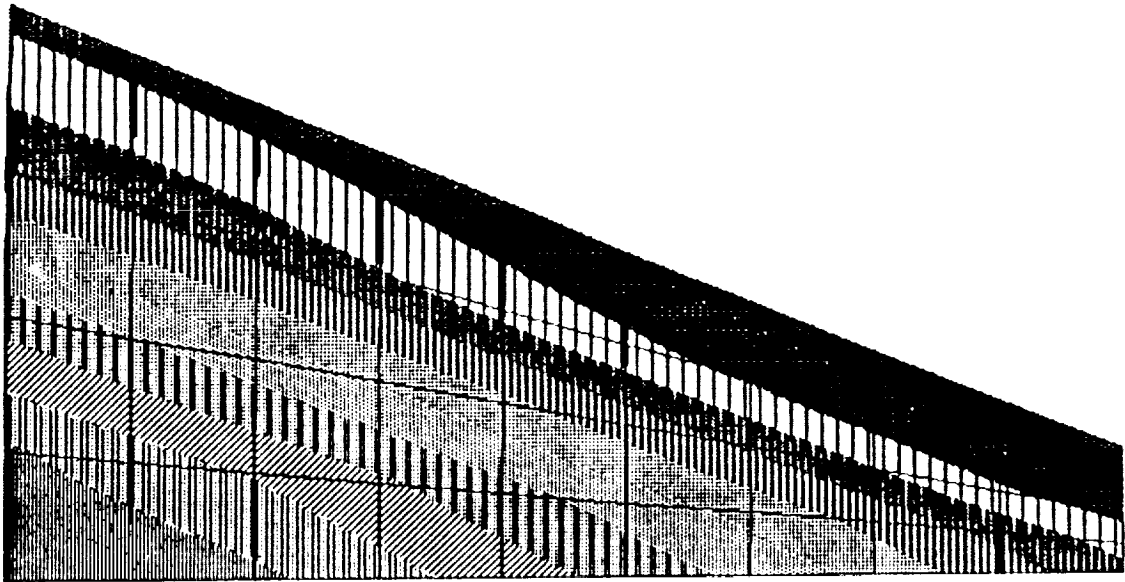


FIGURE IX.12: Finite element models for Longbow delta wing and swing wing

## NORMAL STRESS DISTRIBUTION



## SHEAR STRESS DISTRIBUTION

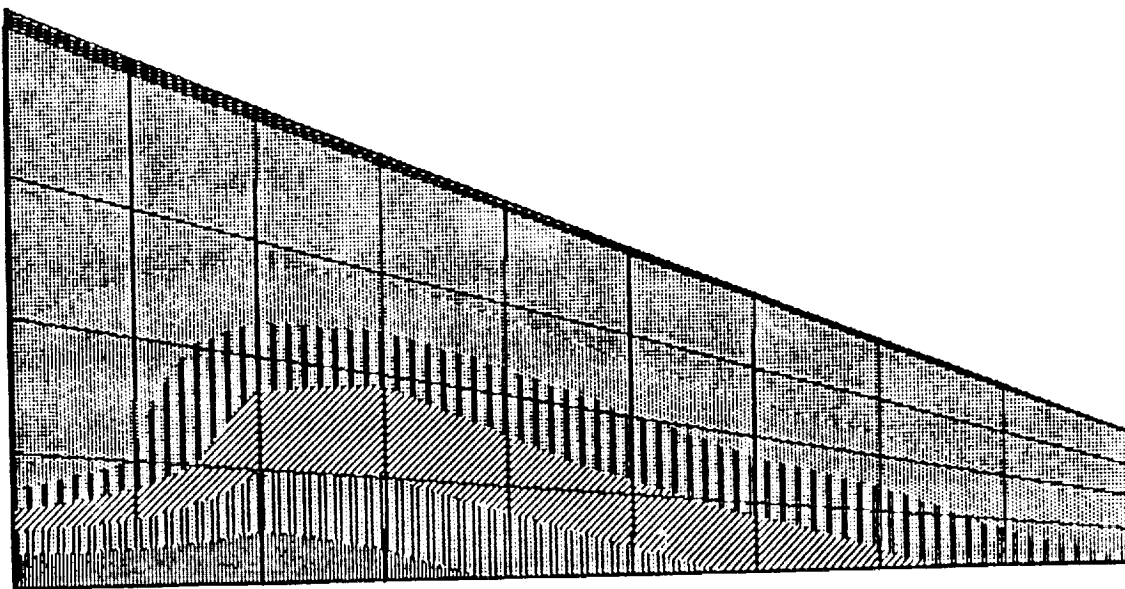
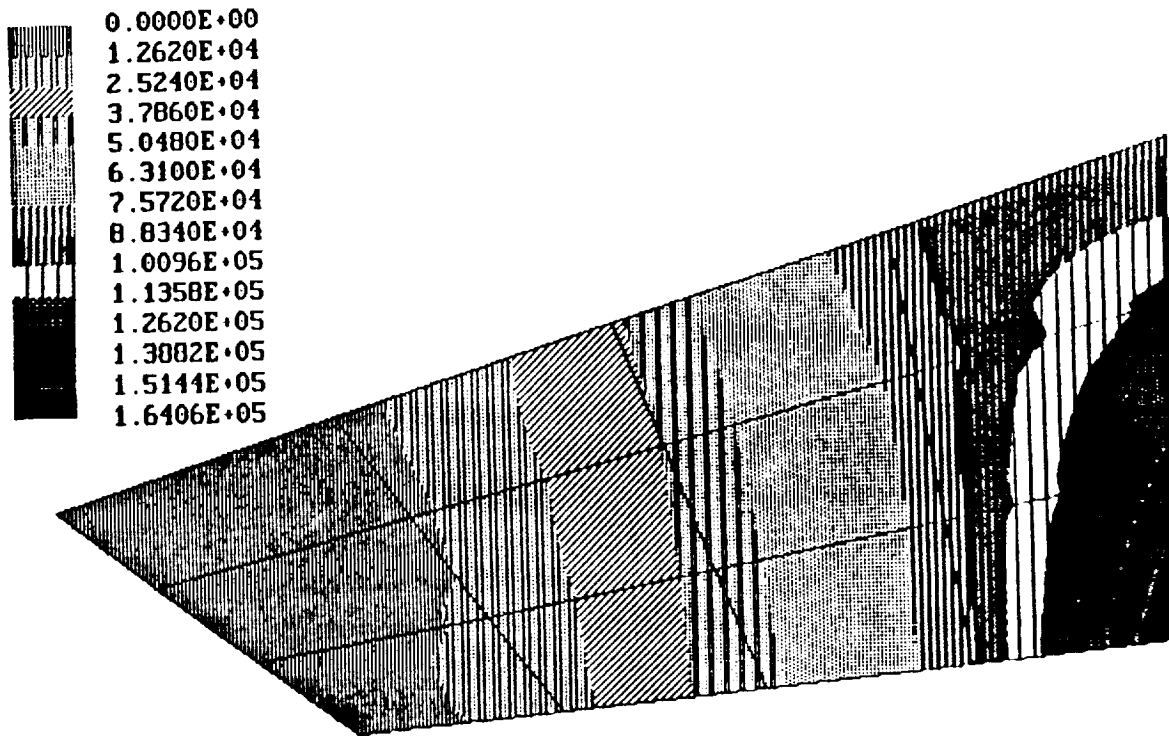


FIGURE IX.13: Normal and shear stress distribution on Longbow upper wing surface caused by a uniformly distributed pressure load.

# 1/2" SWING WING (3G LOAD)

## MAJOR STRESS



# 1/2" SWING WING (3G LOAD)

## MAX SHEAR/2ND MJ

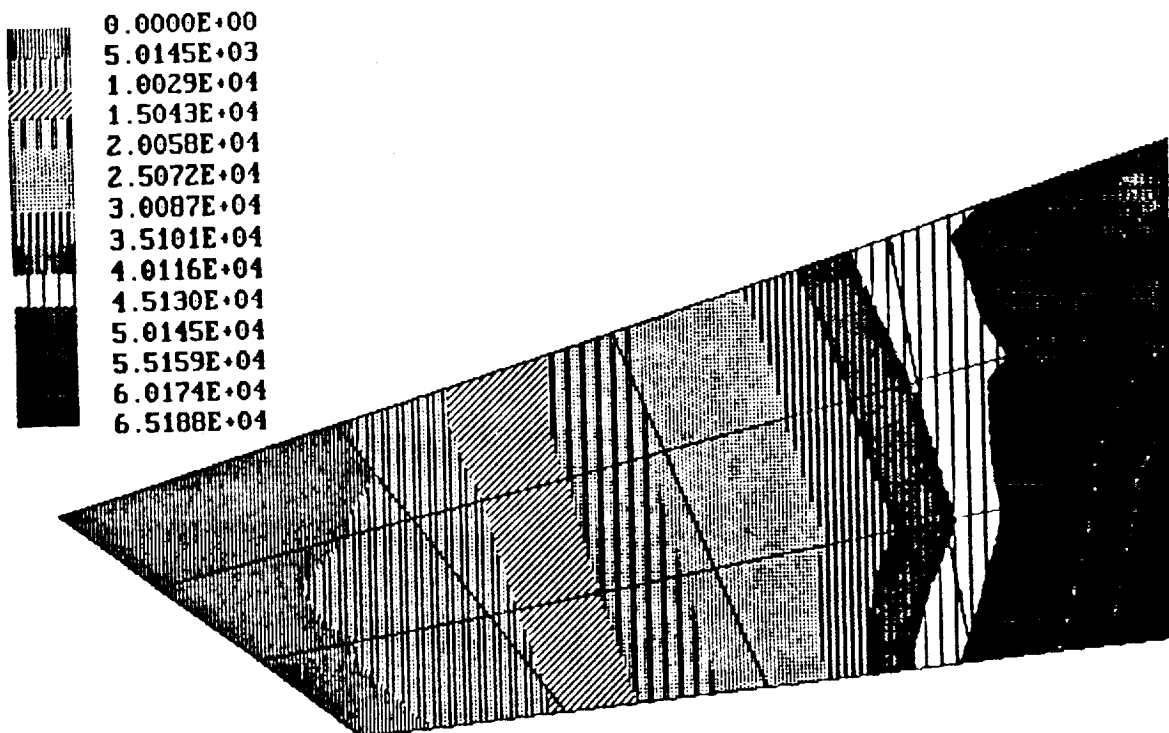


FIGURE IX.14: Major normal stress and maximum shear stress distribution on 1/2" swing wing caused by 40% of a uniformly distributed 3g pressure load.

## **G. FUSELAGE**

The most severe loads for the fuselage were encountered during catapult launch and arrestment. The maximum gross weight of 65,000 lbs was used to calculate the forces on the fuselage during launch. The maximum force generated by a C13-1 catapult to achieve 150 knots end speed was 252,000 lbs. At the maximum landing weight of 42,000 lbs and landing speed of 137 kts, the peak hook point load was 160,000 lbs.

## **H. WEIGHT**

Given the the shape, engines and structure, a weight estimation was made as suggested by Nicolai. A FORTRAN code was used to determine estimated weights for all component groups (i.e. -Avionics).

## **I. CENTER OF GRAVITY**

With the weight of each component, it was now possible to calculate the center of gravity (CG) for the full-up aircraft. Given the shape of LONGBOW, an even distribution of weight throughout the airframe produced a CG much further aft than desired. To reduce the stability problems associated with this aft CG, the high density components, such as fuel, were moved as far forward as the volume of the aircraft allowed. The weight of each component is shown in Table IX.1, along with the position of the component with reference to the nose. The final placement of the fuel is shown pictorially in Section X. Table IX.1 is for the wings forward configuration, and shows a fully loaded CG of 36.19 feet from the nose, or 95.2% MAC. With the

the wings swept, the CG moves back to 36.74 feet from the nose, or 96.7% MAC when fully loaded.

By burning the fuel from the aft tanks first, the CG moves forward to a minimum of 78.5% MAC as shown in Figure IX.15. The CG travel curve is shifted aft for the wings swept configuration.

Shown with the CG calculations in Table IX.1 are the moments of inertia for the wings forward configuration. Similar calculations were made for the swept wing configuration for the stability and control analysis.



## Center of Gravity and Moments of Inertia

Compon.	Weight	X	Z	Y	b <sub>x'</sub>	b <sub>y'</sub>	l <sub>z z'</sub>	b <sub>x y'</sub>	l <sub>y z'</sub>	b <sub>x z'</sub>
Fuselage	3800	30	2.5	0	738.1737	107035.2	106297	0	0	8858.084
Lt Wing	3000	28	0.5	-13	15781.38	73125.82	88860.57	-33940.4	-606.079	1305.402
Rt Wing	3000	28	0.5	13	15781.38	73125.82	88860.57	33940.45	606.0794	1305.402
Lt Engine	5500	39.5	6	-5	10427.67	272871.7	270991.3	-33761.7	-5128.36	40514.08
Rt Engine	5500	39.5	6	5	10427.67	272871.7	270991.3	33761.73	5128.365	40514.08
V Fins	78	47	-4	0	38.78908	5394.107	5355.318	0	0	-455.772
Stabs	240	54	0	0	0	21751.72	21751.72	0	0	0
Fuel 1	2000	27	1.5	-20	25004.66	45455.96	70180.89	-33567.5	-1864.86	2517.561
Fuel 2	2000	27	1.5	20	25004.66	45455.96	70180.89	33567.48	1864.86	2517.561
Fuel 3	3000	24	0.5	-6	3380.058	53731.27	57064.71	-13427	-279.729	1118.916
Fuel 4	3000	24	0.5	6	3380.058	53731.27	57064.71	13426.99	279.729	1118.916
Fuel 5	11500	48	2.5	-8	25109.56	825756	846397.7	-137254	-7148.63	42891.78
Fuel 6	11500	48	2.5	8	25109.56	825756	846397.7	137253.7	7148.629	42891.78
Fuel 7	2000	16	1	0	62.16199	15975.63	15913.47	0	0	994.5919
Av Bay 1	250	34	0.3	-3	70.63157	8983.107	9052.34	-792.565	-6.99322	79.25654
Av Bay 2	250	34	0.3	3	70.63157	8983.107	9052.34	792.5654	6.993224	79.25654
AIM * 2	2460	25	1	0	76.45925	47863.49	47787.03	0	0	1911.481
Ducts	1059	26	5	0	822.8694	23073.26	22250.39	0	0	4278.921
Ramps	295	16	4.5	0	185.6701	2532.907	2347.237	0	0	660.1604
Access.	2000	40	5	0	1554.05	101013.2	99459.19	0	0	12432.4
Cockpit	700	21	2	0	87.02679	9681.731	9594.704	0	0	913.7813
MLG	1200	42	5	0	932.4299	66724.68	65792.25	0	0	7832.411
NLG	500	10	1	0	15.5405	1569.59	1554.05	0	0	155.405
Sigma	64832				164061.1	2962463	3083197	0	0	214435.4
Aircraft					149576.5	227897.9	363116.6	0	0	15942.7
Xc <sub>cg</sub> =36.7 Zc <sub>cg</sub> =2.68 Yc <sub>cg</sub> =0.0										
					b <sub>x</sub>	b <sub>y</sub>	l <sub>z z</sub>	b <sub>x y</sub>	b <sub>y z</sub>	b <sub>x z</sub>

Table IX.1

# Center of Gravity Travel

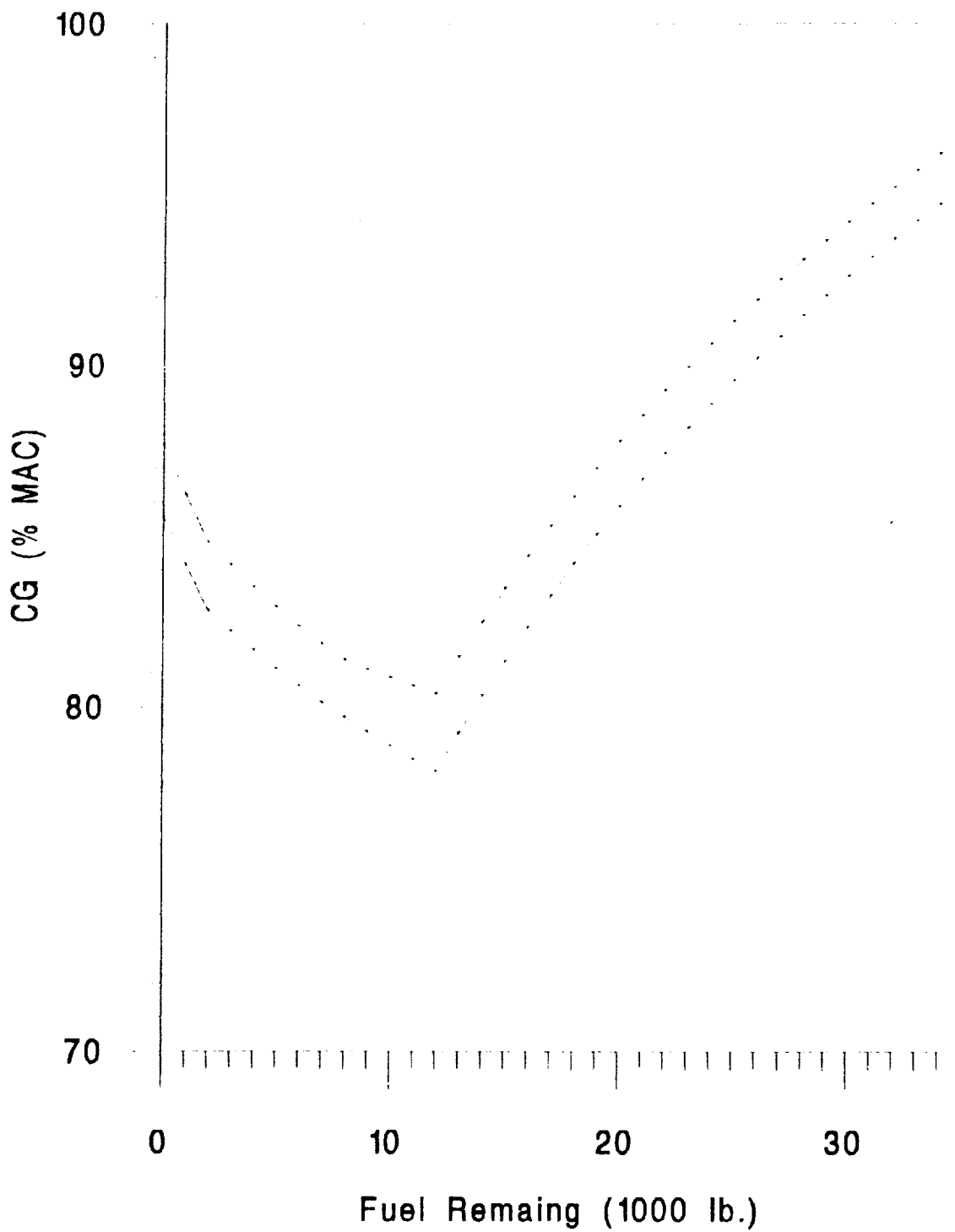


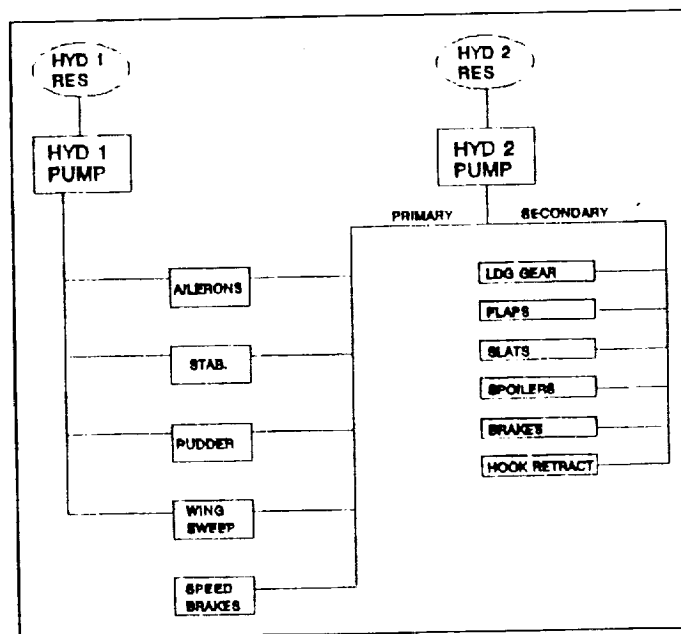
Figure IX.15



## X. Aircraft Systems

### A. Hydraulic System

The Longbow's hydraulic power consists of two systems, HYD 1 and HYD 2, as shown in Figure X.1. Each system is powered by one 8000 psi engine driven hydraulic pump. HYD 1 and HYD 2 each independently power the tandem flight control and the wing sweep actuators.



Hydraulic System  
Figure X.1

HYD 2 is divided into a primary and secondary system. HYD 2 primary powers the flight control actuators and wing sweep as previously stated, and also powers the speed brakes. HYD 2 secondary powers the landing gear, flaps, slats, spoilers, nose

wheel steering, brakes, canopy and hook retract.

An isolation valve divides HYD 2 into the primary and secondary circuits, and is both manually and automatically controlled. After takeoff, when the computer determines that the landing gear, flaps, and slats are fully retracted, the flight position of the isolation valve is automatically selected. The hydraulic devices on the HYD 2 secondary circuit are no longer operational. When the landing gear handle is moved to the landing position, the isolation valve is opened, permitting operation of the devices powered by HYD 2 secondary.

If the HYD 2 secondary system fails, the isolation valve automatically moves to the flight position, preventing further loss of HYD 2 fluid. If this occurs it will be necessary to use emergency landing gear extension, emergency flaps/slats, and auxiliary brakes to land the aircraft.

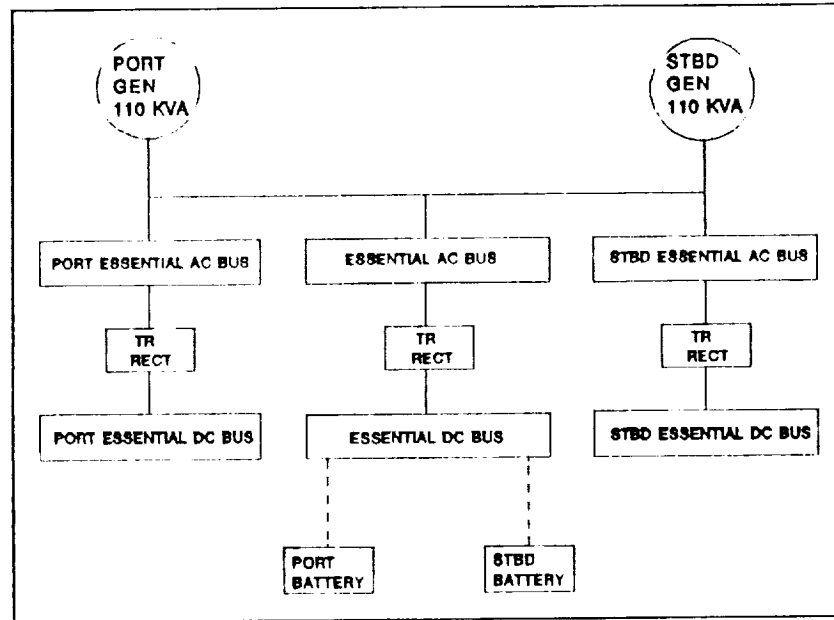
The Longbow is equipped with an emergency hydraulic system that will power the elevator, aileron, and rudder actuators in the event of a HYD 1 and HYD 2 failure. The electrically driven emergency hydraulic pump is actuated when the pressure in HYD 1 or HYD 2 drops below 3000 psi.

HYD 1 and HYD 2 are each equipped with relief valves and automatic level sensing reservoirs. In the event of a loss of hydraulic fluid the component which is causing the fluid loss will be isolated

We chose 8000 psi hydraulic pumps vice 3000 psi in order to realize the 25% weight reduction associated with a hydraulic system of this pressure.

## B. Electrical System

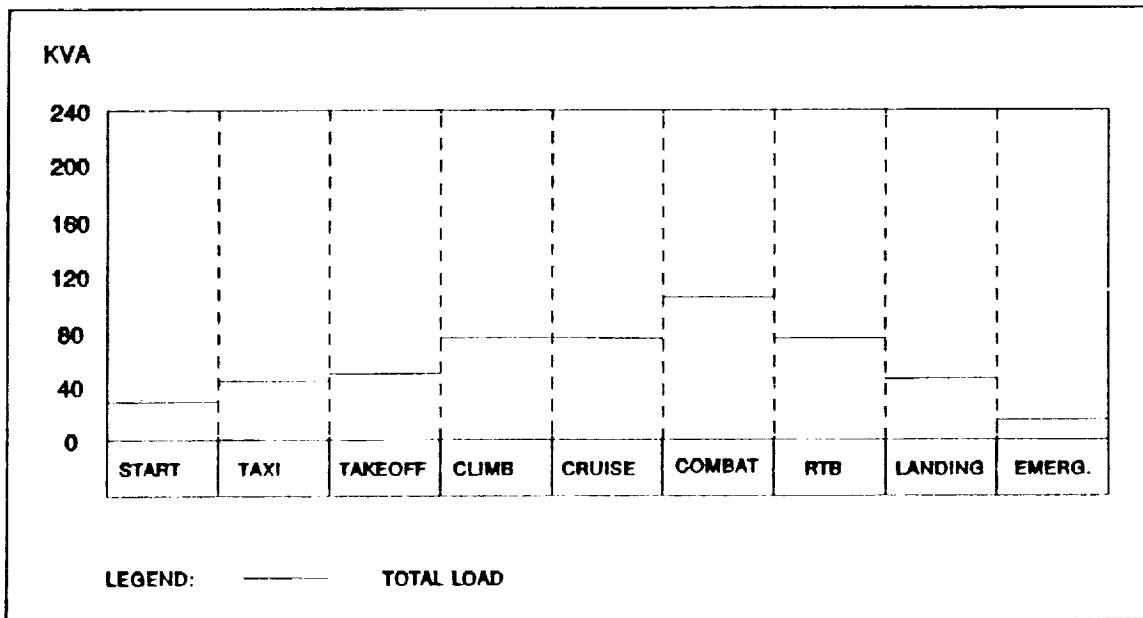
The normal electrical power supply for the aircraft, shown in Figure X.2, is provided by two engine driven generators rated at 110 KVA.



Electrical System  
Figure X.2

The power requirement was determined using an electric load profile as shown in Figure X.3. The Longbow's power requirements vary with the phase of flight. The primary portion of the power generated is used by the avionics, flight controls and pitot heat.

In order to meet weight requirements, it was determined that both generators would be needed to furnish the total power required. In the event of a single generator failure, only the essential items would be powered. If only one generator was required to furnish all electrical power, then each generator would need to be larger, and as a result heavier.



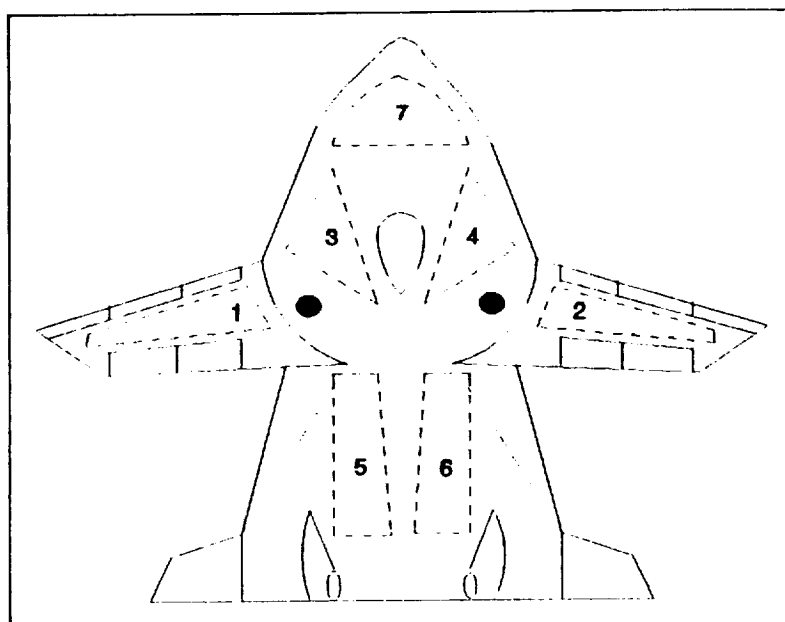
Electric Load Profile  
Figure X.3

Two nonparallel transformer/rectifiers convert AC electrical power to DC. All essential items can be operated on the emergency power system, consisting of two nickel-cadmium batteries. Each battery is maintained by a continuous charge from DC power via the transformer rectifiers.

An auxiliary power unit is provided to allow for unassisted starts.

### C. Fuel System

The Longbow's fuel system consists of four fuel cells (Figure X.4). Each fuel cell is self-sealing, foam filled, and equipped with full time ullage inerting. Due to the Longbow's high operating altitudes, each fuel tank is fitted with an independent fuel transfer pump.



Fuel System  
Figure X.4

The fuel tanks were sized to most efficiently utilize available aircraft volume. Ten percent of fuel tank volume is available for internal components such as foam, transfer pumps and fuel lines. The volume and JP-5 capacity of each fuel tank is as follows:

Fuel Tank	Volume (FT <sup>3</sup> )	Capacity (LBS JP-5)
1	39.32	2000
2	39.32	2000
3	58.99	3000
4	58.99	3000
5	226.11	11500
6	226.11	11500
7	39.32	2000

Table X.1: LONGBOW Fuel Tank Capacities

The total capacity of the Longbow's fuel system is 35000 LBS of JP-5. The wing tanks and aft fuselage fuel tank feed into the forward fuselage fuel tank. The wing tanks begin to transfer when the aft fuselage fuel tank is empty. Fuel is delivered to the engines via redundant sumps, and engine driven suction fuel pumps. In case of fuel pump failure, gravity feed will continue to supply fuel to the engines.

In order to decrease the Longbow's vulnerability, fuel system components will be located inside the fuel tanks, fuel lines will be self-sealing, and fuel runs will be minimized.

All fuel tanks will have a fuel dumping capability.

Inflight refueling will be accomplished through a retractable aerial refueling probe, which will deliver fuel to both the forward and aft fuselage fuel tanks.

The Longbow will be equipped with a computer controlled fuel management system to control aircraft's center of gravity.

#### **D. Environmental Control System**

The environmental control system regulates the environment of the cockpit and the electronic equipment. The system provides cockpit airconditioning and pressurization, windshield and canopy defogging, electronic equipment cooling and pressurization, rain removal, deicing, anti-g suit inflation and hydraulic reservoir pressurization. High pressure bleed air is taken from compressor sections of each engine and passed through an expansion turbine. As energy is expended to drive the turbine, the bleed air is cooled to approximately 400 degrees F. A portion of this air is used for

rain removal and deicing. The remainder of the bleed air passes through a second expansion turbine where it is cooled further. This air is used for the cooling and pressurization functions.

#### E. Survivability

Survivability enhancement features have been incorporated into the design of the Longbow. These features will reduce both the susceptibility and vulnerability of the aircraft. The survivability design of the Longbow is optimized for the high altitude supersonic interceptor mission, where the primary threat is surface to air missiles and enemy fighters.

The susceptibility reduction concepts incorporated into the design of the Longbow are as follows:

1. Threat Warning - Radar and missile warning receivers.
2. Noise Jammers and Deceivers - Self protection jammer.
3. Signature Reduction - Low radar/IR cross section.
4. Expendables - Chaff and Flare dispensing system.

The vulnerability reduction concepts incorporated into the design of the Longbow are as follows:

1. Component Redundancy with Separation - Dual engines, hydraulic systems, mission computers, fuel sumps and quad-redundant flight control system.

2. Component Location -

- a. Harder components located in front.
- b. Compactly grouped non-redundant critical components.
- c. Components located to prevent cascading damage.
- d. Components located to reduce presented area from below

(direction of most probable threat).

3. Passive Damage Suppression -

- a. Ballistically resistant components.
- b. Self-sealing fuel tanks and fuel lines.
- c. Failsafe damage modes of critical components.
- d. Onboard inert gas generating system (OBIGGS) for ullage inerting.
- e. Fuel tank foam.
- f. Dry bay fire walls.

4. Active Damage Suppression -

- a. Ignition and hydraulic ram detection followed by Halon dispensing for suppression.
- b. Overheat detection followed by Halon dispensing for extinguishing.

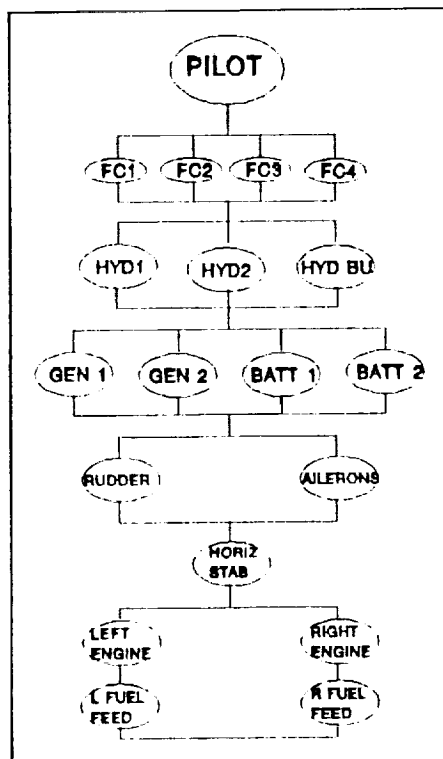
5. Component Shielding - Shielding of engine turbines and compressors.

6. Component Elimination -

- a. Suction fuel pump vice positive pressure pump.
- b. Onboard oxygen generation system (OBOGS) vice LOX bottle.

The Longbow's Kill Tree is for an "A" level attrition kill (ie. out of control in 5 minutes) and is shown in Figure X.5. A vulnerability analysis for the Longbow revealed that the Probability of Kill given a single hit from directly below the aircraft is .034. Assuming a susceptibility of .01, the Longbow's probability of kill given a single shot is .00034. The survivability measure for this scenario is .99966.





Kill Tree  
Figure X.5

## F. Avionics and Cockpit Design

The Longbow's avionics will represent a dramatic advance over the current systems. In aircraft like the F/A-18, F-16C or F-15E, the avionics suite consists of a set of subsystems - a radar, two individual radios, threat warning receiver, IFF, etc. These systems utilize low speed multiplex buses to pass information among subsystems and the cockpit. The large number of controls and displays requires that the pilot interpret a great quantity of information. A lack of redundancy among subsystems can result in loss of mission capability when a single component is disabled.

The Longbow's avionics system design will be viewed as a single subsystem. This subsystem will draw from a highly

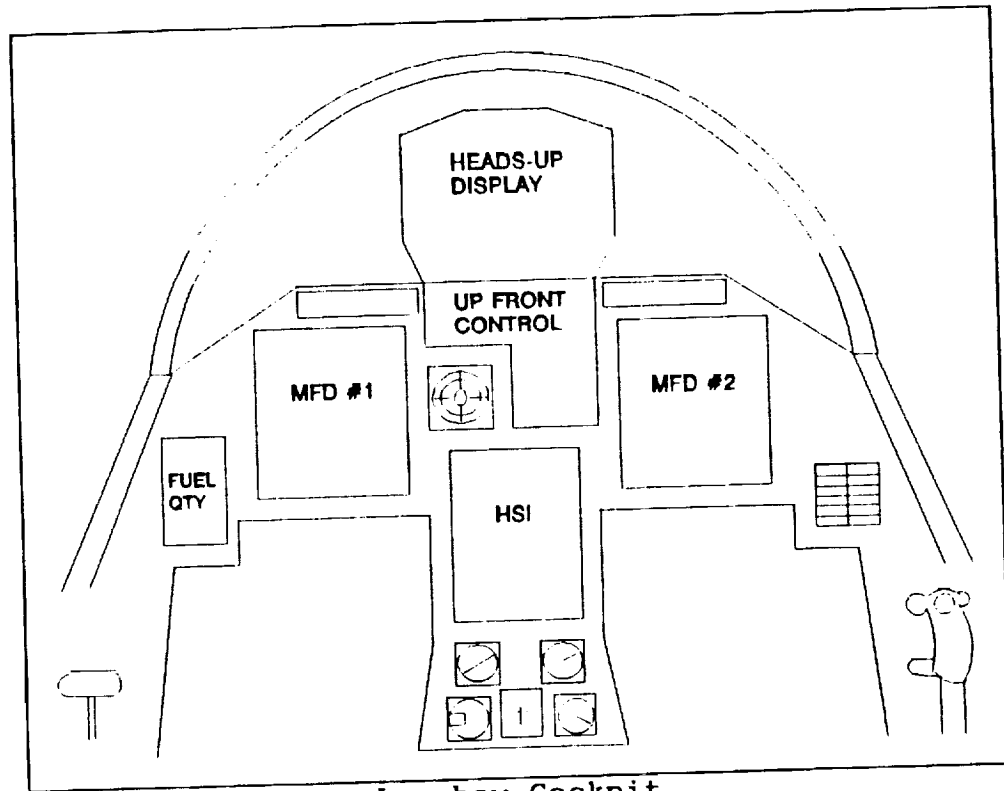
integrated set of resources, each of which can perform multiple tasks in order to accomplish the mission when components have failed or have been damaged.

This highly integrated system will consist of multiple apertures and antennas that are linked with all of the receivers and transmitters through digital signal processing. All of the apertures will be capable of functioning as both sensors and transmitters. For instance, a single aperture will function as a communications transmitter for one portion of the mission, and then act as a threat warning sensor for another.

The key to this avionics configuration is modularity. Very High Speed Integrated Circuits (VHSIC) will permit enormous information processing and storage capacity in small packages. Each module will be capable of performing all avionics functions. The aircraft's mission computers will determine which function is performed by which module. If a module fails, a spare can be brought on line. If damage or failures are numerous during a high tasking portion of the mission, then the remaining modules can be reallocated to higher priority tasks. It is estimated that as few as 60 to 120 modules will handle the avionics of the Longbow.

The cockpit of the Longbow is equipped with three multi-function displays and a wide angle heads-up display, as shown in Figure X.6. The center MFD functions as the primary map display of the aircraft. Each MFD will be capable of displaying all of the aircraft's standard displays. The Longbow's cockpit differs from all previous Naval aircraft in that it is equipped with a side stick controller. The side stick was chosen over the center stick

in that it frees up space in the cockpit for larger displays, and it provides for a more relaxed position for the pilot.



Longbow Cockpit  
Figure X.6

The Longbow cockpit design will incorporate the Hands ON Throttle And Stick (HOTAS) concept. HOTAS alleviates the pilots need to remove his hands from the throttle and control stick in order to perform a significant number of flight and mission functions. This system will increase the pilot's situational awareness, resulting in a more lethal weapons system.

Two mission computers and a conformal multi-mode radar completes the basic design of the Longbow's avionics package.

## G. Maintainability

The Longbow will be one of the most maintainable aircraft in the fleet. The targeted MMH/FH is 23. An approximate 10% improvement over the F/A-18. This goal will be attained by using components with a greater MTBF, improved training systems for maintenance personnel, an airframe mounted accessories drive, EMAIN, external fastener standardization, and larger access panels.

The EMAIN system will utilize a variety of sensors to monitor engine and airframe data. The flight data computer will continuously record parameters such as airframe strain, engine temperatures, engine RPM, oil pressure, etc. This information can then be downloaded to a hand held computer similar to that which is currently being used by B-2 maintenance personnel. Data can then be analyzed for any conditions requiring maintenance. The need for multiple publications, maintenance logs, and records will also be alleviated by the hand held unit.

The Longbow's Airframe Mounted Accessories Drive (AMAD) will make it simpler and quicker to replace the aircraft's engines. Mounting system components such as hydraulic pumps and generators on the airframe vice the engine greatly reduces the steps required to effect an engine change.

The superior maintainability of the Longbow will translate into fewer lost sorties and significant cost savings.

## H. Supportability

Supportability is always a concern for carrier based aircraft. The Longbow is designed to use the support equipment which is currently aboard our aircraft carriers. Nitrogen, hydraulic, and fuel servicing procedures will be nearly identical to the procedures used in the fleet today.

During the initial conceptual design phase, the design team considered using alternative fuels for the Longbow. Hydrogen and JP-4 were two of the fuels considered. Hydrogen was ruled out because of the large storage volume necessary aboard both the aircraft and the ship. The safety aspects of using hydrogen also eliminated that fuel from consideration.

JP-4 was considered because it provides a greater heating value than JP-5 while displacing a similar volume. The problem with JP-4 is that it has a low flash point resulting in a high vapor pressure. This is not compatible with shipboard operations.

JP-5 was ultimately selected for the Longbow. It has a relatively high flashpoint and is currently used for all carrier based aircraft.

Another supportability consideration was the avionics design. Although different than existing avionics on aircraft such as the F/A-18, the modularity and multitask ability of the Longbow's Very High Speed Integrated Circuits will significantly reduce the need for many different types of spare parts.

## I. Carrier Suitability

The Longbow will meet all carrier suitability requirements. It is compatible with MK-7 mod 3 arresting gear and C13-1 catapults, including wind over deck requirements for each of these systems. The max gross weight is well below the maximum elevator capacity of 130,000 pounds.

Carrier elevator dimensions are 85 x 52 feet. The dimensions of the Longbow are 57 x 57 feet with the wings in the swept back configuration. Therefore, like other carrier aircraft, the Longbow will be "tail over water" when being transported on the elevators.

The Longbow exceeds the established catapult takeoff, carrier approach, and waveoff rate of climb criteria. Using the Naval Air Engineering Center's Publications NAEC 607770 "Design Requirements, Catapulting Arrangement, Nose Gear Type Launch" and NAEC MISC OA136 "Catapult Performance/Load Factor Curves" it was determined that the Longbow's catapult end speed and approach speed would be 150 and 137 knots respectively. At these airspeeds, in the landing configuration, a catapult launch weight of 65,000#, and an approach speed of 42,000# the Longbow exceeded all requirements as shown in Table X.2.

	NAVAIR CRITERIA	Longbow
HORIZONTAL ACCEL. AT THE END OF THE CATAPULT STROKE	.065g	.43g
ROTATION CL	less than 0.9 CLmax	0.74 CLmax
LONGITUDINAL ACCEL. AT APPROACH WEIGHT	at least 5 ft/sec <sup>2</sup>	23 ft/sec <sup>2</sup>
APPROACH SPEED	greater than 1.1 Vs	1.32 Vs
50 FOOT ALTITUDE CORRECTION AT APPROACH SPEED WITH NO POWER ADDITION	within 5 seconds	0.3 seconds
SINGLE ENGINE WAVEOFF RATE OF CLIMB	500 ft/min	881.5 ft/min

Longbow Carrier Suitability  
Table X.2

Note: (1) The single engine rate of climb calculation assumes an increase in drag of 36% from the windmilling engine and new trim condition.

## J. Landing Gear

The design of the Longbow's landing gear was driven by the aircraft's requirement to be carrier based. The Longbow's gear meets the requirements set forth in MIL-STD 8863B and 8552. The main landing gear and nose gear tire selection was based on the maximum tire loading. Roskam's method was used to calculate strut diameter and stroke. The placement of the Longbow's landing gear, Figure IV.4 was a function of available internal volume, aircraft center of gravity, NAVAIR guidance on required JBD clearance and shuttle battery position, and tip back and touch down angle restrictions. The specifications for the Longbow's landing gear are shown in Table X.3.

Main Gear Tires	42 x 13-18 28TL
Nose Gear Tires	22 x 6.6-10 20TL
Main Gear Tire Loaded Radius	17.2 IN
Nose Gear Tire Loaded Radius	9.4 IN
Maximum Main Gear Tire Speed	200 KTS
Maximum Nose Gear Tire Speed	196 KTS
Main Gear Strut Diameter	4.84 IN
Main Gear Strut Stroke	15.75 IN
Nose Gear Strut Diameter	4.84 IN
Nose Gear Strut Stroke	13.2 IN
Nose Gear Maximum Dynamic Load	39760.6 LBS
Touch Down Angle	21 DEG
Tip Back Angle	27.6 DEG

LONGBOW Landing Gear Specifications  
 Table X.3



## VIII. PERFORMANCE

### A. TAKEOFF/LANDING

All takeoff characteristics were computed based on full flap extension and Combat Rated Thrust.

Figure VIII.1 shows the calculated roll distance and the FAR required distance to a height of 50 feet above the runway. This analysis assumes a dry concrete runway and a friction coefficient of 0.04 ( $\mu$ ).

For landing (Figure VIII.2), the braking friction coefficient was 0.40 and the residual thrust was five percent of the maximum for a given altitude. Because the LONGBOW will roll out at a negative attitude, no residual lift is generated.

### B. SPECIFIC ENERGY

Specific energy plots are shown in Figs. VIII.3 and VIII.4. In the high Mach region, the gradient between energy levels becomes extremely steep. In this region, the engines have moved to a ramjet cycle, and thrust is limited by mass flow. Associated with the increase in thrust is an increase in fuel consumption. Since the LONGBOW is designed specifically for flight at  $M=3.0$ , the increased thrust above that required to attain Mach 3.0 is unnecessary and the increased fuel usage is unwanted. Therefore the thrust of the engine is held constant above  $M=3.0$ , resulting in the steep energy gradient above  $M=3.0$ .

The diagrams are based on maximum thrust at all velocities and the wings are swept according to the schedule in Figure IV.9.

### C. PERFORMANCE MAPS

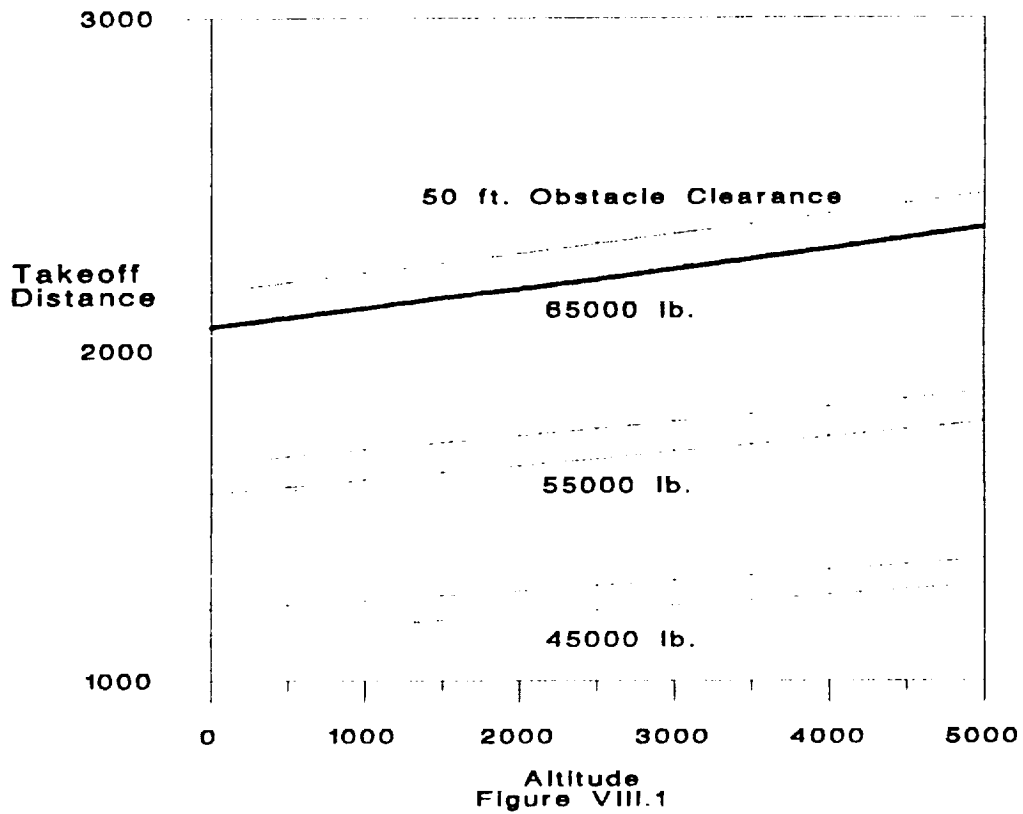
The performance maps shown in Figs. VIII.5 and VIII.6 are

calculated as per Anderson. The lift line is for a lift coefficient of 0.65 with the wings sweeping according to schedule.

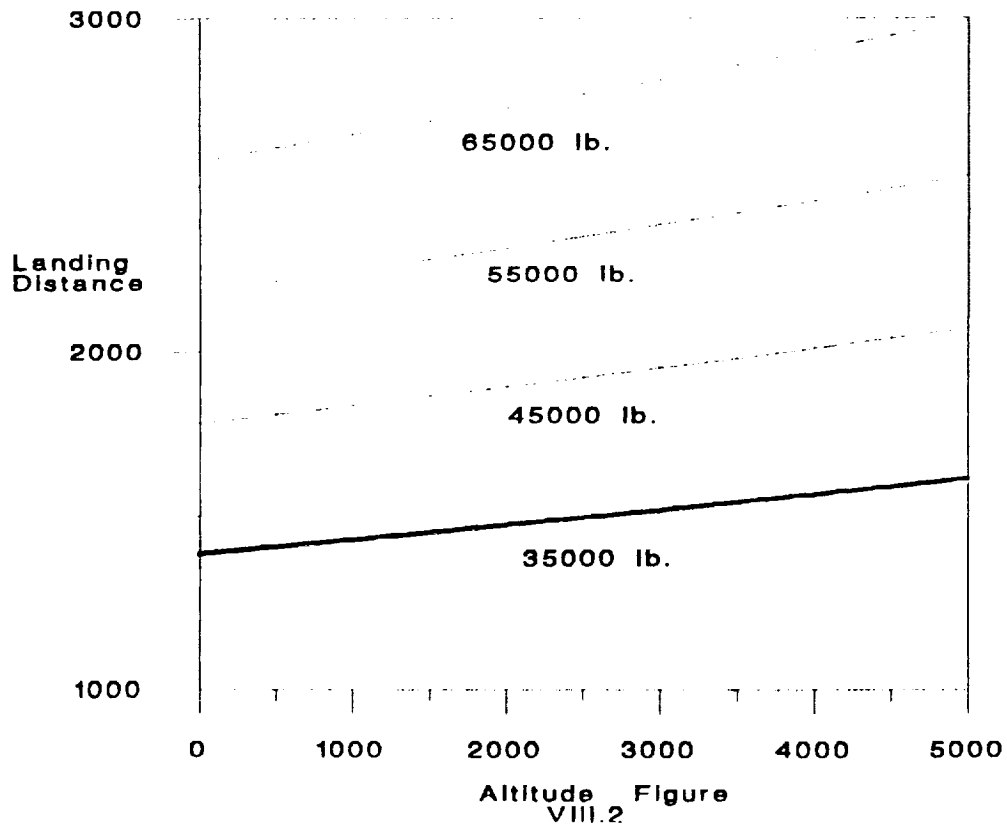
#### D. LOITER/RANGE

Figure VIII.7 shows the range given a loiter time. The profile assumes loitering at  $M = 0.6$ , an outbound leg at  $M = 3.0$ , and a return leg at  $M = 0.8$ . The profile starts with a maximum rate climb to 50000 ft. and holding at  $M = 0.6$ . The outbound leg is flown at  $M = 3.0$ , and the return leg is flown at  $M = 0.8$ . The descent is flown at  $M = 0.6$  and is commenced 120 nm from the CVN. Five thousand pounds of fuel is remaining upon arrival at the CVN at "low holding" altitude ( below 5000 ft.).

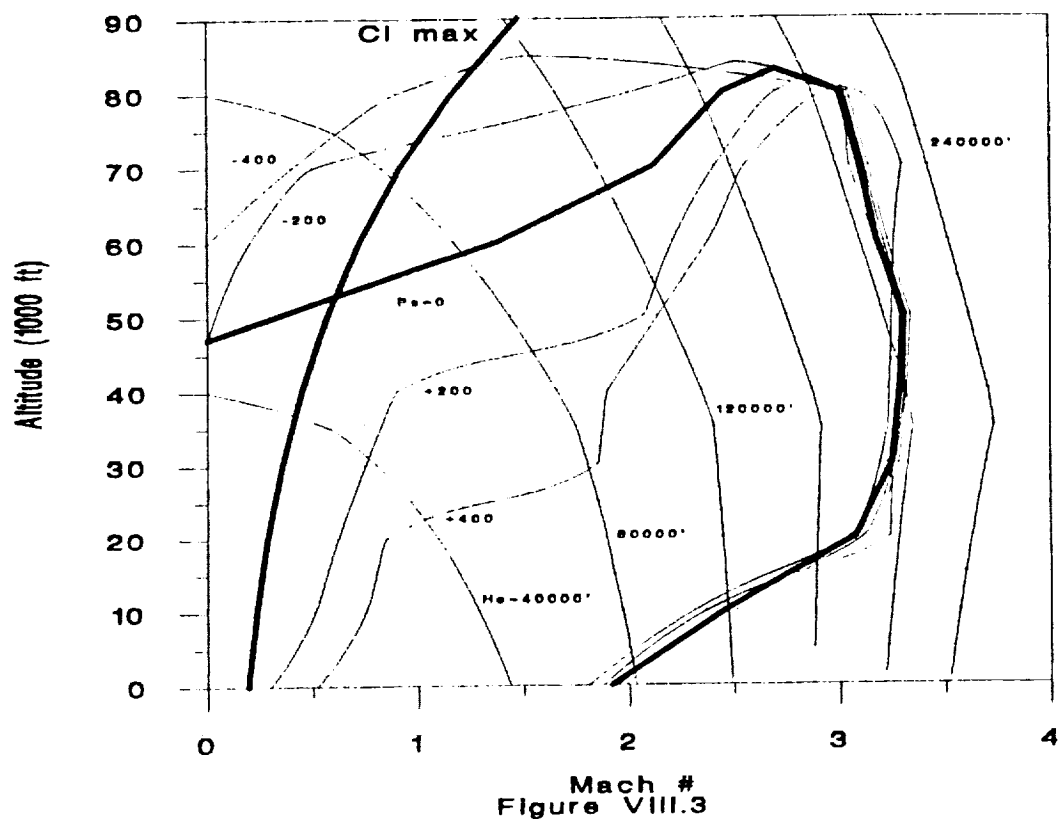
## Takeoff Roll



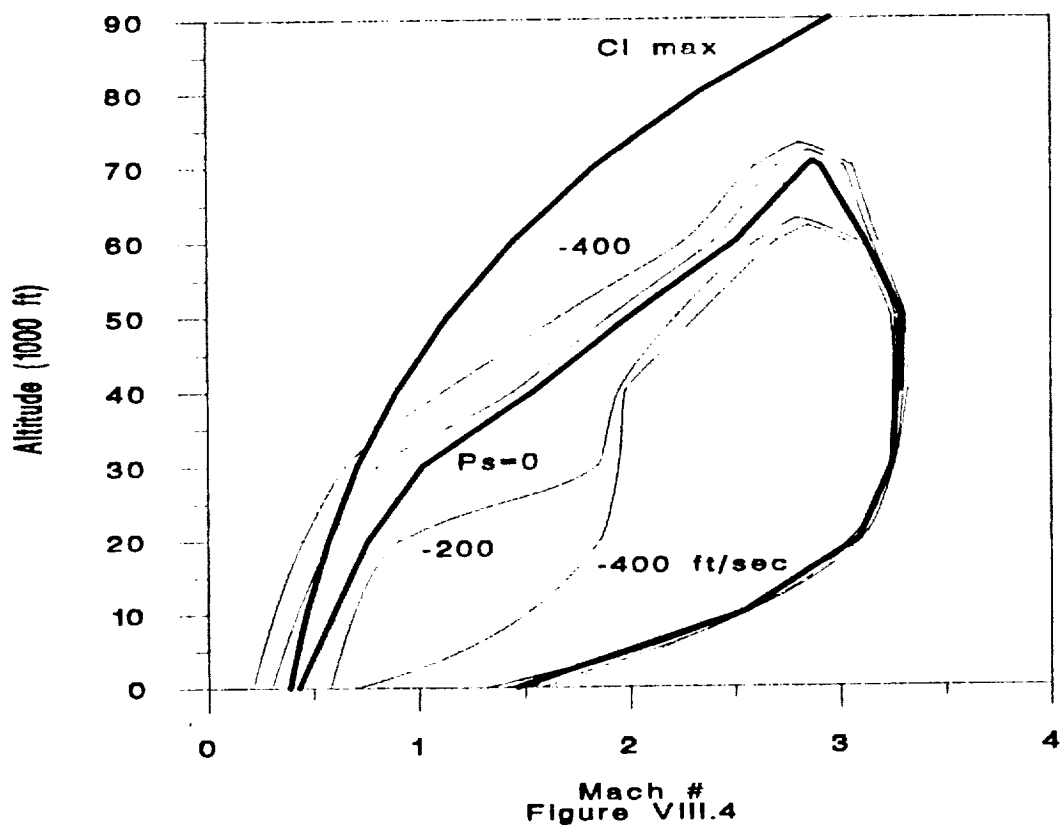
## Landing Roll



# Specific Energy at $Nz = 1.0$



# Specific Energy at $Nz = 4.0$



# Turn Rate at Sea Level (55000 lb.)

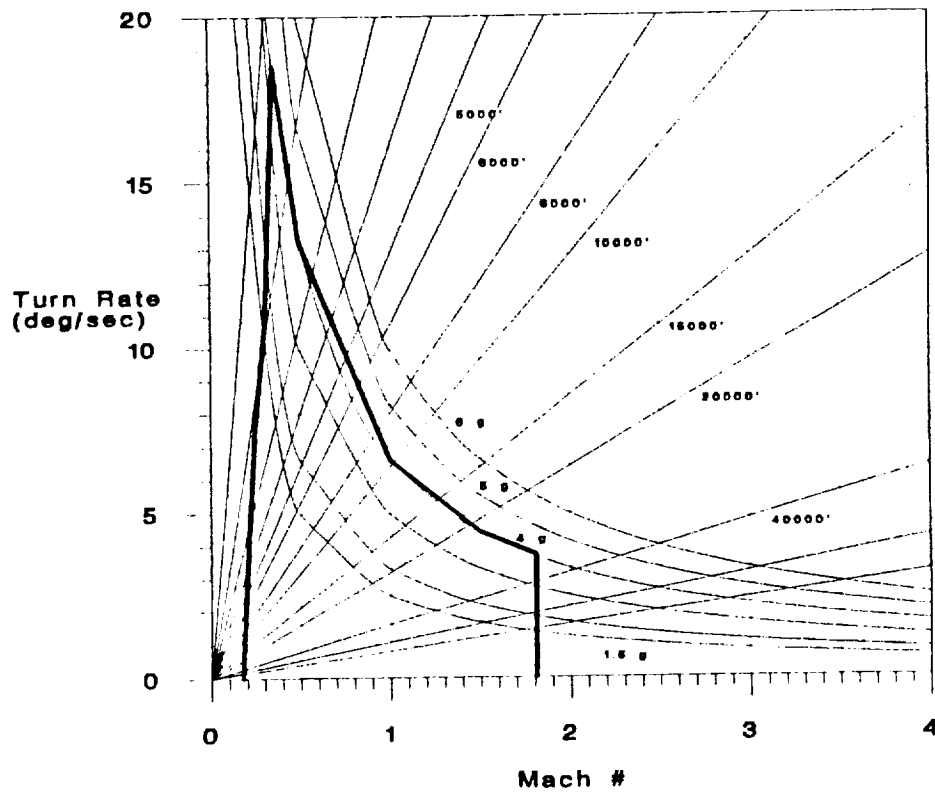


Figure VIII.5

# Turn Rate at 50000 ft. (55000 lb.)

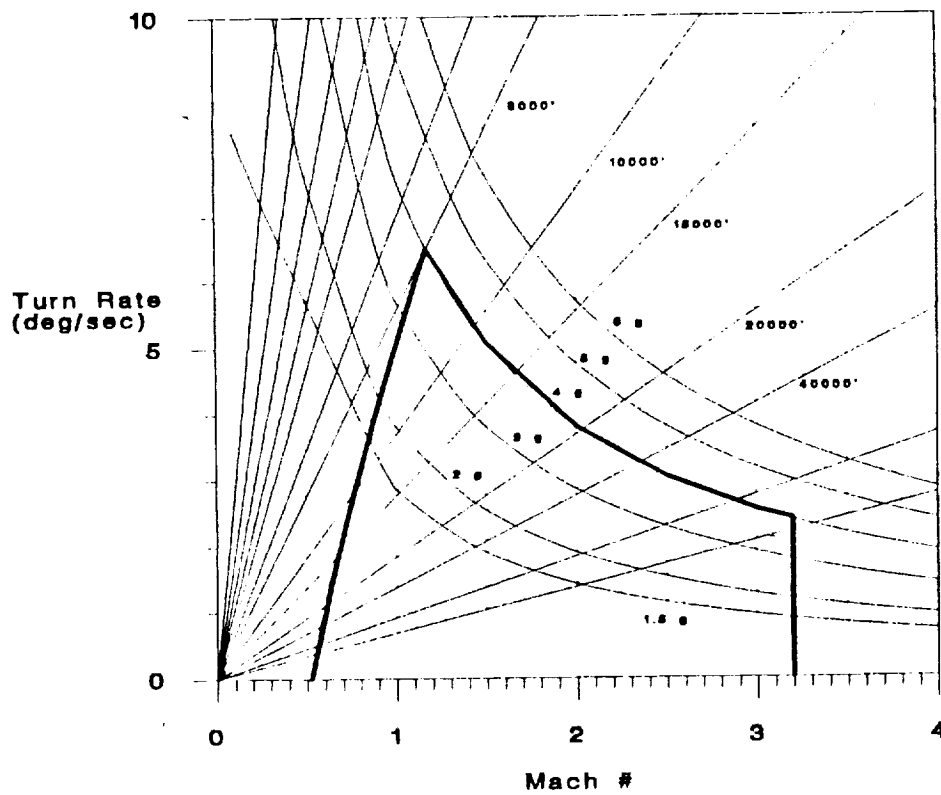


Figure VIII.6

# Loiter Time vs. Range

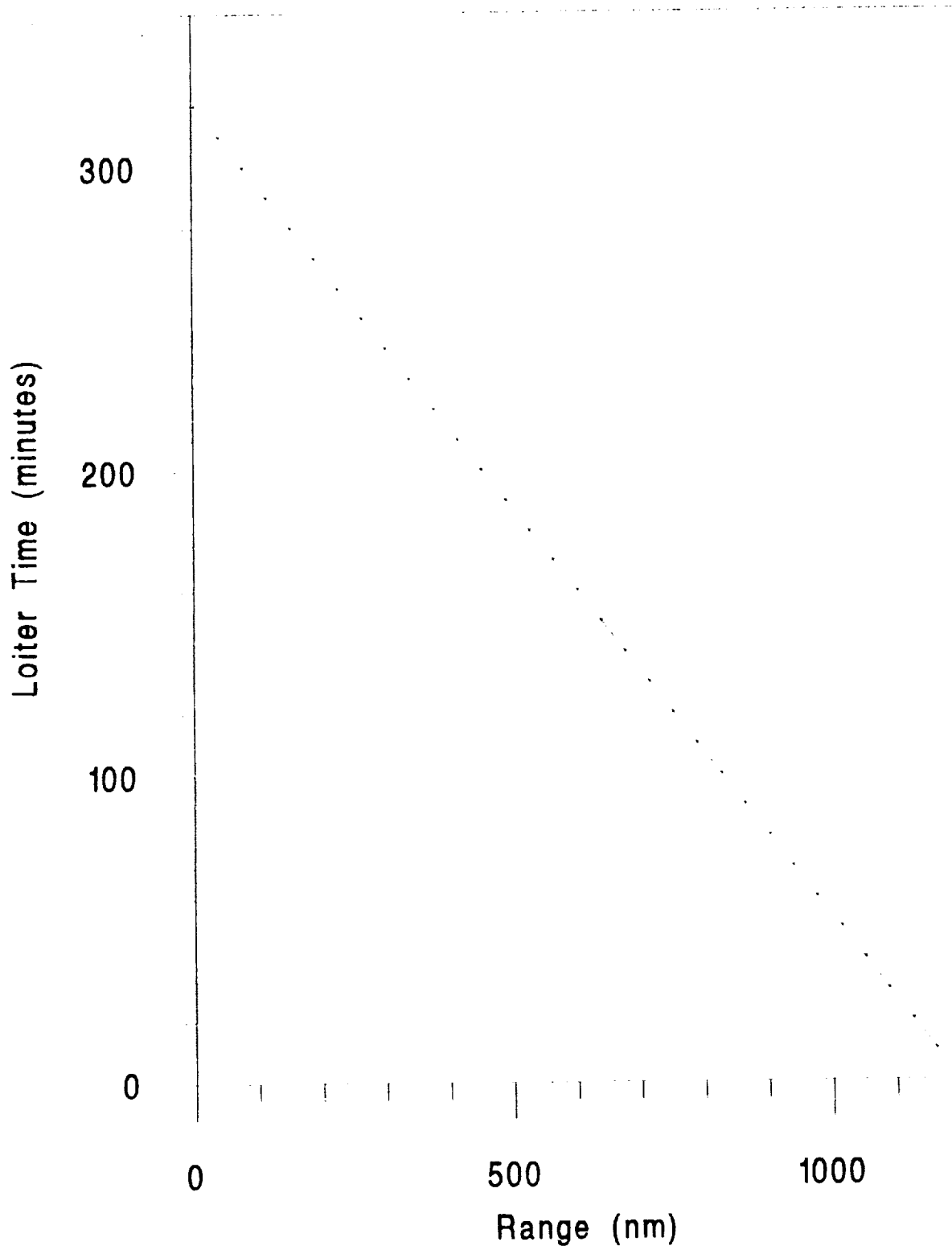


Figure VIII.7

## **XI. COST**

### **A. GENERAL**

Knowing full-well that the cost of an aircraft is determined early in the design cycle, FASTGUYS Corporation considered cost at each point in the design process. Whenever possible, existing technology and materials were used to keep costs down while still satisfying mission requirements. The total life cycle cost for the Longbow will consist of:

- 1) Research, Development, Test and Evaluation (RDT&E)
- 2) Production
- 3) Operations and Maintenance (O & M)

RDT&E includes costs for detail design, and manufacturing and testing of four test aircraft (2 FQ&P aircraft, 1 structural test vehicle and 1 systems/OT&E aircraft). Production cost consists of engineering, manpower and materials to manufacture 250 production aircraft. O&M are the costs incurred in operating the vehicle for a 10 year period, including manpower, maintenance, spares and fuel.

Two cost estimation methods were used: Nicolai's and Earles'. All dollar values are in 1993 dollars.

### **B. NICOLAI COST ESTIMATION**

Nicolai's cost estimation method involves using empirical formulas that relate airplane weight, speed and number of airplanes produced to cost. These formulas are based on costs for 32 aircraft built between 1945 and 1970. Additional costs were added

by this design team to account for the technological challenges associated with a high speed aircraft, including integration of waverider design features, material development for high thermal environment and advanced avionics. The total RDT&E + Production costs using the methods presented in Nicolai resulted in a cost per aircraft of \$46.9M, as shown in Figure XI.1. As shown in Table XI.1 life cycle costs were estimated for a 10 year period.



<b>DT&amp;E COSTS*</b>		
Airframe Engineering		\$231,140,964
Development Support		132,599,497
Flight Test Aircraft		206,112,922
Eng's and Avionics	\$ 4,037,844	
Manufacturing Labor	73,154,520	
Mat'l and Equipment	9,266,005	
Tooling	110,144,465	
Quality Control	9,510,087	
Flight Test Operations		28,600,125
Test Facilities (0.25 FTO)		<u>7,150,031</u>
	Subtotal	605,603,542
	Profit (10%)	<u>60,560,354</u>
	<b>TOTAL DT&amp;E COST</b>	<b>\$666,163,896</b>
<b>PRODUCTION COSTS*</b>		
Engine and Avionics		\$ 176,655,700
Manufacturing Labor		638,678,498
Material and Equipment		238,869,735
Sustaining Engineering		262,924,518
Tooling		120,453,994
Quality Control		15,659,019
Manufacturing Facilities		<u>32,475,000</u>
	Subtotal	1,485,716,467
	Profit (10%)	<u>148,571,647</u>
	<b>TOTAL PROD COST</b>	<b>\$1,634,288,114</b>

\* 1970 Dollars

Amortize DT&E costs over 250 aircraft production run:

$$\text{Unit Cost (1970\$)} = \frac{(\text{DT\&E}) + (\text{PRODUCTION})}{250 \text{ AIRCRAFT}} = \$9,201,808/\text{AIRCRAFT}$$

$$\text{UNIT COST (1993\$)} = \text{UNIT COST (1970\$)} \times 5.1 = \boxed{\$46,900,000} \text{ PER AIRCRAFT}$$

Figure x1.1  
 LONGBOW DT&E and PRODUCTION COSTS  
 (NIKOLAE ESTIMATION METHOD)

ITEM	COST/year(\$M)
AIRCREW: 20 crew/sqd*15 sqd*\$100K/crew/year=	\$30
MAINT: 20 MMH/FH*\$20/hr*15FH/wk*52wk/yr	70.2
OVERHEAD: \$1M/yr/sqd*15sqd=	15
POL: \$750/hr*10FH/wk/ac*52wk/yr*15ac/sqd*15sqd=	87.75
DEPOT/AIMD: \$450K/sqd/yr*15sqd=	6.75
TOTAL YEARLY COSTS=	\$209.7
	10 YR COST(\$M)
10 year operations and maintenance costs=	\$2097
One time spares cost (10% of initial unit cost)=	4.69
TOTAL 10 YEAR O&M COST=	\$2,102
O&M COST PER AIRCRAFT (250 AIRCRAFT RUN)=	\$ 8.4/acft
TOTAL LIFE CYCLE COST PER AIRCRAFT (INCLUDES RDT&E AND PRODUCTION FROM PREVIOUS TABLE)	\$ 55.3 MILLION PER AIRCRAFT

Abbreviations: sqd=squadron yr=year  
hr=hour FH=flight hour  
MMH=Maintenance Man Hour M=Million  
O&M=operations and maint K=Thousand  
AIMD=intermediate maintenance POL=fuel and oil

Table XI.1  
LONGBOW 10 YEAR OPERATIONS AND MAINTENANCE COST ESTIMATE  
Nicolai Method (\$1993)

### C. EARLES COST ESTIMATION

This method relies on the cost estimation methods put forward by Mary Eddins Earles in her book "Factors, Formulas and Structures for Life Cycle Costing", 1981. The results of this cost estimation are presented in Table XI.2.

ITEM	\$ Millions	\$ Millions
<b>RDT&amp;E</b>		\$ 3804
Airframe	\$948	
Engines	229	
Avionics	128	
Support	2499	
<b>INVESTMENT</b>		\$ 9621
Flyaway	\$7677	
Spares	36	
Technical Data	1403	
Training	505	
<b>OPERATING AND SUPPORT (10 years)</b>		\$ 2415
POL	\$1014	
Maintenance	797	
Other	604	
<b>TOTAL FLEET LIFE CYCLE COST</b>		\$ 15840
<b>TOTAL LIFE CYCLE COST PER AIRCRAFT</b>		<b>\$ 63.4 M</b>

Earles Life Cycle Cost Estimate (\$1993)  
Table XI.2

#### D. Cost Comparison

Averaging the costs from the tables for Nicolai and Earles cost estimations results in an expected cost per aircraft of \$ 59.4 million, as shown in Figure XI.2.

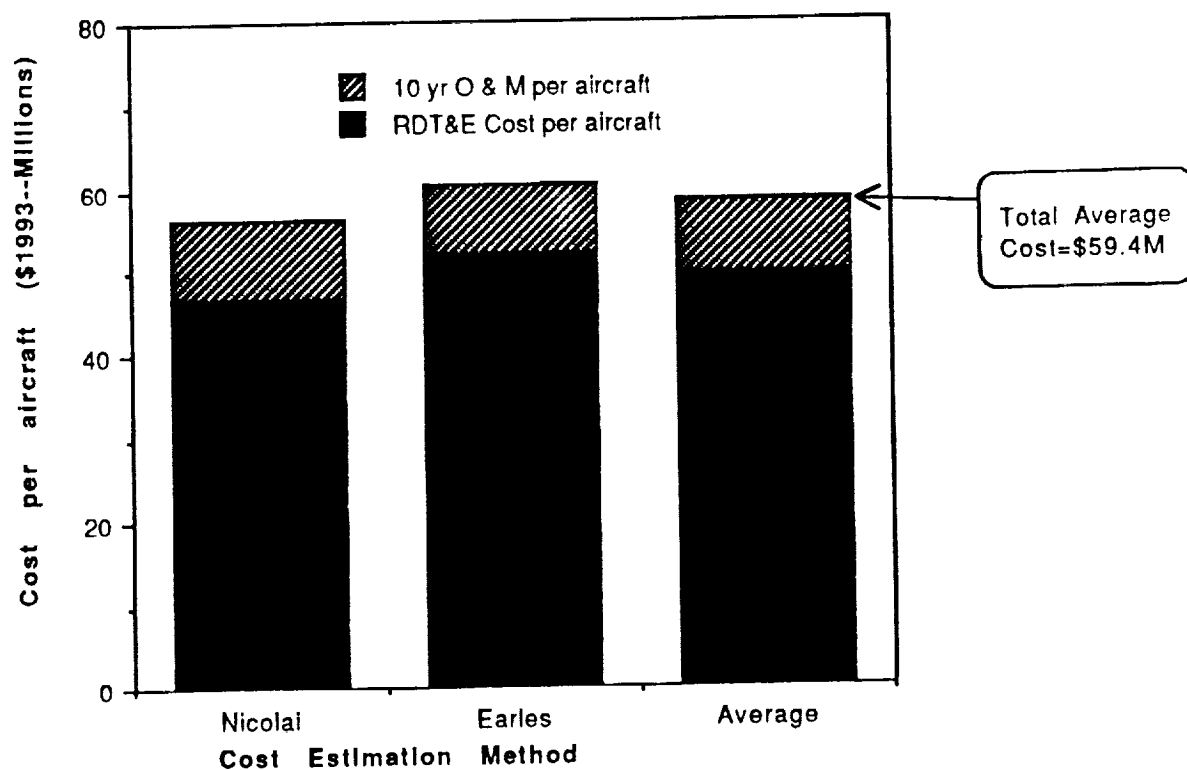


Figure XI.2: LONGBOW Life Cycle Cost Summary

## **XII. MANAGEMENT**

### **A. Organizational Structure**

The LONGBOW design team is comprised of seven experienced Naval Aviators who gave up flying airplanes because they thought it would be more fun to design them for FASTGUYS Corporation. As shown in Figure XII.1, each member of the design team was assigned a primary area of responsibility. In addition, each person had secondary and tertiary areas of interest in which they assisted other team members on a workload-permitting basis. Much as with the successful Lockheed "Skunk Works", the success of the design team stemmed from the fact that it was a small, highly skilled group of technically oriented personnel. In addition, the tenants of Total Quality Leadership (TQL) were implemented to ensure common design goals. Each team member was equipped with the required authority to make decisions on his area of responsibility without the encumbrance of layer upon layer of bureaucratic oversight.

### **B. Houses of Quality**

One of the primary tools utilized by the design team to assist in focusing the design effort was use of "houses of quality". Mission requirements were an integral part of this ongoing analysis to ensure that the Customer's needs were met. Individual requirements were ranked according to their relative importance and then compared with controlling factors to help in defining the cause-and-effect relationship that is so crucial to an efficient

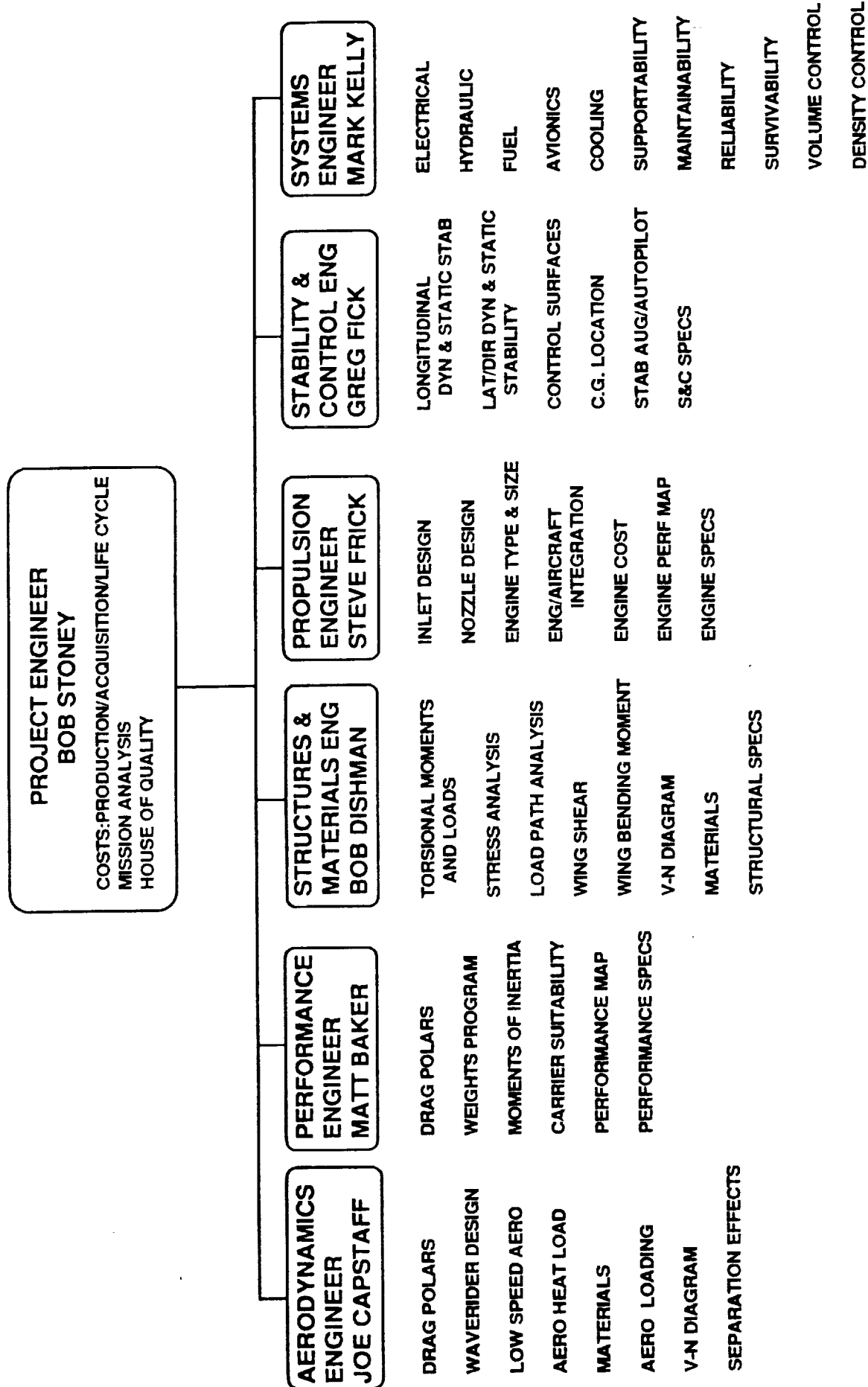


Figure XII.1  
Longbow Design Team Organizational Structure--FASTUYS CORP

design process. The rating system was as follows:

++ Strong positive influence

+ Mild positive influence

- Negative influence

-- Strong negative influence

Several sample houses of quality are depicted in Fig XII.2.

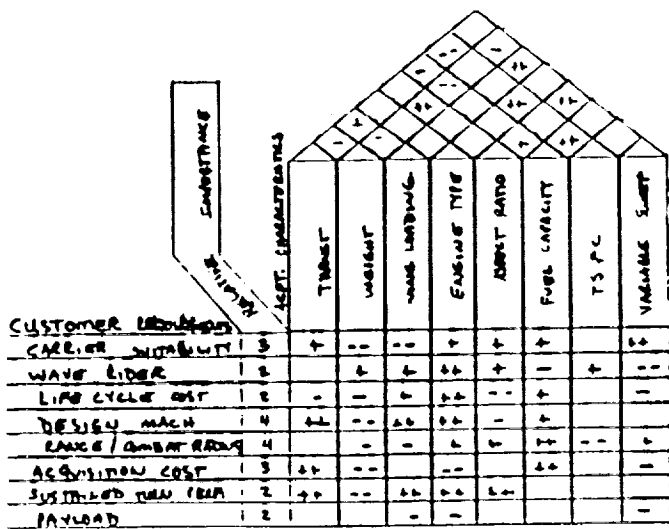


FIGURE A CUSTOMER REQUIREMENTS VERSUS ACFT CHARACTERISTIC

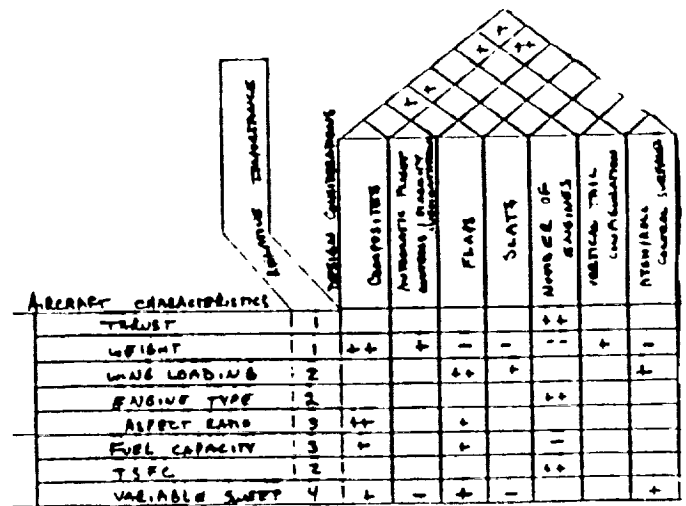


FIGURE B ACFT CHARACTERISTICS VS. DESIGN CONSIDERATION

Figure XII.2  
Sample Houses of Quality

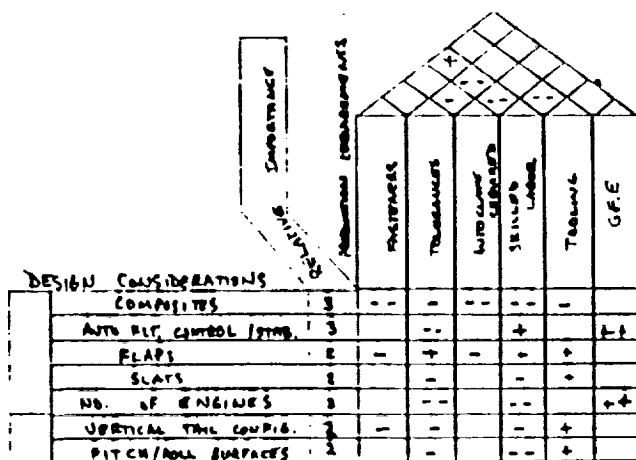


FIGURE C DESIGN CONSIDERATIONS VS. PRODUCTION REQUIREMENTS

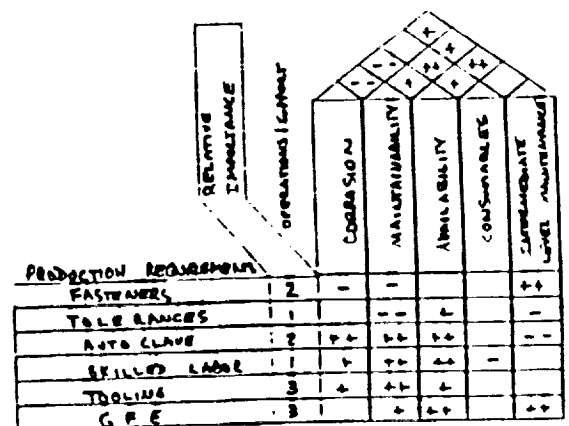


FIGURE D PRODUCTION REQUIREMENTS VS. OPERATIONS/SUPPORT



### **XIII. PRODUCTION FACILITIES**

The Longbow aircraft will be fabricated and assembled at a single production facility located in Jacksonville, Fla. Here, all major forms of transportation including port facilities are available for receipt of large as well as small components from suppliers and subcontractors. Rail lines into the facility complex and quick access to major highways will serve to minimize shipping and handling costs. Except for engines, weapons, and avionics, which will be produced by subcontractors, all major components will be fabricated at this central facility. The final assembly of all aircraft components will then be completed in the central plant.

FASTGUYS, INC. will incorporate the latest technology in Computer Aided Design (CAD) into all facets of the design structure in order to maximize information exchange and time savings, and expedite incorporation of any required design changes. State of the art tooling, both Government Furnished Equipment and company assets will be utilized in order to minimize production time while maximizing quality. Computer aided robotics will also be utilized when deemed necessary. All of these innovations along with TQL management philosophy will assure the highest level of quality while reducing production time and cost. Maximum production efficiency and thus minimum cost per unit is obtained through a steady procurement plan as shown in Table XIII.1 below.

YEAR	# OF ACFT	COMMENTS
1999	2	Prototypes
2000	2	Stat & Dyn Loads Tests
2001	16	Spool-up
2002	30	
2003	40	Full Scale Production
2004	40	
2005	40	
2006	40	
2007	30	Down Scale Production
2008	10	Final Lot

Table XIII.1  
Production Plan

#### XIV. SUMMARY

The LONGBOW design team has completed the preliminary design for an airplane to fulfill the Customer's mission requirements for a high speed, long range Deck Launched Interceptor and Reconnaissance platform. Highlights of the Longbow's capabilities include:

- Design Mach Number of 3
- Advanced, survivable, maintainable systems
- Designed for low cost
- Carrier suitable
- Meets or exceeds all specifications except mission radius

The LONGBOW's combat radius fell short of the RFP's 1500 nm target. The team strongly believes that, given the likely aerodynamic and propulsion technology of the next 20 to 30 years, achieving a 1500 nm radius at speeds of Mach 3 to 5 is not possible while still keeping the airplane small enough to operate on the current CVN. Increase range at slower speeds is possible, in fact achievable in large part by current platforms. Achieving the 1500 nm radius will require either a breakthrough technology or redesign of the CVN configuration to accommodate a larger, heavier airplane.

Several other areas will require further study during the detailed design process. These include refinement of the behavior of the airflow around the body at Mach 3 , Radar Cross Section issues, and Stability and Control system architecture and validation.

## REFERENCES

MIL-F-8785C, Flying Qualities of Piloted Aircraft

MIL-STD-805A, Field of View

MIL-STD-2069, Survivability

MIL-A-8860, Strength and Rigidity

MIL-A-8861, Flight Loads

MIL-A-8863, Carrier Suitability

MIL-STD-8552, Landing Gear Design

MIL-A-8870, Vibration and Flutter

MIL-A-2066, Carrier Launch and Arrestment

Nicolai, L., Fundamentals of Aircraft Design, METS Inc., 1975.

Martin, C.L., Taguchi's Parameter Design Optimization method Applied to Aircraft Systems, Georgia Institute of Technology, December 1989.

Earles, Mary E., Factors, Formulas and Structures for Life Cycle Costing, Eddins-Earles, 1981.

Oates, Gordon C., Aerothermodynamics fo Gas Turbine and Rocket Propulsion, AIAA, 1984.

Lewis, Mark J., The Use of Hypersonic Waveriders for Aero-assisted Orbital Manoeuvring, JBIS, January 1993.

Mattingly, Jack D.; Heiser, William J. and Dailey, Daniel H., Aircraft Engine Design, AIAA, 1987.

"Aircraft Design Short Course", Lecture Notes, University of Dayton, Dayton, OH, January 1977.

Grayson, M., Principles of Guided Missile Design, D. Van Nostrand Company, Inc., 1960.

White, F.M., Heat Transfer, Addison-Wesley Publishing Company, 1984.

Allen, D.H. and Haisler, W.E., Introduction to Aerospace Structural Analysis, John Wiley and Sons, 1985.

AIAA-73-820, "The F-12 Series Aircraft Aerodynamic and Thermodynamic Design in Retrospect", Lockheed California Co..

SAE Aerospace applied Thermodynamics Manual, Society of American Engineers, February 1960.

Niu, M.C., Aircraft Structural Design, Canmilt Press Ltd., 1988.

Roskam, Jan, Airplane Design, Layout Design of Landing Gear and Systems, Roskam Aviation and Engineering Corporation, 1969.

Roskam, Jan, Aircraft Systems, Roskam Aviation and Engineering Corporation, 1970.

Raymer, Daniel P., Aircraft Design: A conceptual Approach, AIAA, 1989.

Ball, Robert E., The Fundamentals of Aircraft Combat Survivability: Analysis and Design, AIAA, 1985.

Anderson, John D., Introduction to Flight, Third Ed., McGraw-Hill Book Co., 1989.

Anderson, John D., Fundamentals of Aerodynamics, Second Ed., McGraw-Hill Book Co., 1991.

Nelson, Robert C., Flight Stability and Automatic Control, McGraw-Hill Book Co., 1989.

